HYBRID FIBER-OPTIC DEVICE FOR SPATIOTEMPORAL CONTROL OF PHOTOSENSITIZER RELEASE AND SINGLET OXYGEN DELIVERY

by

MATIBUR RAHAMAN ZAMADAR

A dissertation submitted to the Graduate Faculty in Chemistry in partial fulfillment of the requirements for the degree of Doctor of Philosophy

The City University of New York

2011

This manuscript has been read and accepted for the Graduate Faculty in Chemistry in satisfaction of the dissertation requirement for the degree of Doctor of Philosophy.

	PROFESSOR ALEXANDER GREER
Date	Chair of Examining Committee
	PROFESSOR MAHESH K. LAKSHMAN
Date	Executive Officer
	PROFESSOR ALEXANDER GREER
	PROFESSOR ROBERTO A SANCHEZ-DELGADO
	PROFESSOR STEPHEN PHILIP FEARNLEY
	Supervision Committee

THE CITY UNIVERSITY OF NEW YORK

Abstract

HYBRID FIBER-OPTIC DEVICE FOR SPATIOTEMPORAL CONTROL OF PHOTOSENSITIZER RELEASE AND SINGLET OXYGEN DELIVERY

BY

MATIBUR RAHAMAN ZAMADAR

Adviser: Professor Alexander Greer

Abstract: This thesis outlined the gradual progress towards the development of the first fiber-optic singlet-oxygen generator designed for releasing singlet oxygen locally, which can surmount the challenges associated with current photodynamic therapy and water disinfection.

We developed a photochemical approach to clean generation of singlet oxygen in aqueous solution with a sensitizer (*meso*-tetra(*N*-methyl-4 pyridyl)porphine) adsorbed onto solid porous Vycor glass (PVG)]. Photophysical analysis revealed that oxygen collision onto the sensitizer adsorbed porous Vycor glass matrix converts ground-state oxygen into singlet oxygen ($^1O_2$) which diffuses into bulk aqueous solution. Singlet oxygen was detected in water by time-resolved methods and by chemical trapping with alkene, N-benzoyl methionine, and anthracene derivative to give hydroperoxide, N-benzoyl sulfoxide, and anthracene endoperoxide derivative. Based on this study, we developed a device that channels light and oxygen through a hollow core fiber optic into the sensitizer adsorbed Vycor glass which acts as a cap. Singlet oxygen was generated on a microscale at the fiber cap site selectively which then diffused out into the surrounding

aqueous solution. A complete Escherichia coli inactivation was observed in 2 h when the fiber cap was immersed in 0.1 mL aqueous samples of $0.1–4.4 \times 10^7$ cells.

The prototype device was further modified to enhance singlet oxygen diffusion in aqueous solution as singlet oxygen has lifetime's ranges from microseconds to milliseconds and the corresponding diffusion distances of singlet oxygen ranges from nanometers to millimeters. Our efforts included $^1O_2$ generation by cleaving off sensitizer molecules away from the fiber optic probe to increase $^1O_2$ formation at a distance from the probe tip. Synthetic methodology was developed to modify the glass probe to release photosensitizer molecules into the surrounding medium by an oxidative self-cleaving mechanism where $^1O_2$ was used as a sole reagent. We successfully attached pyropheophorbide photosensitizer containing a photosensitive electron rich alkene covalently to porous Vycor glass which is triggered for release on-site by visible light irradiation, via dioxetane decomposition to give two carbonyl fragments. The cleaved photosensitizer diffuses into solution to produce singlet oxygen at a distance from the glass surface which also improves the photooxidation efficiency of the heterogenous photosensitizer. Finally, a review of the literature on 'singlet oxygen as a reagent in organic synthesis' was accomplished, which represent the last chapter of the thesis.

ACKNOWLEDGMENTS

This dissertation would not be possible without help of many people in many ways. I am truly grateful for all that they have done and would like to take the time to acknowledge them. First and foremost, I would like to express my sincere appreciation and gratitude to my mentor Professor Alexander Greer for his ever-willing support, dedication, inspiration and valuable insights that enriched my knowledge during my Ph.D. studies. As my mentor, Professor Greer introduced me to the fascinating world of physical—organic chemistry. His drive, passion for science, and his challenge in exploring new ideas encouraged me to grow up as a young scientist. I am truly grateful to my mentor for giving me the opportunity to work on different projects towards the development of fiber optic singlet oxygen generator and also a book chapter which I included in my thesis (chapter 5).

I would like to thank the members of my dissertation committee, Professor Roberto A. Sanchez-Delgado (Brooklyn College) and Professor Stephen Philip Fearnley (York College), for taking their time for my annual committee meetings, which were of great help for me, approving my dissertation and the defense.

I would like to take some opportunity to express my deep appreciation to our collaborators. Naveen Gandra in Professor Ruomei Gao reaseach group at Jackson State University helped us to get singlet oxygen luminescence study and measuring singlet oxygen life time in solution (chapter 1). Professor Harry D. Gafney at Queens College, City University of New York helped us by providing some valuable suggestions in the early phase of the development of Vycor based heterogeneous sensitizer project. Dr. Jovan Giaimuccio in Professor Gerald J. Meyer research group at Johns Hopkins

University helped us for nanosecond transient absorption study which showed a details understanding of the nature of quenching of excited state of sensitizer adsorbed Vycor glass with ground state molecular oxygen at the water—solid interface (chapter 2). Professor Catherine McEntee at Brooklyn College, City University of New York helped us for of E. *colie* inactivation study.

I would like to take some time to express my sincere thanks to Dr. David Aebisher with whom I worked on different projects from the beginning of the development of fiber optic singlet oxygen generator. He is the person whom I learn first how to conduct organic photochemistry reaction. His constant inspiration and excellence guidance, and wonderful suggestions always helped me to develop my knowledge in the area of organic photochemistry.

I wish to thank all my teachers from Graduate Center and Brooklyn College and acknowledge their significant contributions to my education and work. I have learned a lot from each of them throughout my Ph.D. program, for which I am very grateful.

I am really grateful to my colleagues; Goutam Ghosh, Mahendran Adiackipillai, Mihaela Minnis, Bonnie I. Kruft, Ashwini Ghogare, and Leda Lee for their great efforts for finishing up of my last project (chapter 4). I deeply appreciate their significant contribution. I am also grateful to Nikolay S. Azar, Alvaro Castillo, Dr. Nahed Sawwan, and Dr. Edyta M. Greer.

My very special thanks go to the most valuable thing I have in life – my family in India. Their faith, unconditional love, and confidence in my abilities and in me is what has produced the person I am today. Thank you for everything.

To My Parents

And All the Other Wonderful People in My Life

TABLE OF CONTENTS

TITLE i

APPROVAL PAGE iii

ABSTRACT iv

ACKNOWLEDGEMENT vi

TABLE OF CONTENTS x

LIST OF SYMBOLS AND ABREVIATIONS xiv

LIST OF FIGURES xvii

LIST OF SCHEMES xxii

LIST OF TABLES xxv

Chapter 1. Singlet Oxygen Chemistry in Water. A Porous Vycor Glass—Supported Photosensitizer 1

1.1 Introduction 1

1.2 Results and Discussion 3

1.2.1 Adsorption of Photosensitizer **1** 3

1.2.2 Spectroscopic Properties of PVG-Adsorbed **1** 5

1.2.3 Detection of Singlet Oxygen 6

1.2.4 Photooxidation of *Trans*-2-methyl-2-pentenoate Anion (**2**) 10

1.3 Conclusion 12

1.4 Experimental Section 12

1.4.1 Materials and Instrumentation 12

1.4.2 Measurements 13

1.4.3 *Meso*-tetra(*N*-methyl-4-pyridyl)porphine (**1**). 15

1.4.4 Heterogeneous Photooxidation of *Trans*-2-methyl-2-pentenoate Anion (**2**)..... 16

1.5 References 18-22

Chapter 2. Photoexcited Sensitizer Quenching by O_2 at the Water—Porous Glass Interface 23

2.1 Introduction 23

2.2 Results and Discussion 25

2.2.1 Time-Dependent Adsorption of Photosensitizer onto PVG. 25

2.2.2 Uniform Photosensitizer Distribution 26

2.2.3 Photosensitizer Penetration Depth 28

2.2.4 Spectral Properties ……..... 30

2.2.5 Time-Resolved Photophysical Studies……..... 31

2.3 Conclusion 37

2.4 Experimental Section 38

2.4.1 Materials and Sample Preparation..... 38

2.4.2 Instruments ……..... 39

2.4.3 Transient Absorption Spectroscopy ……. 39

2.4.4 Computational Methods ……..... 40

2.5 References 41-44

Chapter 3. Singlet Oxygen Delivery Through the Porous Cap of a Hollow-Core Fiber Optic Device……..... 45

3.1 Introduction 45

3.2 Results and Discussion 46

3.3 Conclusion 52

3.4 Experimental Section 53

3.4.1 General Aspects 53
3.4.2 Fiber Modifications 54
3.4.3 Cap Preparation, Adsorption and Desorption Studies 54
3.4.4 Methionine Trapping Studies 55
3.4.5 Further experiments 55
3.5 References 57-58

Chapter 4. Fiber Optic-Guided Photosensitizer Drug Delivery 59
4.1 Introduction 59
4.2 Results and Discussion 61
4.2.1 Synthesis of the Sensitizer-Fiber Cap (Scheme 1) 61
4.2.2 Requirements for Sensitizer Loading Onto the Fiber Cap 66
4.2.3 Fiber Optic-Initiated Photocleavage of the Attached-Sensitizer 70
4.3 Conclusion 74
4.4 Experimental Section 75
4.4.1 Materials and Instrumentation 75
4.4.2 Construction of the Fiber Optic Apparatus 76
4.4.3 Synthesis and Characterization 77
4.4.4 Sensitizer Coverage Measurements 81
4.4.5 Oxygen Flow Measurements 82
4.5 References 101

Chapter 5. Singlet Oxygen as a Reagent in Organic Synthesis 102
5.1 Introduction 102
5.2 Dioxetanes 104

5.2.1 Background Information 104
5.2.2 Adamantyl-Substituted Alkenes..... 106
5.2.3 Alkoxy-Substituted Alkenes 107
5.2.4 Phenyl- or MethylSubstituted Alkenes ……. 109
4.2.4.1 Diphenylindene Photooxidation..... 109
4.2.4.2 Electron-Transfer Photooxidation..... 109
5.2.5 Summary ……. 109
5.3 Endoperoxides..... 111
5.3.1 Background Information 111
5.3.2 Arenes ……..... 114
5.3.2.1 Benzenes... 114
5.3.2.2 Naphthalenes…..... 116
5.3.2.3 Anthracenes, Polyacenes, and Carbon Nanotubes….
..... 117
5.3.3 Electron Transfer Photooxidation ……. 119
5.3.4 Conjugated Dienes ……. 119
5.3.4.1 Acyclic Dienes.. 119
5.3.4.2 Cyclopentadienes and Cyclohexadienes.. 120
5.3.4.3 Heterocycles and Cyclohexatriene..... 121
5.3.5 Summary 125
5.4 Hydroperoxides..... 126
5.4.1 Background Information 126
5.4.2 Simple Alkenes 126
5.4.3 ‘Ene’ Reactions Confined in Zeolites 129
5.4.4 Summary ……. 130
5.5 Tandem Singlet Oxygen Reactions ……..... 130
5.5.1 Background Information..... 130

5.5.2 Bisperoxides..... 131

5.5.2.1 Phenyl-Substituted Alkenes.. 131

5.5.2.2 Cyclic Alkenes.. 132

5.5.3 Rearrangment to a Hemiketal Hydroperoxide.. 135

5.5.4 Rearrangements to Spiro Compounds… 136

5.5.5 Summary... 139

5.6 Conclusion 140

5.7 References.....141-148

LIST OF SYMBOLS AND ABBRIVIATIONS

Å	angstrom
Ac	acetyl
Ac_2O	acetic anhydride
B3LYP/6-31G(d)	Becke-style-Parameter Density Functional Theory
brine	saturated aqueous sodium chloride solution
br	broad
^oC	degree Celsius
calcd	calculated
CCl_4	carbon tetrachloride
kcal	kilocalorie
^{13}C NMR	carbon-13 nuclear magnetic resonance
δ	chemical shift in ppm
d	doublet
DCM	Dichlorometane
DMAP	4-(Dimethylamino)pyridine
DFT	Density Functional Theory
DMF	N,N-dimethylformamide
ε	dielectric constant
EDC	1-Ethyl-3-(3-dimethylaminopropyl)carbodiimide
Et_2O	diethyl ether
EtOAc	ethyl acetate
eq	equivalent

g	gram
GC	gas chromatography
GCMS	gas chromatography mass spectroscopy
h	hour
^{1}H NMR	proton nuclear magnetic resonance
HPLC	high pressure liquid chromatography
Hz	hertz
IR	infra-red spectroscopy
J	coupling constant
L	liter
LAH	lithium aluminum hydride
m	multiplet
MeOH	methanol
mg	milligram
min	minute
mL	milliliter
mmol	millimole
NaH	sodium hydride
$NaBH_4$	sodium borohydride
NBS	N-bromosuccinimide
NaI	sodium iodide
n-BuLi	*n*-Butyllithium
*p*H	potential of hydrogen

*p*Ka	ionization constant
ppm	parts per million
q	quartet
rt	room temperature
s	singlet
t	triplet
THF	tetrahydrofuran
TLC	thin layer chromatography
TMPyP	meso-tetra(N-methyl-4-pyridyl)porphyrine
TsOH	*p*-toluenesulfonic acid
UV	ultra-violet spectroscopy

LIST OF FIGURES
Chapter 1

Figure — Page

1. Plot of the moles of H^+ ions arising from PVG silanol deprotonation calculated from the decrease in pH of the aqueous solution during the adsorption of **1** onto PVG. Each point is taken at a 30-minute increment over a total of 3 hours 5

2. Normalized absorption spectra of **1-ads** and **1**: (1) the solid line is of **1-ads** in air, in which uncoated PVG was used as a blank, and (2) the dashed line is an H_2O solution of **1**, in which H_2O was used as a blank. The inset is an expanded view of the visible portion of the spectra……..... 6

3. Singlet oxygen phosphorescence (1270 nm) decay from **1-ads** carried out in H_2O (dots) and D_2O (solid line). The above traces have been corrected, in which an uncoated PVG sample served as a blank and was subtracted from the background……..... 8

4. Time-resolved quantum yield measurement. $^1O_2$ emission intensity as a function of absorbance in D_2O with the excitation wavelength of 532 nm. Solid squares represent meso-tetra(4-sulfonatophenyl)porphine dihydrochloride with $\Phi_\Delta = 0.63$ in D_2O. The open circles represent free **1** measured to be $\Phi_\Delta = 0.43 \pm 0.07$ in D_2O……. 9

5. Photooxidation of trans-2-methyl-2-pentenoate anion by **1-ads** as a function of irradiation time in D_2O [solid squares ($y = 2x10^{-5}x + 6x10^{-6}$; $r^2 = 0.9394$)] and H_2O [hollow squares ($y = 1x10^{-5}x + 9x10^{-6}$; $r^2 = 0.9832$)]. ……..... 11

6. Absorption spectra of *meso*-tetra(4-sulfonatophenyl)porphine (dashed line) and **1** (solid line) in H_2O solution. The inset is an expanded view of the visible portion of the spectra, in which the two compounds are optically matched at 532 nm…..... 15

Chapter 2

Figure Page

1. The adsorption of a PVG sample at λ_{max} =525 nm that was sitting in a solution containing **1**. The PVG sample was removed at the indicated times. The plateau region at 14 hours corresponds to 8.83×10^{-7} mol **1** adsorbed onto one gram of PVG……..... 26

2. Rectangular shape of **1** (left) estimated from a B3LYP/6-31G(d) optimized structure and the corresponding computed solvent accessible map (right). 28

3. A low-magnification (60x) cross-sectional optical image. The red areas indicate the depth of **1** accessed into PVG. The image shows 0.32 mm penetration depth on each face for 0.9×10^{-6} mol **1** adsorbed onto a 1.5 mm PVG sample. The horizontal line in the middle of the PVG sample corresponds to where two glass layers meet due to the commercial fabrication process. ……..... 29

4. Absorption spectra of **1** in water (blue line), and **1-ads** at different loadings: 0.9×10^{-8} (green line), 0.9×10^{-7} (red line), and 0.9×10^{-6} (black line) moles of **1** adsorbed on PVG. The spectra were normalized at 532 nm. Except for the green line (0.9×10^{-8} mols **1** adsorbed onto PVG), the Q-band maximum is at 525 nm.…..... 31

5. Nanosecond transient absorption spectra observed at 500 ns after pulsed-light excitation (417 nm, 1.6 mJ/pulse) of **1** in water solution (inset) and **1** at the water/PVG interface. Data points were collected every 10 nm from 450-550 nm. 32

6. Time-resolved absorbance observed at 470 nm after pulsed with 417-nm light at 0.6 mJ/pulse. 0.9×10^{-7} mole **1** adsorbed onto PVG with increasing percents of O_2. The O_2:N_2 ratios ranged from 0:100 to 32:68 in H_2O solution. 33

7. Lifetime quenching as a function of O_2 concentration of a H_2O solution containing 0.9×10^{-7} mole **1** adsorbed onto PVG (in black, left). Amplitude quenching as a function of O_2 concentration of a H_2O solution containing 0.9×10^{-7} mole **1** adsorbed onto PVG (in blue, right). Samples were excited with a 10 ns 417-nm light pulse (0.6 mJ/pulse) and the transient absorption was monitored at 470 nm…… 35

Chapter 3

Figure Page

1. (A) A schematic drawing showing the compressed oxygen-to-fiber coupling and the use of a modified cuvette. Oxygen gas is delivered through a pipette at the top of the cuvette and enters the proximal end of the fiber to the left, which is protruding into the cuvette cavity. (B) A portion of the experimental set-up showing the LED, the 10X objective, and modified cuvette, in which green light is focused into the fiber. 48

2. Image of the HC-580 fiber inserted into silica cap (length = 2.38 mm, bore diameter = 0.38 mm). Green light exited the distal end of the fiber. The absorption of light by the sensitizer occurs in the PVG cap. 50

3. Photooxidation of *N*-benzoyl-DL-methionine anion **2** with the fiber device. 51

4. Photooxidation of *trans*-2-methyl-2-pentenoate anion **4** via "external" visible-light irradiation (Ref. 1). 52

Chapter 4

Figure Page

1. Concept of sensitizer photocleavage from the porous cap flowing oxygen and visible light through a hollow optical fiber… 61

2. The FTIR spectrum of functionalized porous glass **1**, in which the C-H_x stretching modes observed at 2851 and 2954 cm^{-1} were assigned to saturated carbons of the spacer methylene groups indicating that **12** and $(CH_3O)_3SiCH_2CH_2CH_2I$ (1:3 ratio) were anchored to the porous Vycor glass surface. The FTIR spectrum of a clean piece of PVG was not identical, no C-H_x stretching modes were observed. 65

3. A low-magnification (10x) cross-sectional optical image. The dark green thin coating shows the depth of **1** accessed into PVG. The image shows ~0.1 mm penetration depth on the outer face of the cylinder-shaped PVG cap **1** (diameter 5.0 mm × length 8.0 mm). .. 66

4. Schematic of the sensitizer functionalized porous cap **1** where oxygen and light come internally from the hollow optical fiber. Typically 0.3 μmol or 0.33% silane **12** was loaded per gram porous Vycor glass. The sensitizer may adopt various conformations on the isotropic PVG material. PVG is a transparent material with ~4 nm diameter pores and a ~200 m^2/g surface area. PVG has interconnected pores and the surface has "stalagmite-like" features that are ~3 nm in length and width… 69

5. Percent photocleavage of **3** released into toluene-d_8 solution from the porous cap **1**. Silane **12** was loaded in 0.06 to 1.1 μmol amounts (0.068 to 1.24%) onto porous Vycor glass per gram and were exposed to visible light (xx mJ/cm^2)..... 70

6. Plot of nanomolarity of **3** arising from fiber tip **1** upon photooxidation over time. Photocleavage of **3** away from the sensitizer device cap **1** into in petrolatum (open diamonds) at 65 °C and into D_2O (solid squares) and toluene-d_8 (open squares) at room temperature. 72

7. Time course of photorelease of **3** into petrolatum at 65 °C and the diffusion of the sensitizer away from the probe tip. 73

8. Time course of photorelease of **3** into toluene-d_8 solution arising from photooxidative cleavage *and* departure from the fiber optic device tip. The absorption spectra show the fourth Q-band of **3** and were normalized at 640 nm: (a) orange, (b) turquoise 0.5 h, (c) blue 1.0 h, (d) green 1.5 h, (e) red 2.0 h, and (f) black 4.0 h. 74

9. ^{1}H NMR of 1,2-Bis(4-bromophenoxy)ethane (**6**) in $CDCl_3$ 84

10. ^{13}C NMR of 1,2-Bis(4-bromophenoxy)ethane (**6**) in $CDCl_3$ 85

11. ^{1}H NMR of *meso*- and *dl*-1,2-Dibromo-1,2-bis(4-bromophenoxy)-ethane (**7**) in $CDCl_3$ 86

12. ^{13}C NMR of *meso*- and *dl*-1,2-Dibromo-1,2-bis(4-bromophenoxy)-ethane (**7**) in $CDCl_3$ 87

13. ^{1}H NMR of *cis*-1,2-Bis(4-bromophenoxy)ethene (**8**) in $CDCl_3$ 88

14. ^{13}C NMR of *cis*-1,2-Bis(4-bromophenoxy)ethene (**8**) in $CDCl_3$ 89

15. ^{1}H NMR of (Z)-4,4'-(ethene-1,2-diylbis(oxy))dibenzaldehyde (**9**) in $CDCl_3$ 90

16. ^{13}C NMR of (Z)-4,4'-(ethene-1,2-diylbis(oxy))dibenzaldehyde (**9**) in $CDCl_3$ 91

17. HRMS of (Z)-4,4'-(ethene-1,2-diylbis(oxy))dibenzaldehyde (**9**) 92

18. ^{1}H NMR of (Z)-(4,4'-(ethene-1,2-diylbis(oxy))bis(4,1-phenylene))-dimethanol (**10**) in $CDCl_3$ 93

19. ^{13}C NMR of (Z)-(4,4'-(ethene-1,2-diylbis(oxy))-bis(4,1-phenylene))- dimethanol (**10**) in $CDCl_3$ 94

20. HRMS of (Z)-(4,4'-(ethene-1,2-diylbis(oxy))bis(4,1-phenylene))-dimethanol (**10**) 95

21. ^{1}H NMR of (Z)-4-[2-(4-hydroxymethyl-phenoxy)-vinyloxy]-benzyl-pyropheophorbide-a (**11**) in $CDCl_3$ 96

22. ^{13}C NMR of (Z)-4-[2-(4-hydroxymethyl-phenoxy)-vinyloxy]-benzyl-pyropheophorbide-a (**11**) in $CDCl_3$ 97

23. HRMS of (Z)-4-[2-(4-hydroxymethyl-phenoxy)-vinyloxy]-benzyl-pyropheophorbide-a (**11**) 98

24. HRMS of pheophorbide (**3**) 99-100

LIST OF SCHEMES

Chapter 1

Scheme Page

1. Kautsky and de Bruijn photooxidation 2
2. Photooxidation of trans-2-methyl-2-pentenoate anion by **1-ads** 11

Chapter 2

Scheme Page

1. Adsorption of photosensitizer **1** onto the PVG surface and production of singlet oxygen……..... 23
2. Mechanism of ^{3}1*-ads quenching by O_2. Dynamic quenching route in black; static quenching route in blue 34

Chapter 3

Scheme Page

1. Singlet oxygen generation in aqueous solution 46
2. Schematic diagram of fiber-optic singlet-oxygen generator 47

Chapter 4

Scheme Page

1. Synthesis of Sensitizer Functionalized Cap 1 64

Chapter 5

Scheme Page

1. Singlet oxygen photooxidation 102
2. 1,2-Dioxetane alkene precursor 105
3. 1,2-Dioxetanes 106

4. Arene precursor 111

5. Endoperoxides from arene 112

6. Diene precursor..... 113

7. Endoperoxides from diene..... 114

8. Reaction of hexamethylbenzene with Singlet oxygen…..... 115

9. Reaction of phenol with singlet oxygen 115

10. Singlet oxygen reaction with diamid-substitued tetracene 118

11. Mechanism of formation of butenolides..... 122

12. Mechanism of *bis*-spiro compound formation from furan deriv 123

13. Mechanism of tris-spiro compound formation from furan deriv 124

14. Reaction of 2-carboxy-4-methoxy-5-(methoxycarbonyl)-1-methylpyrrole with singlet oxygen..... 124

15. Reaction with cycloheptatriene derivative with singlet oxygen…..... 125

16. Reaction of tetramethylethene with singlet oxygen 127

17. Reaction of 2-methyl-5-oxo-cyclo-2-enecarboxylic acid with singlet oxygen..... 128

18. Reaction of dec-2-en-4-ol with singlet oxygen reaction 129

19. Reaction of 2-methyl-2-pentene with singlet oxygen..... 130

20. Reaction of 2,3,5,6-tetraphenyl-[1,4]dioxine with singlet oxygen..... 131

21. Reaction of 2,3-dipheyl-1*H*-indene with singlet oxygen..... 132

22. Reaction of benzhydrylidene-cyclobutane with singlet oxygen..... 132

23. Reaction of 6,6-diethoxyfulvene with singlet oxygen..... 133

24. Reaction of 1,4-cyclohexadiene with singlet oxygen..... 134

25. Reaction of tetrahydronapthalene with singlet oxygen 134

26. Reaction of 5-isopropyl-3,8-dimethyl-1,2,6,7,8,8a-hexahydro- azulelene

with singlet oxygen 134

27. Reaction of biphenylene with singlet oxygen..... 135

28. A tandem singlet oxygen reaction with *Z*- or *E*-silylated furan 136

29. Mechanism of singlet oxygenation of 2-methyl-5-trimethylsilylfuran 137

30. A tandem singlet oxygen [2 + 4]-cycloaddition and "ene" reaction 138

31. Reaction of 2',3',5'-tris-(*O-tert*-butyldimethylsilyl)guanosine with singlet oxygen..... 139

LIST OF TABLES

Chapter 2

Table Page

1. Stern-Volmer Quenching Constants as a Function of Coverage of **1** onto Porous Vycor Glass or of **1** in Fluid Water Solution 36

Chapter 3

Table Page

1. Quantities of oxygen delivered through a 30-cm segment of the HC-580 fiber into 100-μL H_2O from an oxygen tank at 40 PSI (room temperature)[1] 50

Chapter 4

Table Page

1. Loading of Pheophorbide Silane **12** onto Porous Vycor Glass 68

2. Oxygen Permeability Through Porous Fiber Tip 68

Chapter 1: Singlet Oxygen Chemistry in Water. A Porous Vycor Glass—Supported Photosensitizer

1.1 Introduction

Singlet oxygen [$^1O_2$ ($^1\Delta_g$)] has a lifetime of microseconds to milliseconds, and can diffuse a distance from where it was generated.[1,2] Remarkably, $^1O_2$ can diffuse across a cell membrane[3,4] and even serve as a signaling molecule.[5-7] The first report of $^1O_2$ as a diffusible intermediate came from Kautsky and de Bruijn in 1931,[8] in which trypaflavine (a sensitizer) and leucomalachite green (an oxygen-acceptor compound) were adsorbed separately on silica gel beads (Scheme 1). Upon photolysis in the presence of O_2, $^1O_2$ was generated on a SiO_2 bead and diffused to another (separate) SiO_2 bead where it was trapped by leucomalachite green.[8-10] Kautsky's "through space" experiment was similar in many respects to the Paneth/Hofeditz lead mirror experiments (thermal decomposition of $PbEt_4$),[11] which provided evidence for free ethyl radicals in the gas phase.[12-14] Other researchers have since conducted similar heterogeneous $^1O_2$ studies. The first heterogeneous photosensitizer (covalently bound) was polymer Rose Bengal synthesized by Neckers et al. in 1972.[15-17] Polymer Rose Bengal was based on Merrifield beads with its origins traced directly to solid phase peptide synthetic chemistry.

Scheme 1

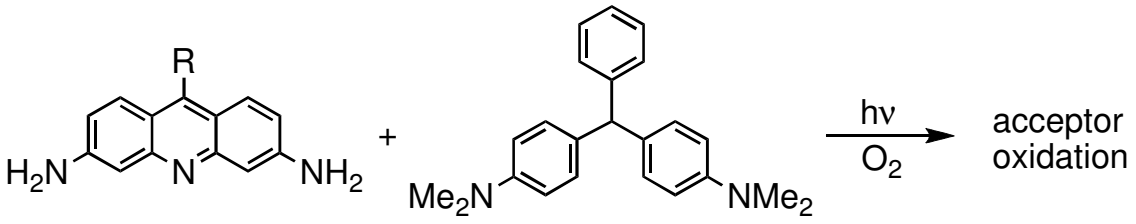

trypaflavine
(R = H and CH_3)

leucomalachite green
($^1O_2$ acceptor)

Silica gel, polymers, alumina, and zeolites have been used as solid supports for $^1O_2$ photosensitizers.[18] However, these solid supports[18a-c] are often used to generate $^1O_2$ in the presence of organic solvents, or in the absence of solvent altogether.

Additional studies could be directed toward $^1O_2$ chemistry in water, and the search for alternative solid supports. We sought a system that does not require covalent attachment of the sensitizer to the solid, but nonetheless binds the two together tightly. Because porous Vycor glass (PVG) develops a negative ζ potential in water (indicating an anionic surface) cations bind tightly.[19,20] Neutral molecules can also bind to PVG,[21-27] but do so more weakly than cations. By taking advantage of the cation-binding ability of PVG in water,[19,20,28-32] one can imagine a similar PVG-binding of a cationic photosensitizer. Raftery et al. have used PVG as a solid support for photocatalysts, such as a TiO_2 monolayer.[33,34] To date, no reports exist on heterogeneous $^1O_2$ photooxidations with PVG as a solid support. *Meso*-tetra(*N*-methyl-4-pyridyl)porphine (**1**) was selected in our study because it is a $^1O_2$ photosensitizer[2] known to photodynamically inactivate *E. coli*.[35] Anions tend not to bind to PVG. Thus, PVG might also yield specificity for $^1O_2$ reactions with anions rather than cations and neutral compounds in the bulk aqueous phase.

We report that cation **1** binds to the PVG anionic silanol sites to give an adsorbed complex. Singlet oxygen is photochemically generated at the solid-liquid interface, and then $^1O_2$ diffuses into the aqueous medium. An anionic alkene is readily oxidized by $^1O_2$ in the surrounding aqueous solution.

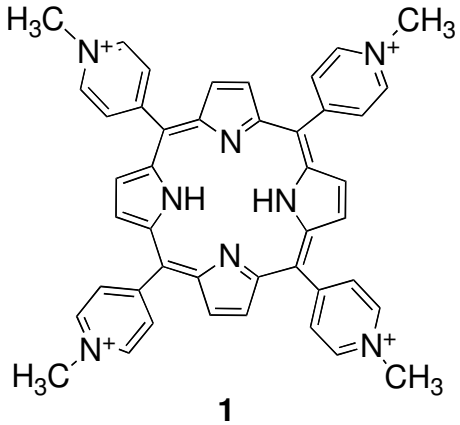

1

1.2 Results and Discussion

1.2.1 Adsorption of Photosensitizer 1. In aqueous solution, cation **1** adsorbs onto PVG and forms a complex. After 48 hours, we find that 1.0×10^{-6} mol **1** adsorbed onto one gram of PVG. Three experiments were conducted to examine aspects of the adsorption process. First, an experiment was carried out in order to determine whether a decrease in pH in the surrounding solution coincides with the adsorption of **1** onto PVG. A concurrent decrease in pH of the aqueous solution is found (plotted as the appearance of moles of H^+ ions, Figure 1), which suggests that **1** cation exchanges onto the anionic silanol sites. The adsorption of **1** over 3 hours corresponded to a pH reduction from 6.12 to 4.14. Figure 1 shows that cationic **1** replaces hydronium ions on the PVG silanol groups. The initial mole ratio of **1** adsorbed:H^+ dissociated is 1:32 (after 30 minutes). After 3 hours, an equilibrium is established and reveals that every mole of **1** adsorbed

leads to the release of 15 moles of H^+ from PVG. Perhaps this decrease in the ratio relates to a tendency for reprotonation of some silanol anion sites over time. Second, to determine if the counter ion (TsO^-) is coadsorbed onto the anionic surface, a 1.69 g PVG sample was placed in 25.0 mL of $1.01x10^{-5}$ M **1** and the aqueous phase was monitored by UV spectroscopy. Adsorption of **1** was accompanied by the appearance of 3.9±0.05 mole equivalent tosylate ion in solution (λ_{max} = 260 nm) measured by a prior constructed calibration curve. The spectroscopic analysis suggested that less than 5% TsO^- counter ion coadsorbs onto PVG, and that the majority of TsO^- remains in the surrounding aqueous solution likely because of the Coulombic interaction disfavoring association of the anion with the anionic silanol surface of PVG. Similarly, Cr^{3+}, Fe^{3+}, and Cu^{2+} are known to cation exchange onto PVG with less than 3% coadsorption of the Cl^- counter ion.[29] Third, repeated washing with water failed to detect **1** by UV-visible absorption (detection limit of **1** is $3.1x10^{-7}$ M at λ_{max} = 422 nm). One may assume the worst case, i.e., desorption below the detection limit ~$3x10^{-7}$ M **1** of our UV-instrument. However, this conclusion is probably incorrect because a control experiment showed that $3x10^{-7}$ M **1** does not lead to the $^1O_2$ chemistry in Sections 3.3 and 3.4. The experimental data lead us to conclude that the adsorbed **1** remains attached to PVG throughout the sensitization and photochemical processes. Thus, the PVG-attached sensitizer is referred to as **1-ads** hereafter.

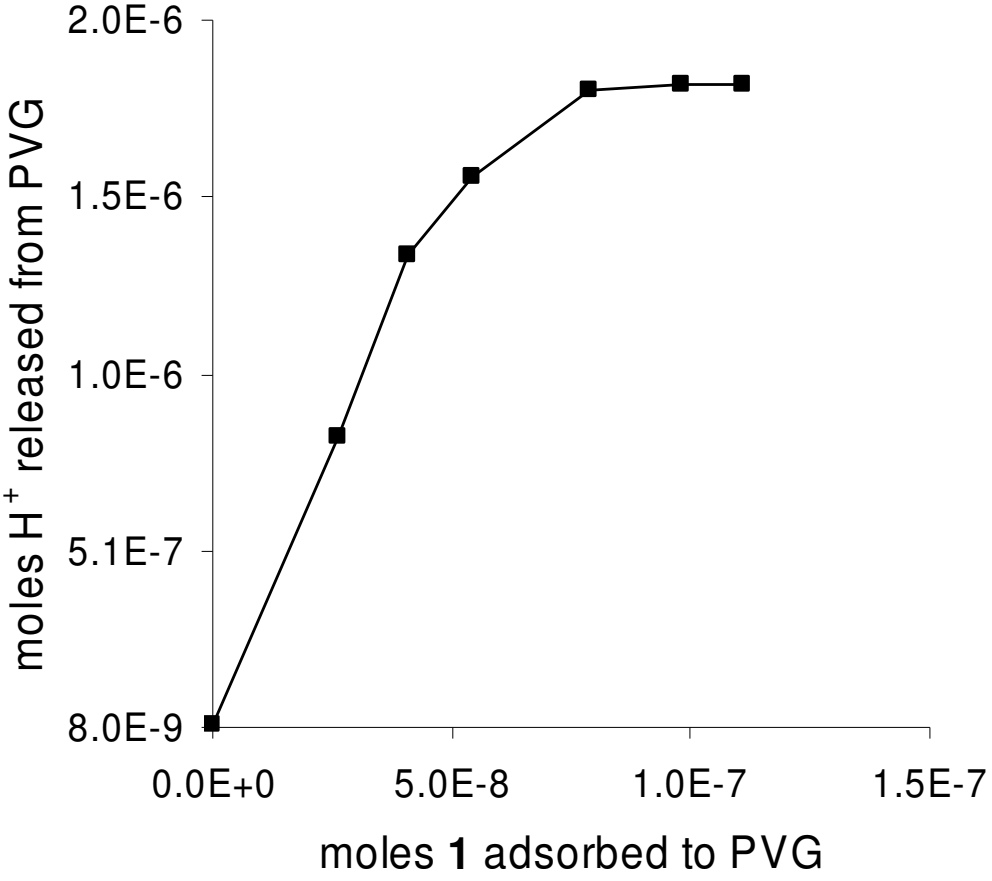

Figure 1. Plot of the moles of H^+ ions arising from PVG silanol deprotonation calculated from the decrease in pH of the aqueous solution during the adsorption of 1 onto PVG. Each point is taken at a 30-minute increment over a total of 3 hours.

1.2.2 Spectroscopic Properties of PVG-Adsorbed 1. Figure 2 shows normalized UV-visible spectra of **1-ads** (in air) and **1** (in H_2O). The spectra are very similar. The λ_{max} of **1-ads** in air is 419 nm. The λ_{max} of **1** in H_2O is 422 nm. There appears to be only a slight decrease of the 500-600 nm absorption of heterogeneous **1** compared to homogeneous **1**. The absorption of **1-ads** consists of a band in the visible region between 500-700 nm indicating that it may be excited upon the absorption of light

in this range. The similarity between the two spectra suggests the **1-ads** may have similar properties to serve as a $^1O_2$ photosensitizer.

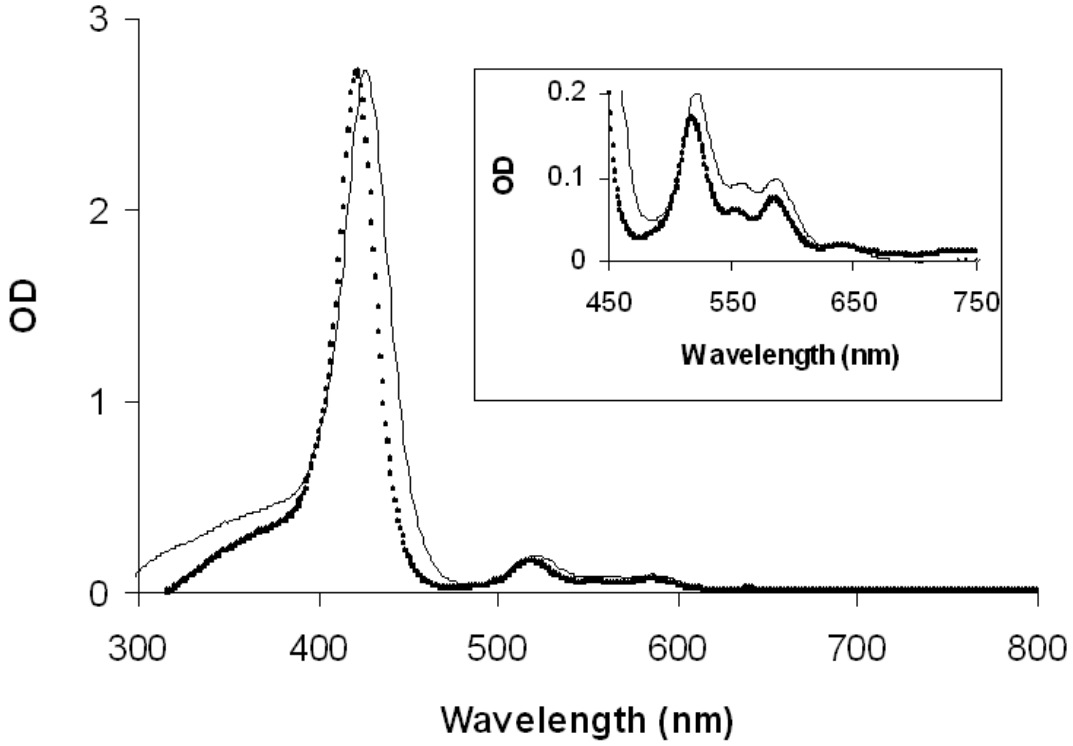

Figure 2. Normalized absorption spectra of 1-ads and 1: (1) the solid line is of 1-ads in air, in which uncoated PVG was used as a blank, and (2) the dashed line is an H_2O solution of 1, in which H_2O was used as a blank. The inset is an expanded view of the visible portion of the spectra.

1.2.3 Detection of Singlet Oxygen. In D_2O, unlike H_2O, $^1O_2$ luminescence is easily detected at 1270 nm from the 532 nm irradiation of **1-ads** (Figure 3). Singlet oxygen luminescence experiment is carried out by our collaborator, Naveen Gandra in Professor Ruomei Gao's research group at Jackson State University. The generation of $^1O_2$ is based on a bimolecular sensitization reaction, represented by the reaction between

the electronically excited sensitizer, **1-ads***, and the acceptor, $^3O_2$. It is possible that **1-ads*** is quenched by O_2 which is adsorbed itself, or simply, O_2 collides with excited **1-ads**. The formation of $^1O_2$ is predominantly a triplet quenching process (eq 3).

$$\textbf{1-ads}^* + {}^3O_2 \rightarrow {}^1O_2 + \textbf{1-ads} \qquad (3)$$

The 1270 nm luminescence decay is exponential and the lifetime of $^1O_2$ in D_2O is found to be 65 μs, which matches the literature value.[41] After $^1O_2$ is generated, its diffusion into the surrounding solution can take place. Ogilby et al.[4] suggested that if one assumes a typical diffusion coefficient for oxygen,[42] D, in liquid ~$3x10^{-5}$ cm^2 s^{-1} then the distance travelled by $^1O_2$ is approximately 62 μm in D_2O. The difficulty in detecting $^1O_2$ in H_2O arises from its short lifetime (3.1 μs)[43] due to efficient electronic to vibronic energy transfer between the two.[44]

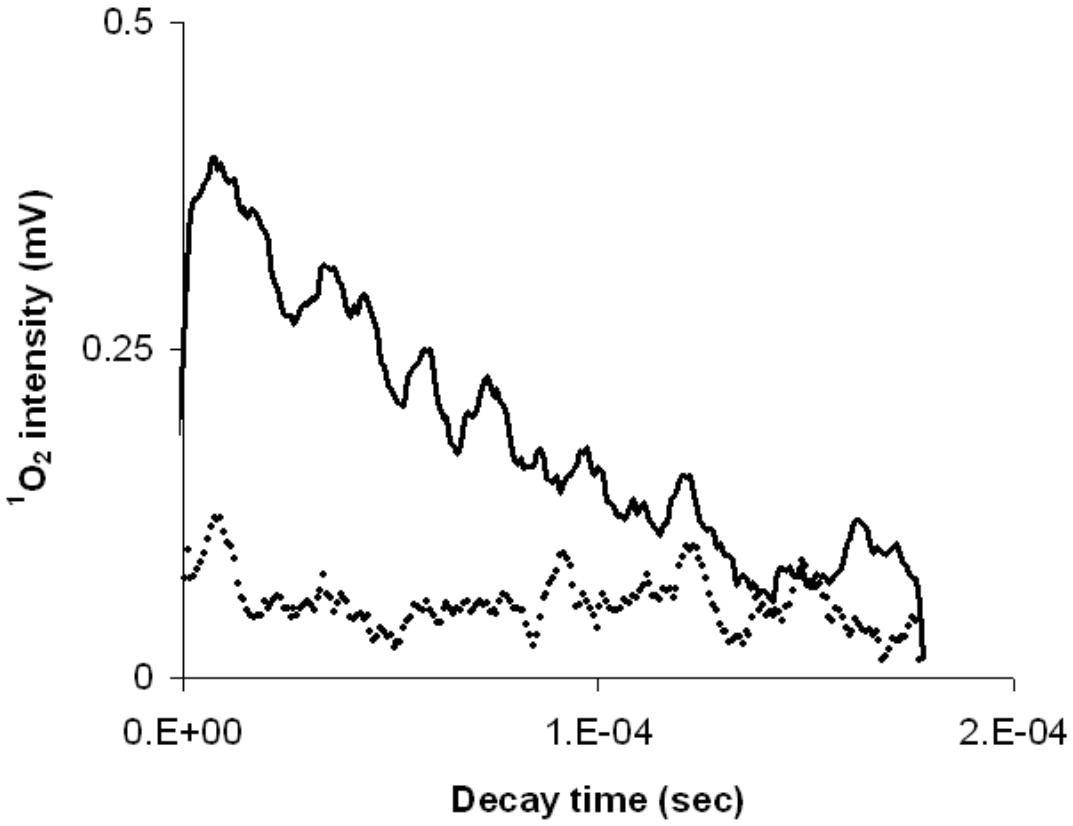

Figure 3. Singlet oxygen phosphorescence (1270 nm) decay from **1-ads** carried out in H_2O (dots) and D_2O (solid line). The above traces have been corrected, in which an uncoated PVG sample served as a blank and was subtracted from the background.

Figure 4 shows $^1O_2$ emission intensity over a range of absorbances for **1** in homogeneous D_2O solution. The literature value of Φ_Δ for the reference sensitizer *meso*-tetra(4-sulfonatophenyl)porphine dihydrochloride is 0.63 in D_2O.[45] Thus, Φ_Δ for the formation for $^1O_2$ from **1** is 0.43±0.07 in D_2O, using *meso*-tetra(4-sulfonatophenyl)porphine dihydrochloride as a reference. Triplet-triplet annihilation appears to be negligible at absorbances ranging from 0.03-0.60 from excitation at 532 nm, as indicated by the $^1O_2$ intensity showing a linear correlation with the absorption of the complexes. Because there is no reference sensitizer-PVG complex, we were not able

to determine the Φ_Δ for the formation of $^1O_2$ with **1-ads**. PVG-adsorbed **1** appears to retain its photosensitization property in aqueous solution. Unlike porous silicon nanocrytsals,[44,46,47] PVG is not found to produce $^1O_2$ in D_2O in the absence of adsorbed **1**. Furthermore, the 1270 nm luminescence of $^1O_2$ in H_2O appears at the noise level of the instrument. However, we show that $^1O_2$ is formed in H_2O by indirect trapping experiments. The results described next show that $^1O_2$ produced in the **1-ads** photosensitized reaction can react with *trans*-2-methyl-2-pentenoate anion (**2**).

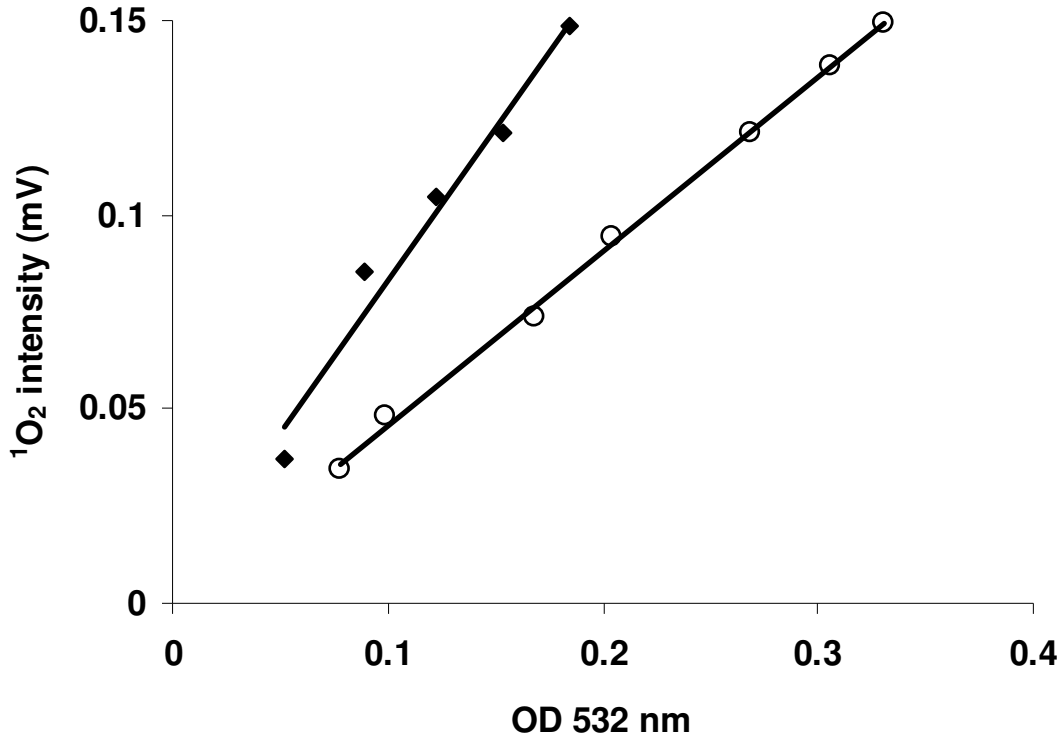

Figure 4. Time-resolved quantum yield measurement. $^1O_2$ emission intensity as a function of absorbance in D_2O with the excitation wavelength of 532 nm. Solid squares represent *meso*-tetra(4-sulfonatophenyl)porphine dihydrochloride with $\Phi_\Delta = 0.63$ in D_2O. The open circles represent free **1** measured to be $\Phi_\Delta = 0.43 \pm 0.07$ in D_2O.

1.2.4 Photooxidation of *Trans*-2-methyl-2-pentenoate Anion (2). Unlike the aerobic UV irradiation of PVG reported to form superoxide,[48] the visible light irradiation of **1-ads** generates $^1O_2$, which can diffuse out of the silica matrix and then trapped by an *trans*-2-methyl-2-pentenoate anion **2** in a surrounding aqueous solution. The **1-ads** sensitized photooxidation of **2** affords one product, hydroperoxide **3** (Scheme 2). Dr. David Aebisher initiated and helped us in conducting experiments to trap singlet oxygen with *trans*-2-methyl-2-pentenoate anion **2** in aqueous solution. The reaction is monitored by NMR. No other products were detected, which would be expected if superoxide were present. Formation of **3** and not regioisomer **5** indicates that the methyl protons are more acidic, in which the resulting double bond is conjugated with the carboxylate group. Hydroperoxide **3** reacted with triphenylphosphine and converted to alcohol **4**, also characterized by NMR. The yield of **3** was dependent on whether the **1-ads** sensitized photooxidation of **2** was conducted in D_2O or H_2O. Figure 5 shows that this $^1O_2$ 'ene' reaction is found to be about two times faster in D_2O than H_2O. Hydroperoxide **3** was formed more rapidly in D_2O than H_2O (cf. 16.9% to 3.9%) after 2 hours. In H_2O, photooxygenation of **2** with **1-ads** formed **3** in 32.8% yield after 8 hours. The results support the conclusion that the reaction of $^1O_2$ with **3** occurs in the surrounding H_2O or D_2O solution. Previous data lead to a similar conclusion that alkene oxidation is more efficient in D_2O than H_2O.[35] The results establish the feasibility of carrying out the heterogeneous sensitization process with **1-ads** in which $^1O_2$ is released into surrounding D_2O and H_2O.

Scheme 2

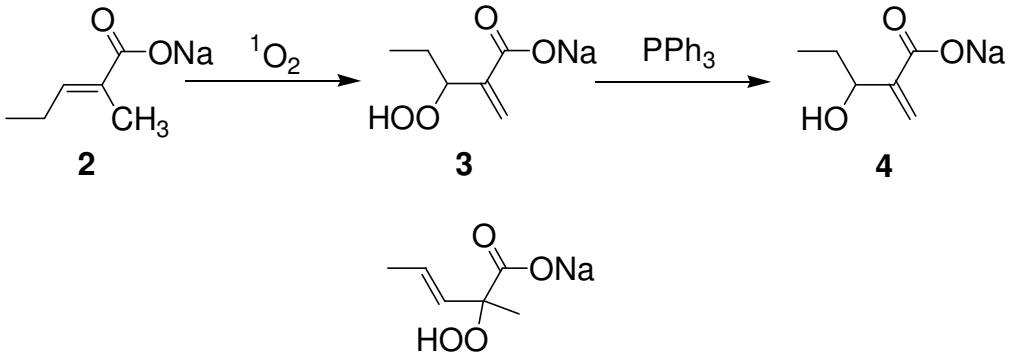

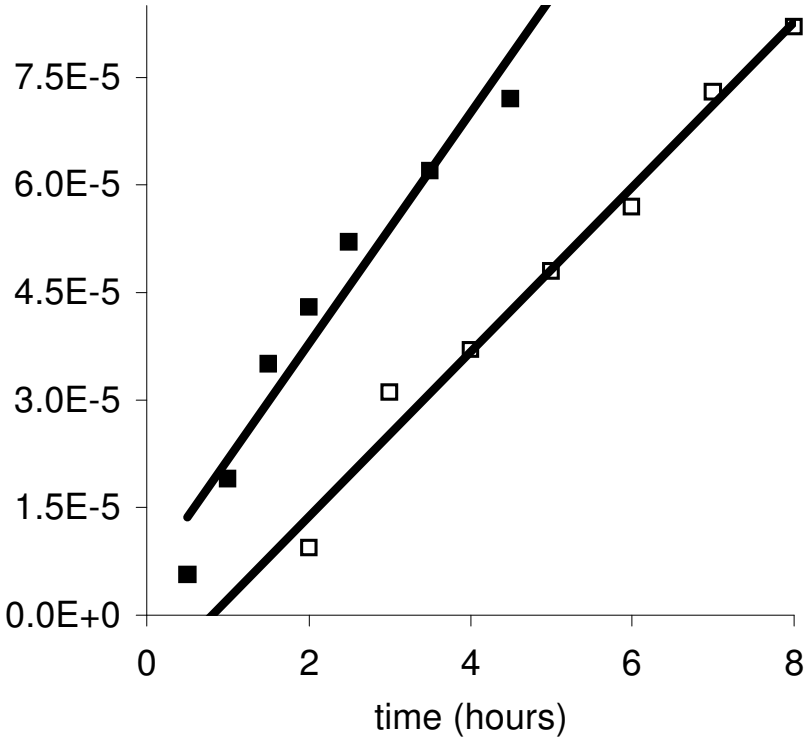

Figure 5. Photooxidation of *trans*-2-methyl-2-pentenoate anion by **1-ads** as a function of irradiation time in D_2O [solid squares ($y = 2x10^{-5}x + 6x10^{-6}$; $r^2 = 0.9394$)] and H_2O [hollow squares ($y = 1x10^{-5}x + 9x10^{-6}$; $r^2 = 0.9832$)].

1.3 Conclusion

PVG is a cation-binding solid. We took advantage of this binding property to examine PVG as a support for the cationic photosensitizer **1**. Sensitizer **1** adsorbed to PVG and gives a stable material, which does not dissociate in water at room temperature. Singlet oxygen is generated in the surrounding aqueous solution upon irradiation of the adsorbed complex. The excited state of **1-ads** is quenched by O_2 to give $^1O_2$, which can be detected in the surrounding aqueous solution. The heterogeneous system described in this paper could have application in ridding wastewater of *E. coli.*

1.4 Experimental Section

1.4.1 Materials and Instrumentation. Reagents were obtained commercially [*meso*-tetra(N-methyl-4-pyridyl)porphine tetratosylate, *meso*-tetra(4-sulfonatophenyl)porphine dihydro-chloride, *trans*-2-methyl-2-pentenoic acid, sodium hydroxide, magnesium sulfate, triphenylphosphine, *p*-toluene sulfonic acid (TsOH), and adipic acid] and used without further purification. The solvents used (methanol, absolute ethanol, deuterium oxide-d_2, and chloroform-d_1) were of spectroscopic or equivalent grade and were used as received. Deionized water was obtained from a U.S. Filter Corporation deionization system. PVG samples (Corning 7930, pore size = 40 Å) were dried in a Fisher Scientific Isotemp muffle furnace at 500 °C and then stored in a desiccator under vacuum (30 mm Hg). Pieces of PVG were in the shape of disks (11.0 mm in diameter and 2.0 mm in thickness) or squares (1.5 cm^2 and 1.0-1.5 mm in thickness). Samples were irradiated with a Q-switched Nd:YAG laser (532 nm, 3-4 ns,

30 mJ, Polaris II-20, New Wave Research Merchantek Products). A liquid N_2 cooled germanium photodetector (Applied Detector Corporation) was used for the determination of quantum yields of $^1O_2$. The steady-state generation of $^1O_2$ was conducted with a Rayonet photoreactor with Sylvania F8T5/CW 8 Watt bulbs that emit at ~425-650 nm. Mass spectrometry data were acquired on an Agilent Technologies 6890N GC/MS instrument with a 5973 Mass Selective Detector (MSD) and a HP-5MS column. UV-visible spectra were collected on a Hitachi UV-VIS U-2001 instrument. NMR data were collected on a Brucker DPX400 NMR instrument.

1.4.2 Measurements. The adsorption process was achieved by placing a 0.28 g PVG sample into 24.7 mL of a 1.0 x 10^{-5} M solution of **1** in deionized water. The amount of photosensitizer adsorbed onto PVG was calculated from the difference in absorbance of the solution before introduction of PVG and the absorbance of the same solution after the PVG's removal [at the λ_{max} of **1** (422 nm)]. The number of moles of photosensitizer adsorbed per gram of PVG was calculated using eq 1,

$$n_{adsorbed} / g\ PVG = \{[(A_i - A_f)/A_i] \times n_i\} / g\ PVG \qquad (1)$$

in which, A_i is the absorbance of the solution prior to introduction of PVG; A_f is the absorbance of the solution after the impregnation interval and removal of the PVG; n_i is the number of moles of sensitizer prior to impregnation; $n_{adsorbed}$ is the number of moles adsorbed onto the PVG; and g PVG is the weight of the PVG in grams.[29] Typically, PVG samples were loaded with 1.0x10^{-6} moles of 1/g PVG. Colorless PVG was converted to deep red on adsorption of 1 after 48 hours. The moles of hydronium ion were calculated from the pH of the surrounding aqueous solution. The experiments were carried out at

room temperature and with O_2-saturated solutions. The phosphorescence of $^1O_2$ at 1270 nm was measured as previously described.[36] The initial $^1O_2$ intensity is extrapolated to t = 0. The data points of the initial 3-4 ns are not used due to electronic interference signals from the detector. The intensity of the pulses at 532 nm were controlled between 20-30 mJ. The quantum yield for production of $^1O_2$ in homogeneous solution is calculated according to eq 2.

$$\Phi_{\Delta\ \text{sample}} / \Phi_{\Delta\ \text{reference}} = S_{\text{sample}} / S_{\text{reference}} \qquad (2)$$

Here $\Phi_{\Delta\ \text{sample}}$ and $\Phi_{\Delta\ \text{reference}}$ are the $^1O_2$ quantum yields for samples and the reference. *Meso*-tetra(4-sulfonatophenyl)porphine was used as a reference sensitizer, in which its absorbance was optically matched with that of 1 at 532 nm (Figure 6). S_{sample} and $S_{\text{reference}}$ represent the slopes obtained from the plot of initial intensity of $^1O_2$ via the absorbance at excitation wavelength 532 nm for the sample and the reference, respectively.

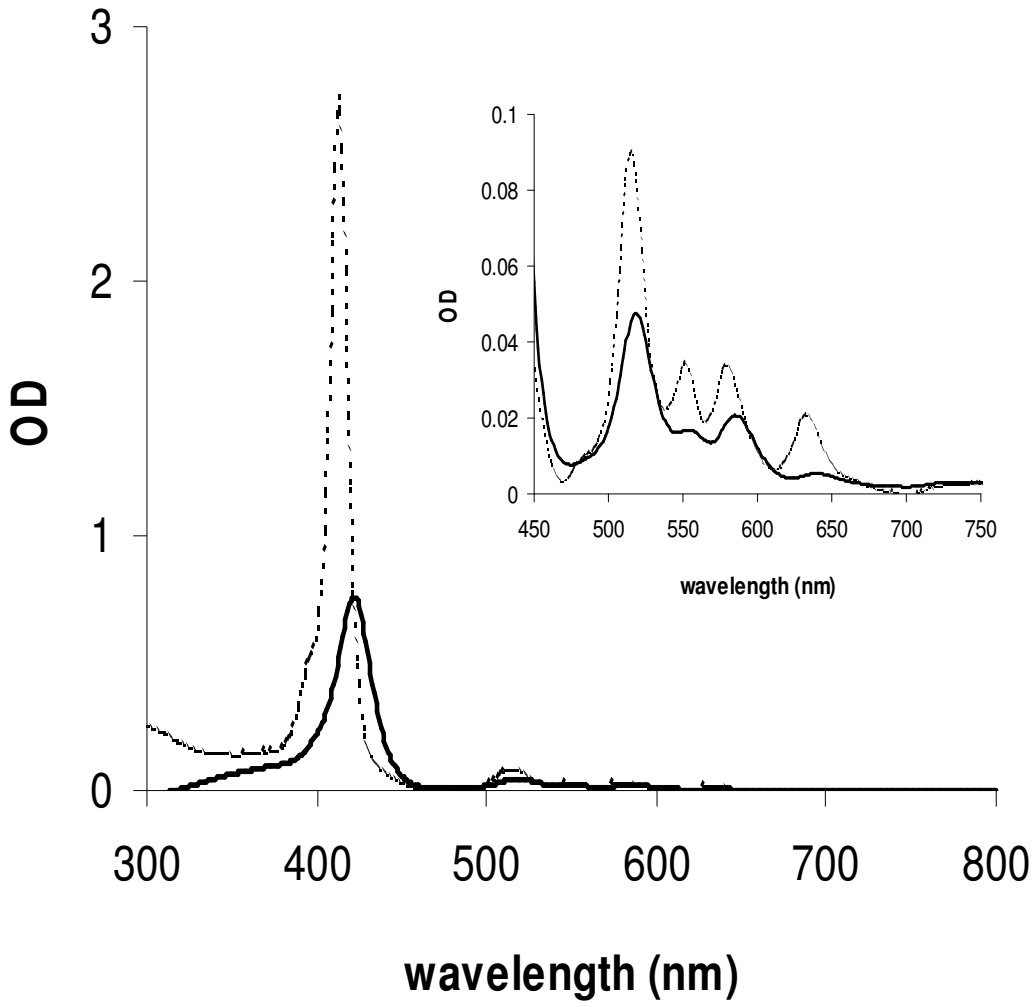

Figure 6. Absorption spectra of *meso*-tetra(4-sulfonatophenyl)porphine (dashed line) and 1 (solid line) in H_2O solution. The inset is an expanded view of the visible portion of the spectra, in which the two compounds are optically matched at 532 nm.

1.4.3 *Meso*-tetra(*N*-methyl-4-pyridyl)porphine (1). Purity of the tosylate of **1** was determined to be 99% based on NMR (integration of peaks in its ^{1}H NMR spectrum) and greater than 95% based on HRMS: ^{1}H NMR (D_2O, 400 MHz) δ 1.50 (s, 12H), 4.63 (s, 12H), 6.43 (bs, 8H), 7.01 (bs, 8H), 8.78 (d, J = 4.6 Hz, 8H), 8.83 - 9.08 (bs, 8H), 9.14

(d, J = 4.6 Hz, 8H). ^{13}C NMR (D_2O, 100 MHz) δ 155.0, 141.6, 138.7, 136.9, 130.8, 126.1, 122.3, 113.3, 46.1, 17.1. Mass spectrum (EI); *m/z* = 676.31 (100), 677.31 (48), 678.31 (12.5), 677.30 (3.0), 679.32 (1.7). HRMS calcd for $(C_{44}H_{36}N_8)^{2+}$ 338.1522 (the base peak represents the loss of four tosylate fragments and two protons), found 338.1525. Literature: ^{1}H NMR (D_2O) δ 9.19 (d, 8H), 9.03 (bs, 8H), 8.71 (d, 8H), 4.77 (s, 12H) at pD 7.0.[37] ^{1}H NMR (DMSO) δ 9.47 (d, 8H), 9.18 (s, 8H), 8.97 (d, 8H), 4.72 (s, 12 H).[38]

1.4.4 Heterogeneous Photooxidation of *Trans*-2-methyl-2-pentenoate Anion (2). Compound **1** ($7.5x10^{-7}$ mol) adsorbed onto 1.58 g PVG was combined with 20 mL of *trans*-2-methyl-2-pentenoic acid (0.25 mmol) and NaOH (0.35 mmol) in deionized H_2O. Presumably *trans*-2-methyl-2-pentenoic acid is a stronger acid and is selectively deprotonated affording **2** since the PVG silanol groups are reported to be pKa ~ 9.[39] Dioxygen was bubbled into the solutions. Photooxygenation was carried out for 4 hours at room temperature with the Rayonet reactor. Aliquots of the H_2O reaction were mixed with D_2O for NMR analysis. 3-Hydroperoxy-2-methylene pentanoic acid (**3**) was detected as the sole product: ^{1}H NMR (D_2O) δ ^{1}H NMR (D_2O) δ 0.91 (t, J = 7.5 Hz, 3H), 1.66 (m, 2H), 4.75 (t, J = 6.5 Hz, 1H), 5.56 (s, 1H), 5.94 (s, 1H); ^{1}H NMR ($CDCl_3$) δ 0.97 (t, J = 7.4 Hz, 3H), 1.71 (m, 2H), 4.82 (t, J = 6.4 Hz, 1H), 6.01 (s, 1H), 6.54 (s, 1H) [Note: 1.66 (in D_2O) and 1.71 ($CDCl_3$) represent ABX3 multiplets]. HRMS calcd for $(C_6H_9O_4)(M - H^+)$ 145.0506, found 145.0506. The percent yield was determined by comparison of the integrated methyl protons of **3** with the methylene protons of adipic acid (internal standard) by ^{1}H NMR spectroscopy. Upon addition of triphenylphosphine (0.08 M), **3** converted to 3-hydroxy-2-methylene pentanoic acid (**4**), a known

compound.[40] Our data agreed with the literature value:[40] ^{1}H NMR (D_2O) δ 1.19 (t, J = 7.1 Hz, 3H), 1.54 (m, 2H), 4.44 (t, J = 6.0 Hz, 1H), 5.45 (s, 1H), 5.76 (s, 1H) (Note: 1.54 represents a ABX3 multiplet).

1.5 References:

(1) Wilkinson, F.; Helman, W. P.; Ross, A. B. *J. Phys. Chem. Ref. Data* **1995**, *24*, 663-1021.

(2) Zebger, I.; Poulsen, L.; Gao, Z.; Andersen, L. K.; Ogilby, P. R. *Langmuir* **2003**, *19*, 8927-8933.

(3) Snyder J. W.; Skovsen E.; Lambert J. D. C.; Ogilby P. R. *J. Am. Chem. Soc.* **2005**, *127*, 14558-14559.

(4) Snyder, J. W.; Skovsen, E.; Lambert, J. D. C.; Poulsen, L.; Ogilby, P. R. *Phys. Chem. Chem. Phys.* **2006**, *8*, 4280-4293.

(5) "Signaling by singlet oxygen in biological systems" Klotz, L.-O., Briviba, K. & Sies, H. in *Antioxidant and Redox Regulation of Genes* (eds Sen, C. K., Sies, H. & Baeuerle, P. A.) 3–20 (Academic, San Diego, 2000).

(6) Flors, C.; Nonell, S. *Acc. Chem. Res.* **2006**, *39*, 293-300.

(7) Laloi, C.; Stachowiak, M.; Pers-Kamczyc, E.; Warzych, E.; Murgia, I.; Apel, K. *Proc. Natl Acad. Sci.* **2007**, *104*, 672–677.

(8) Kautsky, H.; de Bruijn, H. *Naturwiss.* **1931**, 19, 1043-1043.

(9) Kautsky, H.; Hirsch, A.; Flesch, W. *Ber.* **1935**, *68B*, 152-62.

(10) Greer, A. *Acc. Chem. Res.* **2006**, *39*, 797-804.

(11) Paneth, F.; Hofeditz, W. *Ber.* **1929**, *62B*, 1335-47.

(12) Eberson, L. *Adv. Phys. Org. Chem.* **2001**, *36*, 59-84.

(13) Roth, H. D. *Pure & Appl. Chem.* **2001**, *73*, 395-403.

(14) Seyferth, D. *Organometallics* **2003**, *22*, 2346-2357.

(15) Neckers, D. C.; Kooistra, D. A.; Green, G. W. *J. Am. Chem. Soc.* **1972**, *94*, 9284-5.

(16) Schaap, A. P.; Thayer, A. L.; Blossey, E. C.; Neckers, D. C. *J. Am. Chem. Soc.* **1975**, *97*, 3741-5.

(17) Blossey, E. C.; Neckers, D. C.; Thayer, A. L.; Schaap, A. P. *J. Am. Chem. Soc.* **1973**, *95*, 5820-2.

(18) A small sample of references on solid supports for the photochemical production of $^1O_2$, includes: (a) Silica gel: Krishna, C. M.; Lion, Y.; Riesz, P. *Photochem. Photobiol.* **1987,** *45,* 1-6. Williams, J. R.; Orton, G.; Unger, L. R. *Tetrahedron Lett.* **1973**, *46,* 4603. van Laar, F. M. P. R.; Holsteyns, F.; Vankelecom, I. F. J.; Smeets, S.; Dehaen, W.; Jacobs, P. A. *J. Photochem. Photobiol. A* **2001,** *144,* 141-151. Iu, K.-K.; Thomas, J. K. *J. Photochem. Photobiol. A* **1993,** *71,* 55-60. Clennan, E. L.; Chen, M.-F. *J. Org. Chem.* **1995**, *19*, 6004. (b) Polymers: Wolf, S.; Foote, C. S.; Rebek, J. Jr. *J. Am. Chem. Soc.* **1978**, *100*, 7770. Ito, H.; Ikeda, T.; Ichimura, K. *Macromolecules* **1993**, *26*, 4533. Bartoschek, A.; El-Idreesy, T. T.; Griesbeck, A. G.; Höinck, L.-O.; Lex, J.; Miara, C.; Neudörfl J. M. *Synthesis* **2005**, 2433-2444. Lee, P. C.; Rodgers, M. A. J. *J. Phys. Chem.* **1984**, *88*, 4385. Kiozumi, H.; Kimata, Y.; Shiraishi, Y.; Hirai, T. *Chem. Commun.* **2007**, 1846-1848. Gao, Y.; Ogilby, P. R. *Macromolecules* **1992**, *25*, 4962. (c) Zeolites: Li, X.; Ramamurthy, V. *J. Am. Chem. Soc.* **1996**, *118*, 10666-10667. Clennan, E. L.; Pace, A. *Tetrahedron* **2005**, *61*, 6665-6691. Stratakis M.; Raptisa, C.; Sofikitia, N.; Tsangarakisa, C.; Kosmasa, G.; Zaravinosa, I.-P.; Kalaitzakisa, D.; Stavroulakisa, D.; Baskakisa, C.; Stathoulopouloua, A. *Tetrahedron* **2006**, *62*, 10623-10632. Robbins, R. J.; Ramamurthy, V. *J. Chem. Soc., Chem. Commun.* **1997,** 1071. (d) Other heterogeneous media, such as micelles or membranes in photochemical and

chemical sources of singlet oxygen: Ma, L.; Chen, B.; Wu, L.-Z.; Peng, M. L.; Zhang, L. P.; Tung, C.H. *Prog. Chem.* **2004**, *16*, 386-392. Sels, B. F.; De Vos, D. E.; Jacobs, P. A. *J. Am. Chem. Soc.* **2007**, *129*, 6916-6926. Aubry, J.-M.; Adam, W.; Alsters, P. L.; Borde, C.; Queste, S.; Marko, J.; Nardello, V. *Tetrahedron* **2006**, *62*, 10753-10761. Li, H.-R.; Wu, L.-Z.; Tung, C.-H. *J. Am. Chem. Soc.* **2000**, *122*, 2446-2451. Lissi, E. A.; Lemp, E.; Zanocco, A. L. Singlet-Oxygen Reactions: Solvent and Compartmentalization Effects. In *Understanding and manipulating excited state processes,* Ramamurthy, V.; Schanze, K. S., Eds. Marcel Dekker Inc.: 2001; Vol. 8, pp. 287-316.

(19) Gafney, H. D.; Wolfgang, S. *J. Phys. Chem.* **1983**, *87*, 5395-5401.

(20) An extensive list of references on the properties of PVG is given in: Janowski, V. F.; Heyer, W. *Z. Chem.* **1979**, *19*, 1.

(21) Pilkenton, S.; Raftery, D. *Solid State Nuc. Mag. Reson.* **2003**, *24*, 236-253.

(22) Xu, W.; Raftery, D. *J. Catal.* **2001**, *204*, 110-117.

(23) Takeuchi, M.; Yamashita, H.; Matsuoka, M.; Anpo, M.; Masakazu, H.; Takashi, I.; Nobuhisa, N. *Catal. Lett.* **2000**, *67*, 135-137.

(24) Hwang, S.-J.; Raftery, D. *Catal. Today* **1999**, *49*, 353-361.

(25) Ebitani, K.; Yamaguchi, Y.; Morikawa, A. *Catal. Lett.* **1997**, *61*, 69-73.

(26) Wada, Y.; Morikawa, A. *Bull. Chem. Soc. Jpn.* **1987**, *60*, 3509-3513.

(27) Anpo, M.; Wada, T.; Kubokawa, Y. *Bull. Chem. Soc. Jpn.* **1977**, *50*, 31-35.

(28) Gafney, H. D. *Coord. Chem. Rev.* **1990**, *104*, 113.

(29) Gafney, H. D.; Shi, W. *J. Phys. Chem.* **1988**, *92*, 2329.

(30) Gafney, H. D. “Photochemistry of metal carbonyls physisorbed on porous Vycor glass” *In* Photochemistry on solid surfaces, Anpo, M.; Matsuura, T. Eds., Elsevier, New York, **1989**, pp. 272.

(31) Gafney, H. D.; Darsillo, M. S.; Paquette, M. S. *Inorg. Chem.* **1988**, *27*, 2815.

(32) Gafney, H. D.; Xu, S.-P. Photocatalytic behavior of tungsten and ruthenium carbonyls on porous Vycor glass in *"Photosensitive metal-organic systems: Mechanistic principles and recent applications"*, Kutal, C.; Serpone, N. Eds. American Chemical Society, **1993**, p. 67.

(33) Reyes-Garcia, E. A.; Sun, Y.; Reyes-Gil, K.; Raftery, D. *J. Phys. Chem. C* **2007**, *111*, 2738-2748.

(34) Pilkenton, S.; Xu, W.; Raftery, D. *Anal. Sci.* **2001**, *17*, 125-130.

(35) Salmon-Divon, M.; Nitzan, Y.; Malik, Z. *Photochem. Photobiol. Sci.* **2004**, *3*, 423-429.

(36) Gandra, N.; Frank, A. T.; Le Gendre, O.; Sawwan, N.; Aebisher, D.; Liebman, J. F.; Houk, K. N.; Greer, A.; Gao, R. *Tetrahedron* **2006**, *62*, 10771-10776.

(37) Tabata, M.; Sakai, M.; Yoshioka, K.; Kodama, H. *Anal. Sci.* **1990**, *6*, 651-656.

(38) Anaissi, F. J.; Engelmann, F. M.; Araki, K.; Toma, H. E. *Solid State Sci.* **2003**, *5*, 621-628.

(39) Iler, R. K. in “The Chemistry of Silica: Solubility, Polymerization, Colloid and Surface Properties and Biochemistry” John Wiley and Son, 1979.

(40) Hout, J. F.; Outurguin, F.; Paulmier, C. *Chem. Lett.* **1991**, *9*, 1599-1602.

(41) Ogilby, P. R.; Foote, C. S. *J. Am. Chem. Soc.* **1982**, *104*, 2069-2070.

(42) Tsushima, M.; Tokuda, K.; Ohsaka, T. *Anal. Chem.* **1994**, *66*, 4551-4556.

(43) Schweitzer, C.; Schmidt, R. *Chem. Rev.* **2003**, *103*, 1685-1758.

(44) Fujii, M.; Nishimura, N.; Fumon, H.; Hayashi, S.; Kovalev, D.; Goller, B.; Diener, J. *J. Appl. Phys.* **2006**, *100*, 124302.

(45) Tanielian, C.; Wolff, C.; Esch, M. *J. Phys. Chem.* **1996***, 100*, 6555-6560.

(46) Kovalev, D.; Gross, E.; Diener, J.; Timoshenko, V. Y.; Fujii, M. *Appl. Phys. Lett.* **2004**, *85*, 3590-3592.

(47) Harper, J.; Sailor, M. J. *Langmuir* **1997**, *13*, 4652-4658.

(48) Anpo, M.; Yun, C.; Kubokawa, Y. *J. Catal.* **1980**, *61*, 267-269.

Chapter 2. Photoexcited Sensitizer Quenching by O_2 at the Water—Porous Glass Interface

2.1 Introduction

Heterogeneous materials have been studied for many years, and chemists discovered that some could be used as supports for the generation of singlet oxygen [$^1O_2$ ($^1\Delta_g$)].[1a-e] We reported that *meso*-tetra(N-methyl-4-pyridyl)porphine (**1**) adsorbed onto porous Vycor glass (PVG), in which a pH decrease of the surrounding solution indicated the displacement of protons from the surface silanol groups via cation exchange (Scheme 1).[2] Singlet oxygen was generated cleanly in aqueous solution upon irradiation of this heterogeneous sensitizer, **1-ads**.[2]

Scheme 1

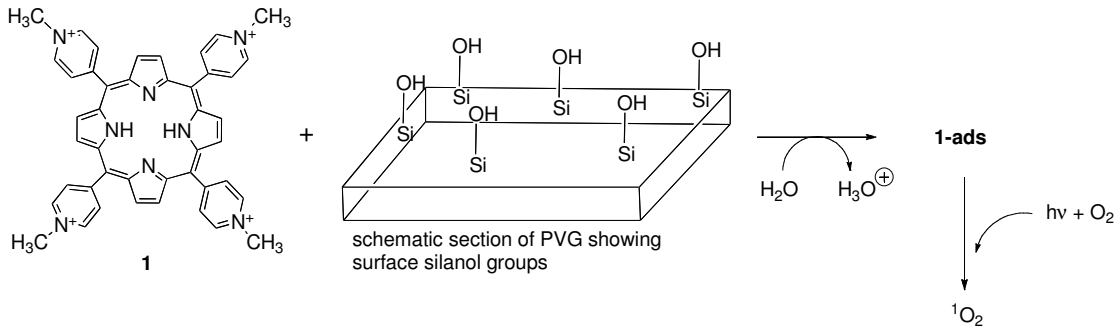

Despite the effectiveness of this and other heterogeneous systems to generate $^1O_2$, surprisingly little is known about the mechanism of sensitizer quenching by O_2 at *water-solid* interfaces. For example, how does the oxygen encounter the excited PVG heterogeneous sensitizer? What mechanism (static or dynamic) converts ground-state O_2 into $^1O_2$, which then diffuses into the bulk solution?

Some detail of the O_2 quenching process may be gleaned from previous studies of *gas-solid* systems. These studies often indicate the static quenching of O_2 — where a

ground state O_2 adduct is formed at the surface — rather than a dynamic encounter of O_2 with the surface. At the gas-solid interface, Gafney showed that photoexcited $Ru(bpy)_3^{2+}$-adsorbed to PVG statically quenches O_2,[3] Avnir showed that photoexcited $Ru(bpy)_3^{2+}$-adsorbed to porous silica and porous glass statically quench O_2 at low temperatures, but dynamically quench O_2 at high temperatures,[4] and Thomas showed that aromatic compounds adsorbed onto nonporous glass statically quench O_2.[5,6] Pore size of silica-adsorbed photosensitizers can be tailored to statically or dynamically quench O_2 in gas-solid systems.[7,8]

Few studies have examined sensitizer quenching by O_2 at organic solvent-solid interfaces[9] or water-solid interfaces.[10] Despite reports on $^1O_2$ production (Φ_Δ) and $^1O_2$ lifetimes (τ_Δ) in homogeneous aqueous media, Nafion membranes,[11] micellar media,[12] water-soluble supramolecular hosts,[13] or aqueous reactions using TiO_2,[14] studies of the quenching mechanism of heterogeneous photosensitizers by O_2 at the *water-solid* interface are uncommon and are in need of elaboration.

We report here a photophysical analysis of how O_2 quenches ^{3}**1*** at the water-PVG interface. We also examined the effects of surface loading and percent coverage of the photosensitizer, and the depth that **1** can penetrate into the PVG material. An assessment of the quenching of the photosensitizer (static or dynamic) could help in the design of heterogeneous systems that attempt to control the exact mode of generation of $^1O_2$ in water.

2.2 Results and Discussion

2.2.1 Time-Dependent Adsorption of Photosensitizer onto PVG. A clean piece of PVG placed into an aqueous solution containing **1**, led to the adsorption of **1** onto PVG. Figure 1 shows the time-dependent adsorption of **1** onto PVG over a 15-hour period. The adsorption process was followed by monitoring the largest of the four Q-bands of **1-ads** at λ = 525 nm. A plateau is reached when there is 8.8×10^{-7} mol **1** adsorbed onto one gram of PVG. Loadings of 1.1×10^{-6} mol **1** onto PVG can be achieved, but only after a 48 to 72-hour period. Once the **1-ads** samples contained the desired surface coverage, they were rinsed with distilled water prior to use.

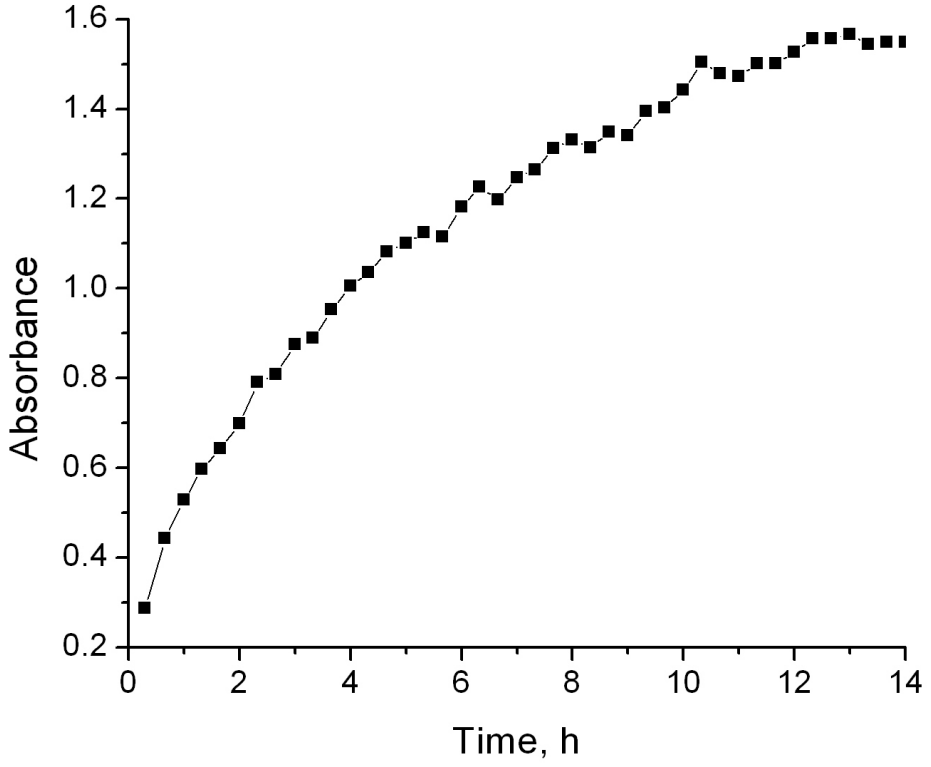

Figure 1. The adsorption of a PVG sample at λ_{max} = 525 nm that was sitting in a solution containing **1**. The PVG sample was removed at the indicated times. The plateau region at 14 hours corresponds to 8.83×10^{-7} mol **1** adsorbed onto one gram of PVG.

2.2.2 Uniform Photosensitizer Distribution. Absorption spectra were recorded at different points on the PVG film to analyze the dispersal of adsorbed **1**. The Q-band absorptions (475-700 nm) are found to be identical to within 0.01 absorbance unit

suggesting that the distribution of **1** is uniform; thus, the surface coverage of **1** adsorbed onto PVG could then be estimated. Two methods were used to determine the surface coverage of **1** adsorbed onto PVG. Both are in qualitative agreement with each other: (1) The amount of uncoated PVG was determined by subtracting 1.0 g PVG from (8.83×10^{-7} mol **1**/g PVG × 679.61 g/mol **1**), which is 0.9994 g. Dividing 8.83×10^{-7} mol **1**/g PVG into (0.9994 g uncoated PVG × 250 m^2/g PVG) yielded 3.5×10^{-9} mol **1**/m^2, indicating that 0.35% of the PVG surface is covered by **1**. (2) Surface coverage was determined by a calculation, in which porphyrin **1** is taken as a rectangular shape (22.2 Å × 22.2 Å × 7.3 Å) multiplied by (8.83×10^{-7} mol **1**/g PVG × 6.02×10^{23} molecules/mol × 10^{-21} $mm^3/Å^3$), which equals 1.91 mm^3/g PVG. The rectangular shape of **1** was estimated based on the B3LYP/6-31G(d) optimized structure and the corresponding solvent accessible contour map (Figure 2), in which the pyridinium rings are nearly orthogonal to the plane of the porphyrin (67°). The corresponding weight of **1**-adsorbed PVG (1.91 mm^3 × 1.38 g PVG/mL) equals 2.64 g PVG. Therefore, the surface coverage of **1** onto PVG was calculated by taking [8.83×10^{-7} mol **1**/(2.64 g PVG × 250 m^2/g PVG)] or 1.4×10^{-9} mol **1**/m^2, yielding 0.13% PVG surface coverage by **1**. Both calculations [(1) and (2), *vide supra*] indicated that <1% of the PVG surface is covered with the photosensitizer **1**. For comparison, the surface coverage of $Ru(bpy)_3^{2+}$ on PVG is <1%,[3] on porous silica is ~6% and porous glass is ~10%.[4]

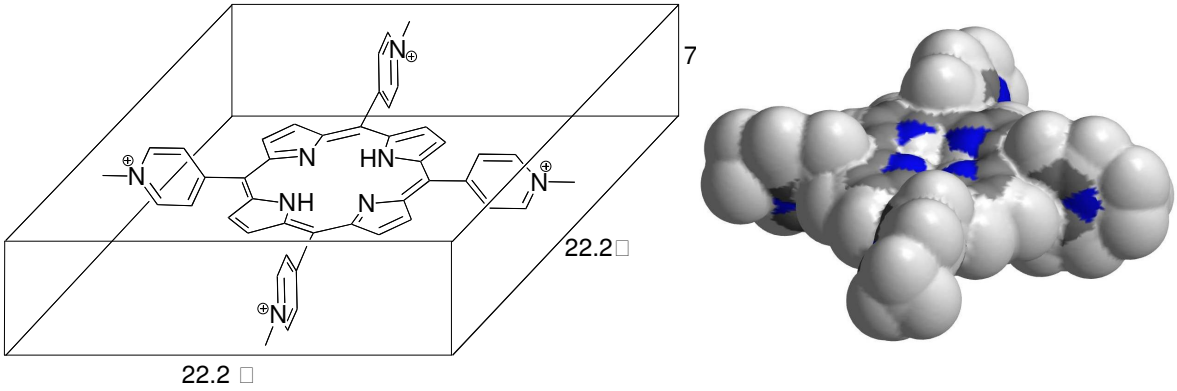

Figure 2. Rectangular shape of **1** (left) estimated from a B3LYP/6-31G(d) optimized structure and the corresponding computed solvent accessible map (right).

2.2.3 Photosensitizer Penetration Depth. The depth that **1** can penetrate into PVG was examined using a microscope equipped with a CCD camera. Figure 3 shows a 1.5 mm thick (sensitizer coated) PVG sample, cut so that the depth of **1** penetrated into PVG could be viewed. The microscope image shows the penetration of **1** reaches a maximum depth of 0.32 mm along all faces of the sample, which corresponds to the plateau region of 8.8×10^{-7} mol **1**/g PVG (Figure 1). Dr. Jovan Giaimuccio in Professor Gerald J. Meyer group at Johns Hopkins University helped us to take low-magnification (60x) cross-sectional optical image of sensitizer adsorbed glass sample (Figure 3). Although O_2 and other gases are permeable and can pass through the connected pores of PVG,[25] **1** neither penetrates to the center of the PVG film nor is **1** localized on the outer surface of PVG. A ten-fold mole increase of **1** resulted in only a 4-fold local increase in

sensitizer distribution into PVG [cf. $0.9x10^{-6}$ mol **1** (penetration depth 0.32 mm) and $0.9x10^{-7}$ mol **1** adsorbed onto one gram PVG (penetration depth 0.09 mm)]. Oxygen is expected to reach the excited sites of **1-ads**, controlled by Knudsen diffusion, in which O_2 collides numerous times within the pore walls, eventually proceeding through the PVG channels. For comparison, $Ru(bpy)_3^{2+}$ penetrates 0.5±0.1 mm into PVG.[3] Streptocyanine dyes also possessed diffusivity into silica gels, influenced by the gel porosities.[26]

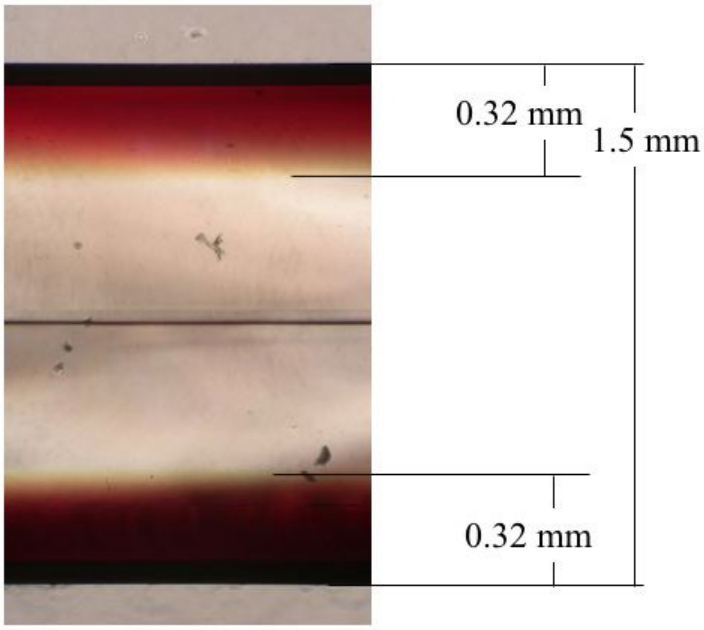

Figure 3. A low-magnification (60x) cross-sectional optical image. The red areas indicate the depth of **1** accessed into PVG. The image shows 0.32 mm penetration depth on each face for $0.9x10^{-6}$ mol **1** adsorbed onto a 1.5 mm PVG sample. The horizontal line in the middle of the PVG sample corresponds to where two glass layers meet due to the commercial fabrication process.

2.2.4 Spectral Properties. Previously, we reported that the spectral features of **1-ads** are nearly identical to **1** in fluid water solution.[2] Here, we report the spectral features measured at different concentrations of **1** adsorbed onto PVG.

Figure 4 shows absorption spectra of **1** in water and **1** adsorbed onto PVG. While the effect of higher coverage dose of **1** produces neither red-shifts nor blue-shifts in the Q-bands, the adsorption of **1** on PVG leads to an unexpected effect on the absorption intensity. Higher coverages of **1** adsorbed onto PVG led to a *decrease* of the Q-band absorption intensity, (cf. 0.9×10^{-8}, 0.9×10^{-7}, and 0.9×10^{-6} mol **1**/g PVG). At higher surface coverage, the absorption spectrum of **1-ads** becomes somewhat similar to that of **1** in aqueous solution (cf. spectra in blue and black, Figure 4). Deducing a possible orientational effect of the porphyrin on the PVG surface is challenging based upon these normalized absorption spectra. Polarization effects are known for porphyrins result in symmetric changes of all the $S_0 \rightarrow S_1$ transitions. However, atomic-level detail is unavailable for PVG and how it may relate to the conformation of adsorbed **1**. Interestingly, recent studies have shown a reduced hydrating ability of ~2.2 H-bonds per water molecule confined in PVG pores compared bulk water with ~3.6 H-bonds per water molecule, pointing to the importance for confinement effects.[27,28]

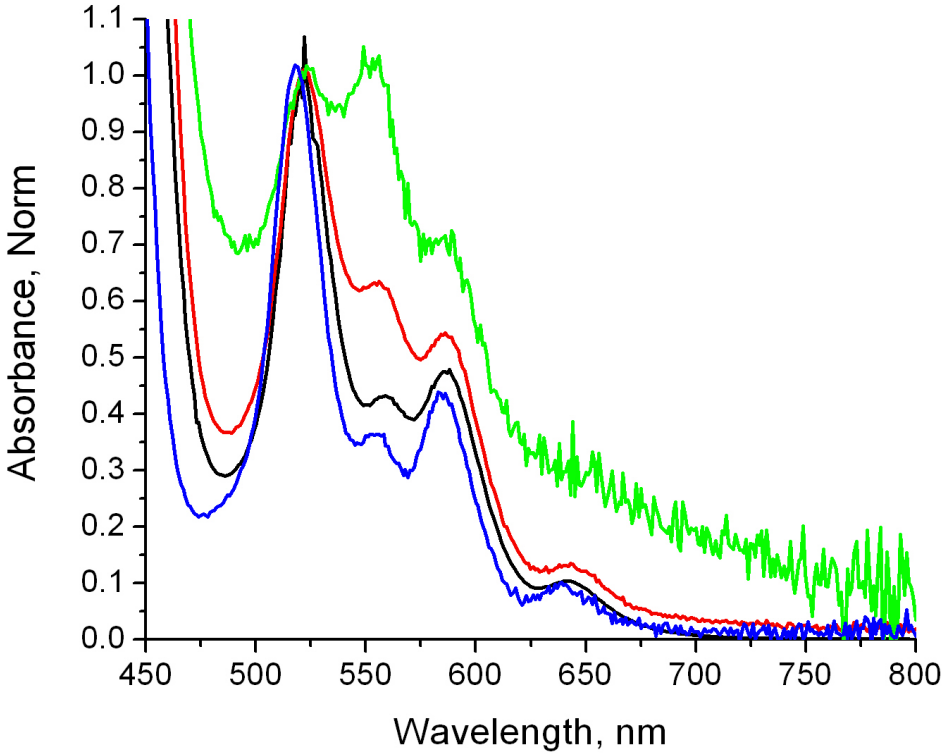

Figure 4. Absorption spectra of **1** in water (blue line), and **1-ads** at different loadings: $0.9x10^{-8}$ (green line), $0.9x10^{-7}$ (red line), and $0.9x10^{-6}$ (black line) moles of **1** adsorbed on PVG. The spectra were normalized at 532 nm. Except for the green line ($0.9x10^{-8}$ mols **1** adsorbed onto PVG), the Q-band maximum is at 525 nm.

2.2.5 Time-Resolved Photophysical Studies. Figure 5 shows a nanosecond transient absorption spectrum generated from pulsed 417-nm light excitation of $0.9x10^{-7}$ mol **1** adsorbed onto one gram PVG in an N_2-purged H_2O solution. The absorption band at ~470 nm was assigned to ^{3}**1*-ads**. Similar transient features were observed for ^{3}**1*** in fluid water (Figure 5, Inset), and also by Reddi et al. for ^{3}**1*** in phosphate buffered solution and in aqueous 2% sodium dodecyl sulfate solution.[29] First-order decay kinetics

were observed for the transient absorption of **^{3}1*-ads**, which decayed cleanly to baseline. The lifetime of **^{3}1*-ads** (τ_0 = 57±1 μs) is similar to **^{3}1*** in fluid aqueous solution (τ_0 = 49±1 μs). Our absorption measurements in the UV-visible region before and after transient absorption experiments revealed no significant change. Dr. Jovan Giaimuccio in Professor Gerald J. Meyer group at Johns Hopkins University has conducted nanosecond transient absorption experiments in order to see the quenching effect of **^{3}1*-ads** with molecular oxygen in aqueous solution. Next we describe how O_2 quenches the transient absorption of **^{3}1*-ads** and **^{3}1*** in water solution.

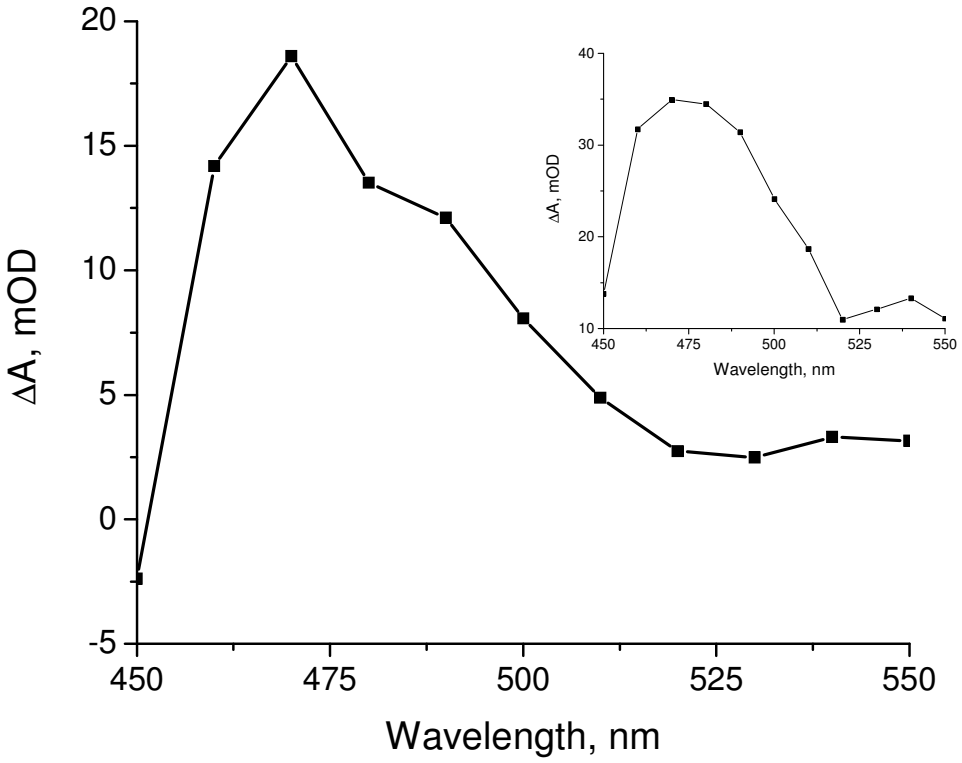

Figure 5. Nanosecond transient absorption spectra observed at 500 ns after pulsed-light excitation (417 nm, 1.6 mJ/pulse) of **1** in water solution (inset) and **1** at the water/PVG interface. Data points were collected every 10 nm from 450-550 nm.

Figure 6 shows the lifetime and the amplitude quenching of the ^{3}**1*-ads** transient absorption by O_2. Photoexcited **1** quenching by O_2 at the PVG/water interface encouraged a Stern-Volmer analysis for insight into quenching mechanism. Two mechanisms were considered: (1) the dynamic encounter of O_2 with an excited site on the surface, and (2) a ground state O_2 adduct formed at the surface with migration of adsorbed O_2 to an excited site (Scheme 2).

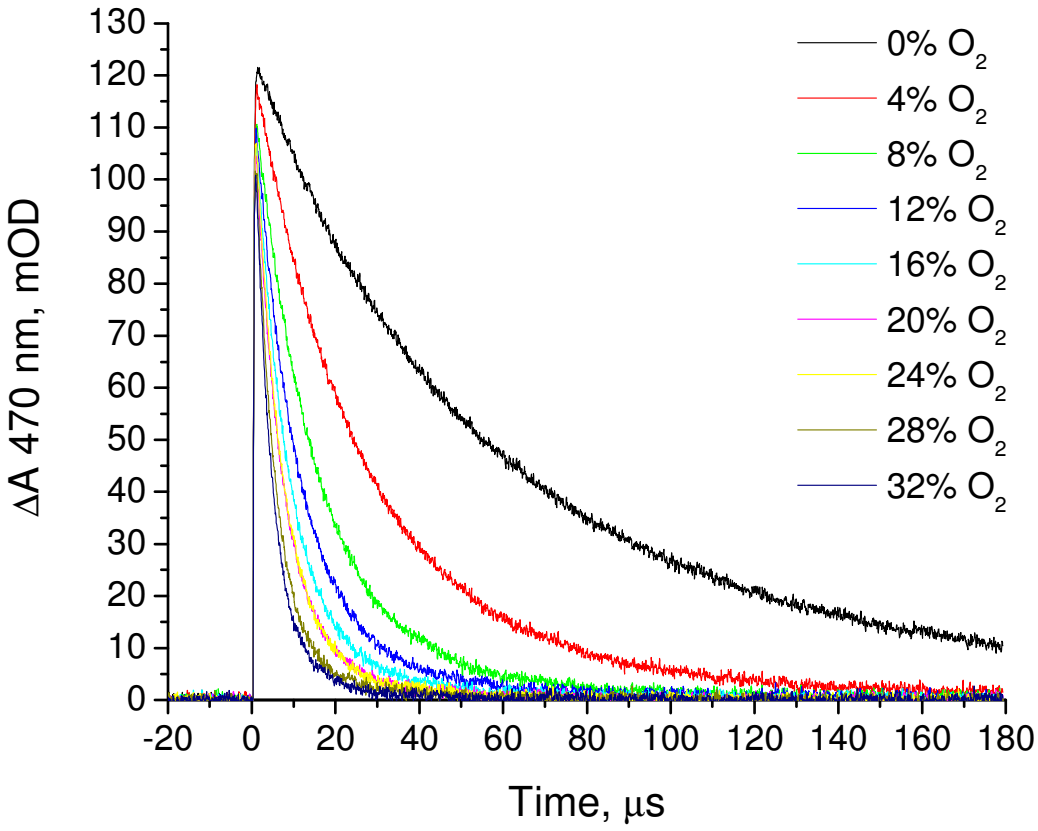

Figure 6. Time-resolved absorbance observed at 470 nm after pulsed with 417-nm light at 0.6 mJ/pulse. 0.9×10^{-7} mole **1** adsorbed onto PVG with increasing percents of O_2. The O_2:N_2 ratios ranged from 0:100 to 32:68 in H_2O solution.

Scheme 2

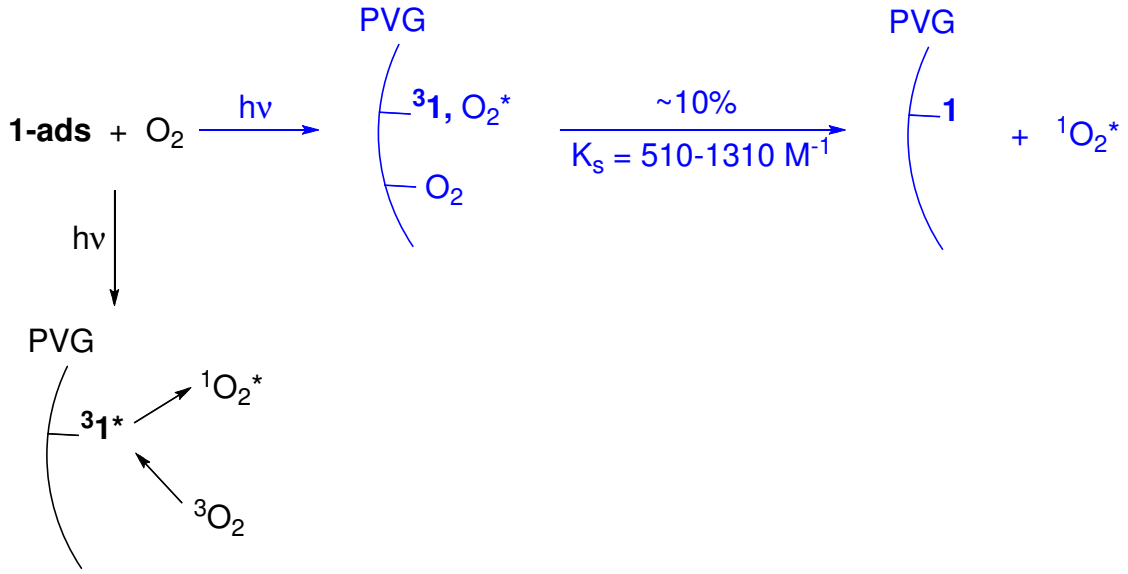

Stern-Volmer data collected at nine O_2 concentrations (from 0 to 0.4 mM) are shown in Table 1 and Figure 7, in which the symbol τ refers to the lifetime of the excited porphyrin, k_q is the rate constant for O_2 quenching, K_D is the Stern-Volmer constant, K_S is the association constant for complex formation between the sensitizer and O_2, and the subscript "0" indicates data in the absence of O_2. The left-axis of Figure 7 shows the plot of τ_0/τ vs $[O_2]$ to be linear over the O_2 concentration examined and corresponded to the Stern-Volmer equation: $\tau_0/\tau = 1 + k_q\tau_0[O_2] = 1 + K_D[O_2]$. For 0.9×10^{-7} moles **1** adsorbed onto one gram PVG, $K_D = 26{,}500\ M^{-1}$ and the quenching rate constant $k_q = 4.6\times10^{8}\ M^{-1}\ s^{-1}$, indicating that 50% of ^{3}**1*-ads** was quenched at an $[O_2]$ of 0.04 mM. For the samples containing 0.9×10^{-6} to 0.9×10^{-8} moles **1** adsorbed onto one gram PVG, the K_D values ranged from 32,000 M^{-1} to 23,700 M^{-1}.

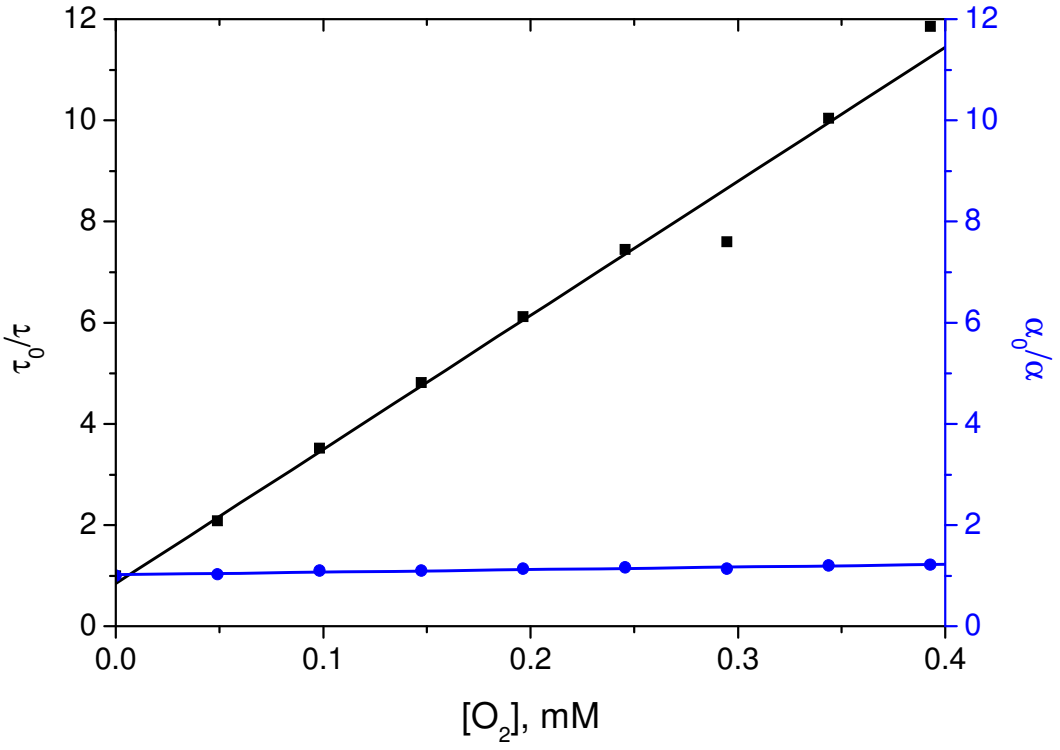

Figure 7. Lifetime quenching as a function of O_2 concentration of a H_2O solution containing $0.9x10^{-7}$ mole **1** adsorbed onto PVG (in black, left). Amplitude quenching as a function of O_2 concentration of a H_2O solution containing $0.9x10^{-7}$ mole **1** adsorbed onto PVG (in blue, right). Samples were excited with a 10 ns 417-nm light pulse (0.6 mJ/pulse) and the transient absorption was monitored at 470 nm.

Table 1. Stern-Volmer Quenching Constants as a Function of Coverage of 1 onto Porous Vycor Glass or of 1 in Fluid Water Solution

Photosens.	Absorbance λ_{520}	K_D (M^{-1})	K_S (M^{-1})	k_q (M^{-1} s^{-1})
1-ads[a,b]	0.87	23700±1320	1310±210	4.2×10^8
1-ads[a,c]	0.25	26500±1220	510±60	4.6×10^8
1-ads[a,d]	0.025	32100±1460	650±80	5.6×10^8
1 in fluid H_2O[e]	~0.2	89600±2600	1160±170	1.8×10^9

[a] The PVG/**1** samples were immersed in water. [b] Sample contained 0.9×10^{-6} mol **1** adsorbed onto PVG. [c] Sample contained 0.9×10^{-7} mol **1** adsorbed onto PVG. [d] Sample contained 0.9×10^{-8} mol **1** adsorbed onto PVG. [e] Homogeneous **1** in deionized water solution.

Interestingly, the bimolecular quenching constant k_q for **1-ads** (k_q = ~5×10^8 $M^{-1}s^{-1}$) is about one-quarter the value measured for **1** in fluid water ($k_q = 1.8\times10^9$ $M^{-1}s^{-1}$). The experiments for **1** in fluid water solution produced a K_D value of 89,600 M^{-1}. Thus, the timescale for O_2 diffusion may be slower in the water-PVG heterogeneous system compared to fluid solution. By analogy, Thomas et al. used the Einstein equation

$<x^2>=6Dt$ to suggest that nitromethane quenching of excited anthracene is 10^3-10^6 times slower in a zeolite compared to fluid solution (cf. 10^{-8}-10^{-11} cm^2 s^{-1}).[41] In our system, the smaller K_D values in the heterogeneous samples may result from reduced directions for access of O_2 to **^{3}1*-ads** compared to O_2 to **^{3}1*** in fluid solution.

The right-hand Y-axis of Figure 7 shows a plot of α_0/α vs $[O_2]$ that was linear over the O_2 concentration examined, and followed the equation: $\alpha_0/\alpha = 1 + K_S[O_2]$. For **1-ads**, we find that the adduct formation constant K_S ranged from 510 M^{-1} to 1310 M^{-1}. From the changes observed in the amplitude in Figure 7, we estimate that ~10% of the quenching occurred via the static quenching mechanism (colored blue in Scheme 2). Indeed, for the static component to account for 50% quenching of **^{3}1*-ads**, 1.5 mM O_2 would be needed. Thus, a ground-state adduct equilibrium of **1** and O_2, and **1-ads** and O_2 appeared to form, but to a minor extent. The above Stern-Volmer analysis suggested that quenching of **^{3}1*-ads** by O_2 is primarily dynamic, the route colored black in Scheme 2. In the absence of aggregation, photosensitizers in fluid solution are often quenched dynamically by O_2.[21]

2.3 Conclusion

We have obtained evidence that O_2 quenches triplet **1*** at the water-PVG interface primarily by a dynamic quenching mechanism. The contribution from static quenching remains low even with loadings of **1** onto PVG that varied by 100 fold. The O_2 quenching constants k_q for **^{3}1*-ads** were only 3-4 times smaller than for **^{3}1*** itself suggesting the heterogeneous system is capable of generating singlet oxygen for its use as a reagent in the surrounding aqueous solution.

2.4 Experimental Section

2.4.1 Materials and Sample Preparation. Deionized H_2O was obtained from a U.S. Filter Corporation deionization system. *Meso*-tetra(N-methyl-4-pyridyl)porphine tetratosylate was purchased commercially and used as received. The PVG was used as a host material and was purchased from Advanced Glass and Ceramics (Corning 7930). The PVG has a void space of ~28% of the volume, average pore sizes of 40 Å, a hydrophilic absorbing surface area of 250 m^2/g, a density of 1.38 g/mL, and transparency in the near-UV (50% T at 351 nm), visible, and parts of the near-IR.[15] Pieces of PVG (1.5 cm × 1.5 cm, thickness: 1.15-1.53 mm) were heated in a muffle furnace at 500 °C and stored in a desiccator under vacuum at 30 mm Hg. The photosensitizer-coated PVG was prepared by soaking 1.4 g PVG into a 20 mL 3.7×10^{-5} M aqueous solution of **1** for 15-64 hours. The amount of **1** adsorbed onto PVG was calculated from the difference in absorbance of the solution before introduction of PVG and the absorbance of the same solution after the removal of PVG.[2,16] For the transient absorption studies, PVG was cut such that each piece fits diagonally into a 1-cm path-length quartz cuvet. Each PVG/**1** sample was placed into the quartz cuvet, which contained deionized water, and was sparged with N_2 gas for 20 minutes. Any bubbles that stuck onto the PVG surface were removed by sonication for a few seconds. Some PVG samples (1.5 cm × 1.5 cm, thickness: 1.53 mm) were cut into 0.3 cm × 1.5 cm pieces and photographed with a microscope.

2.4.2 Instruments. Photographic images were taken with a Nikon TE200 microscope equipped with an Orca 100 monochrome charge-coupled device (CCD) camera and a Hamamatsu Camera Controller (C4742-95). The light source used was a 100-W mercury arc lamp. The objective used was a Plan Apo 60×Oil DIC. Images were recorded and analyzed with CamMedia software.[17] Absorption spectra were collected with a Hitachi UV-VIS U-2001, a Hewlett-Packard 8453 diode array, or a Varian Carey 14 spectrophotometer. In some experiments with the Carey 14 instrument, the Q-bands of **1** at 525, 552, 585, and 640 nm were followed because the intense Soret band at 422 nm gave absorbances of 2.5 or greater, which saturated the UV-vis detector. A Quantel Brilliant B Nd:YAG laser (417 nm, 0.6-1.6 mJ/pulse) was used in the transient absorption experiments.[18,19]

2.4.3 Transient Absorption Spectroscopy. The PVG samples used in these experiments contained 0.9×10^{-8} to 1.1×10^{-6} mol **1**/g PVG. Room-temperature time-resolved measurements were conducted as previously described.[20] The PVG samples were excited at 417 nm, but oriented so that reflected laser light was directed at a 45° angle away from the detector on the transient absorption apparatus. Each kinetic trace is an average of 64 laser pulses. The triplet of **1-ads** was monitored at 470 nm, in which a 435 nm long pass filter was placed in front of the detector monochrometer to block scattered laser light. The data points in the transient absorption experiments were collected every 10 nm from 450-550 nm. An MKS Instruments Multi Gas Controller (MKS 647C) was used to control the flow of O_2 and N_2 through two MKS Instruments flow controllers. The flow controllers were set for a flow rate of 100 standard cubic centimeters per minute (sscm). Gas correction factors (GCFs) programmed into the

MGC were utilized to correct for specific heat, density, and molecular structure of O_2 and N_2. The samples were purged with different ratios of an O_2:N_2 stream of gas for 5 minutes before each kinetic trace was taken. The oxygen concentration of a solution bubbled with the O_2:N_2 gas stream were determined by using Henry's Law.[21,22]

2.4.4 Computational Methods. Density function theoretical (DFT) calculations were conducted by the exchange-correlation of B3LYP along with Pople basis set 6-31+G(d) with the use of the Gaussian 03 program package.[23] The solvent accessible surface was computed by the method of Lee and Richards.[24]

2.5 References

(1) Recent examples include: (a) *polymers and polymer blends*: Koizumi, H.; Kimata, Y.; Shiraishi, Y.; Hirai, T. *Chem. Comm.* **2007**, 1846-1848. A. P. Schaap *The Spectrum* **2007**, *20*, 4-13. Zebger, I.; Poulsen, L.; Gao, Z.; Andersen, L. K.; Ogilby, P. R. *Langmuir* **2003**, *19*, 8923-8933. (b) *Quantum dots*: Ma, J.; Chen, J.-Y.; Idowu, M.; Nyokong, T. *J. Phys. Chem. B.* **2008**, *112*, 4465-4469. Tsay, J. M.; Trzoss, M.; Shi, L.; Kong, X.; Selke, M.; Jung, M. E.; Weiss, S. *J. Am. Chem. Soc.* **2007**, *129*, 6865-6871. Samia A. C. S.; Dayal S.; Burda C. *Photochem. Photobiol.* **2006**, *82*, 617-25. (c) *Silica, silica nanoparticles, xerogels, and exchange resins*: Cantau, C.; Pigot, T.; Manoj, N.; Oliveros, E.; Lacombe, S. *Chem. Phys. Chem.* **2007**, *8*, 2344-2353. Feng, K.; Wu, L.-Z.; Zhang, L.-P.; Tung, C.-H. *Tetrahedron* **2007**, *63*, 4907-4911. Ishii, K.; Shiine, M.; Kikukawa, Y.; Kobayashi, N.; Shiragami, T.; Matsumoto, J.; Yasuda, M.; Suzuki, H.; Yokoi, H. *Chem. Phys. Lett.* **2007**, *448*, 264-267. Chirvony, V.; Chyrvonaya, A.; Ovejero, J.; Matveeva, E.; Goller, B.; Kovalev, D.; Huygens, A.; de Witte, P. *Adv. Mat.* **2007**, *19*, 2967-2972. Greer, A. *Acc. Chem. Res.* **2006**, *39*, 797-804. Roy, I.; Ohulchanskyy, T. Y.; Pudavar, H. E.; Bergey, E. J.; Oseroff, A. R.; Morgan, J.; Dougherty, T. J.; Prasad, P. N. *J. Am. Chem. Soc.* **2003**, *125*, 7860-7865. (d) *Modified* TiO_2: Naito, K.; Tachikawa, T.; Fujitsuka, M.; Majima, T. *J. Phys. Chem. C* **2008**, *112*, 1048-1059. Jaczyk, A.; Krakowska, E.; Stochel, G.; Macyk, W. *J. Am. Chem. Soc.* **2006**, *128*, 15574-15575. Tatsuma, T.; Tachibana, S.; Miwa, T.; Tryk, D. A.; Fujishima, A. *J. Phys. Chem. B* **1999**, *103*, 8033-8035. (e) *Zeolites*: Cojocaru, B.; Laferriere, M.; Carbonell, E.; Parvulescu, V.; Garcia, H.; Scaiano, J. C. *Langmuir* **2008**, *24*, 4478-4481. Pace, A.; Pierro, P.; Buscemi, S.; Vivona, N.; Clennan, E. L. *J. Org. Chem.* **2007**, *72*,

2644-2646. Jockusch, S; Sivaguru, J.; Turro, N. J.; Ramamurthy, V. *Photochem. Photobiol. Sci.* **2005**, *4*, 403-405.

(2) Aebisher, D.; Azar, N. S.; Zamadar, M.; Gafney, H. D.; Gandra, N.; Gao, R.; Greer, A. *J. Phys. Chem. B* **2008**, *112*, 1913-1917.

(3) Gafney, H. D.; Wolfgang, S. *J. Phys. Chem.* **1983**, *87*, 5395-5401.

(4) Samuel, J.; Ottolenghi, M.; Avnir, D. *J. Phys. Chem.* **1992**, *96*, 6398-6405.

(5) Krasnansky, R.; Koike, K.; Thomas, J. K. *J. Phys. Chem.* **1990**, *94,* 4521.

(6) Krasnansky, R.; Thomas, J. K. *J. Photochem. Photobiol. A: Chem.* **1991**, *57*, 81-86.

(7) Drake, J. M.; Levitz, P.; Turro, N. J.; Nitsche, K. S.; Cassidy, K. F. *J. Phys. Chem.* **1988**, *92*, 4680-4684.

(8) Wellner, E.; Rojanski, D.; Ottolenghi, M.; Huppert, D.; Avnir, D. *J. Am. Chem. Soc.* **1987**, *109*, 575-576.

(9) Ruetten, S. A.; Thomas, J. K. *J. Phys. Chem. B.* **1999**, *103*, 1278-1286.

(10) Xiong, Z.; Xu Y.; Zhu L.; Zhao J. *Environ. Sci. Tech.* **2005**, *39*, 651-657.

(11) Zhang, D.; Wu, L.-Z.; Yang, Q.-Z.; Li, X.-H.; Zhang, L.-P.; Tung, C.-H. *Org. Lett.* **2003**, *5*, 3221-3224. Wetzler, D. E.; Garcia-Fresnadillo, D.; Orellana, G. *Phys. Chem. Chem. Phys.* **2006**, *8*, 2249-2256.

(12) Rodgers, M. A. J.; Lee, P. C. *J. Phys. Chem.* **1984**, *88*, 3480-3484; Lee, P. C.; Rodgers, M. A. J. *J. Phys. Chem.* **1984**, *88*, 4385-4389. Matheson, I. B. C.; Rodgers, M. A. J. *J. Phys. Chem.* **1982**, *86*, 884-887. Lee, P. C.; Rodgers, M. A. J. *J. Phys. Chem.* **1983**, *87*, 4894-4898.

(13) Natarajan, A.; Kaanumalle, L. S.; Jockusch, S.; Gibb, C. L. D.; Gibb, B. C.; Turro, N. J.; Ramamurthy, V. *J. Am. Chem. Soc.* **2007**, *129*, 4132-4133.

(14) Daimon, T.; Nosaka, Y. *J. Phys. Chem. C* **2007**, *111*, 4420-4424.

(15) Elmer, T. H. in ASM Engineered Materials Handbook; Schnieder, S. J., Jr., Ed.; ASM: Materials Park, OH, 1991; Vol. 4, pp 427.

(16) Gafney, H. D.; Shi, W. *J. Phys. Chem.* **1988**, *92*, 2329.

(17) Bauer, L. A.; Reich, D. H.; Meyer, G. J. *Langmuir* **2003**, *19*, 7043-7048.

(18) Staniszewski, A.; Morris, A. J.; Ito, T.; Meyer, G. J. *J. Phys. Chem. B* **2007**, *111*, 6822-6828.

(19) Staniszewski, A.; Heuer, W. B.; Meyer, G. J. *Inorg. Chem.* **2008**, *47*, 7062-7064.

(20) Argazzi, R.; Bignozzi, C. A.; Heimer, T. A.; Castellano, F. N.; Meyer, G. J. *Inorg. Chem.* **1994**, *33*, 5741-5749.

(21) Iu, K.-K.; Ogilby, P. R. *J. Phys. Chem.* **1988**, *92*, 4662-4666.

(22) Battino, R. Ed. *IUPAC Solubility Data Series, Volume 7, Oxygen and Ozone*; Pergamon: Oxford, 1981.

(23) Frisch, M. J., Trucks, G. W., Schlegel, H. B., Scuseria, G. E., Robb, M. A., Cheeseman, J. R., Montgomery, J. A., Jr., Vreven, T., Kudin, K. N., Burant, J. C., Millam, J. M., Iyengar, S. S., Tomasi, J., Barone, V., Mennucci, B., Cossi, M., Scalmani, G., Rega, N., Petersson, G. A., Nakatsuji, H., Hada, M., Ehara, M., Toyota, K., Fukuda, R., Hasegawa, J., Ishida, M., Nakajima, T., Honda, Y., Kitao, O., Nakai, H., Klene, M., Li, X., Knox, J. E., Hratchian, H. P., Cross, J. B., Bakken, V., Adamo, C., Jaramillo, J., Gomperts, R., Stratmann, R. E., Yazyev, O., Austin, A. J., Cammi, R., Pomelli, C., Ochterski, J. W., Ayala, P. Y., Morokuma, K., Voth, G. A., Salvador, P., Dannenberg, J. J., Zakrzewski, V. G., Dapprich, S., Daniels, A. D., Strain, M. C., Farkas, O., Malick, D. K., Rabuck, A. D., Raghavachari, K., Foresman, J. B., Ortiz, J. V., Cui, Q., Baboul, A.

G., Clifford, S., Cioslowski, J., Stefanov, B. B., Liu, G., Liashenko, A., Piskorz, P., Komaromi, I., Martin, R. L., Fox, D. J., Keith, T., Al-Laham, M. A., Peng, C. Y., Nanayakkara, A., Challacombe, M., Gill, P. M. W., Johnson, B., Chen, W., Wong, M. W., Gonzalez, C., and Pople, J. A. *Gaussian 03*, revision B.05; Gaussian, Inc.: Pittsburgh, PA, 2003.

(24) Lee, B.; Richards, F. M. *J. Mol. Biol.* **1971**, *55*, 379-380. Richards, F. M. *Ann. Rev. Biophys. Bioeng.* **1977**, *6*, 151-176.

(25) Knagge, K.; Smith, J. R.; Smith, L. J.; Buriak, J.; Raftery, D. *Solid State Nuc. Mag. Res.* **2006**, *29*, 85-89. Preethi, N.; Shinohara, H.; Nishide, H. *Bull. Chem. Soc. Jpn.* **2006**, *79*, 1308-1311. Uchytil, P.; Petrickovic, R.; Seidel-Morgenstern, A. *J. Membrane Sci.* **2007**, *293*, 15-21. Shiojiri, K.; Yanagisawa, Y.; Yamasaki, A.; Kiyono, F. *J. Membrane Sci.* **2006**, *282*, 442-449. Yang, J.; Cermakova, J.; Uchytil, P.; Hamel, C.; Seidel-Morgenstern, A. *Catal. Today* **2005**, *104*, 344-351.

(26) Hellriegel, C.; Kirstein, J.; Braeuchle, C.; Latour, V.; Pigot, T.; Olivier, R.; Lacombe, S.; Brown, R.; Guieu, V.; Payrastre, C.; Izquierdo, A.; Mocho, P. *J. Phys. Chem. B* **2004**, *108*, 14699-14709.

(27) Gleb, L. D.; Gubbins, K. E. *Langmuir* **1998**, *14*, 2097-2111.

(28) Thompson, H.; Soper, A. K.; Ricci, M. A.; Bruni, F.; Skipper, N. T. *J. Phys. Chem. B* **2007**, *111*, 5610-5620.

(29) Reddi, E.; Ceccon, M.; Valduga, G.; Jori, G.; Bommer, J. C.; Elisei, F.; Latterini, L.; Mazzucato, U. *Photochem. Photobiol.* **2002**, *75*, 462-470.

Chapter 3. Singlet Oxygen Delivery Through the Porous Cap of a Hollow-Core Fiber Optic Device

3.1 Introduction

We reported a photochemical approach to the clean generation of singlet oxygen in aqueous solution with a porous glass sensitizer [*meso*-tetra(*N*-methyl-4-pyridyl)porphine **1** adsorbed onto porous Vycor glass (PVG)].[1,2] The porous glass sensitizer involved oxygen "collision" onto the matrix for the conversion ground-state O_2 into $^1O_2$, reflecting $^1O_2$ diffusion into the bulk aqueous solution (Scheme 1).[2] Singlet oxygen was detected in water by time-resolved methods or reaction with an alkene molecule to give a hydroperoxide.[1] Our attention to a *porous* glass sensitizer stemmed from a desire to fix the photosensitizer to the end of a hollow fiber optic through which O_2 flows to "deliver" singlet oxygen site-selectively on the micro-scale. Few reports have appeared on heterogeneous sensitizers coupled to fiber optics,[3-7] or the production of singlet oxygen by heterogeneous sensitizers in water.[8,9] Clearly, at present, methods that generate singlet oxygen are not coupled into maneuverable delivery devices. We report here the first study of a hybrid sensitizer/fiber optic device for singlet oxygen generation at the fiber tip. The prototype device is based on micro-optic technology[10] for localizing singlet oxygen in water, and has the potential for use in cancer treatment and in water disinfection.

Scheme 1

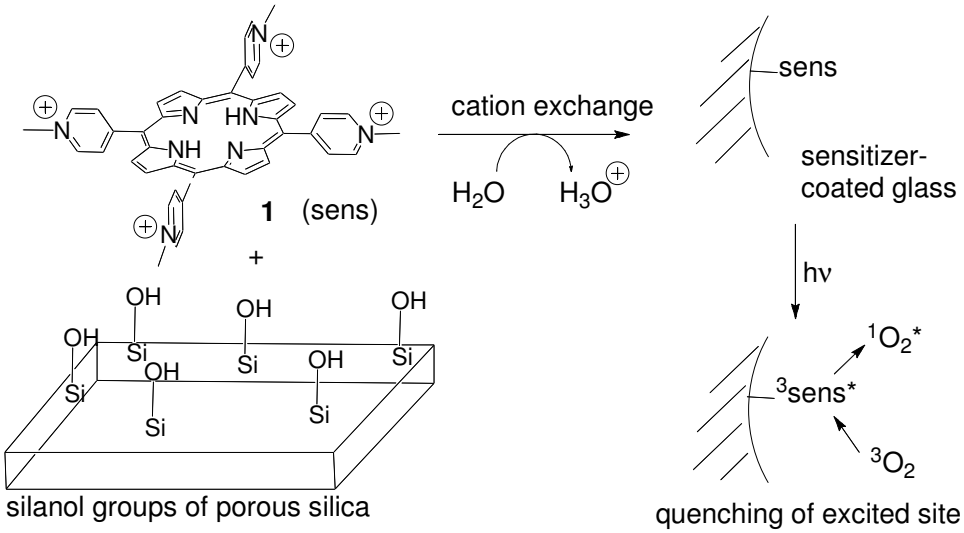

3.2 Results and Discussion

The singlet oxygen fiber device consisted of a porous Vycor cap coated with **1** as sensitizer placed on the end of a hollow core photonic bandgap fiber. Compressed oxygen was delivered through the core of the fiber to the cap and into water solutions containing *N*-benzoyl-DL-methionine anion (0.02 M) as an indirect method to analyze singlet oxygen production. Oxygen flowed through the fiber and irradiation with 532-nm laser light focused into the proximal end of the fiber led to the sulfoxide as the only product at the distal end in water. The same product was observed in D_2O and in H_2O. The experimental evidence suggesting the viability of the device in Scheme 2 includes the following:

Scheme 2

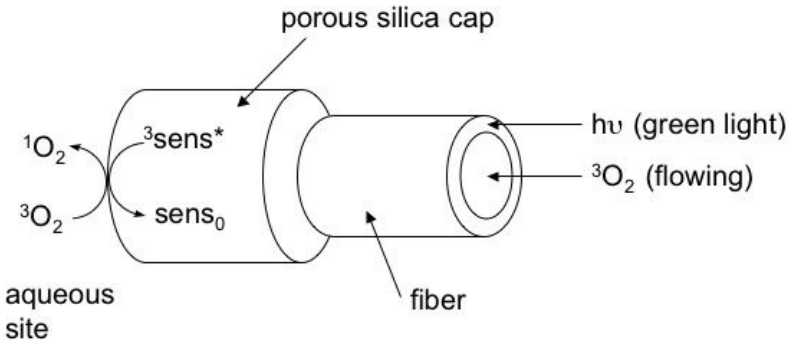

A hollow core photonic bandgap fiber HC-580 (capable of transmitting 520-630 nm light, core diameter of 4.9 µm, acrylate coating diameter of 220 µm) was coupled to a green-LED or a 10-Hz Nd:YAG laser operating at 532 nm. The equation from Gaussian optics for the focal length with optimum mode matching to the single-mode HC-580 fiber accounts for the preferred use of a 10X objective.[11] A Newport laser-to-fiber coupler with 0.1-µm xyz translation resolution aligned the microscope objective to focus green light into the optical fiber, and a Teflon-lined fiber chuck upon tightening accommodated the 220 µm fiber. The 532-nm beam exiting the distal end of the 30-cm length of fiber was 0.15 mW (LED) and 0.11 mJ/pulse (Nd:YAG). The intensity of the light exiting the fiber is a function of its length. The attenuation is ~1 dB/m and bending the fiber does not increase the attenuation noticeably.

Previous studies of gas and light passage through hollow optical fibers[12,13] suggested that ground-state O_2 could be delivered through our HC-580 fiber. A 406-µm channel was mechanically drilled through one side of a polystyrene cuvette (10 mm light path length, 12.5 mm^2×45 mm) using a micro diamond-head drill. The fiber was inserted into a ferrule collar glued into the hole in the cuvette with ethyl cyanoacrylate glue, where a 2 mm segment of the fiber protruded into the center of the cuvette (Figure 1A,B). The cuvette was placed into the center of the laser-to-fiber coupler, where the 532-nm

beam passes though the opposite (unmodified) side of the quartz cuvette and entered the fiber (Figure 1B). A 3-mm hole was drilled into the square polytetrafluoroethylene cuvette cover (12.5 mm^2) glued to the cuvette. A plastic 200 µL pipette tip was inserted to about ¼ of its length and glued in place. The top of the cuvette was connected to an oxygen tank, where compressed oxygen flowed 40 PSI into the cuvette. The flow rate of oxygen through the uncapped hollow fiber was 0.12 mL/hour.

A **B**

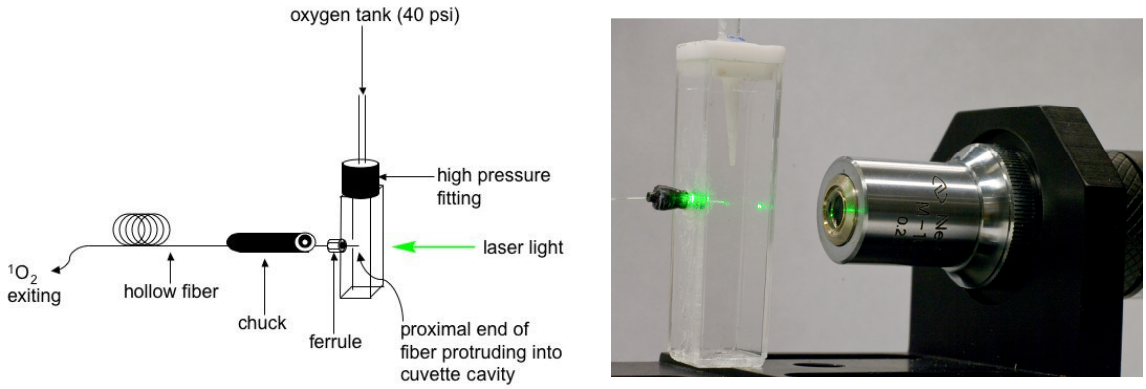

Figure 1. (A) A schematic drawing showing the compressed oxygen-to-fiber coupling and the use of a modified cuvette. Oxygen gas is delivered through a pipette at the top of the cuvette and enters the proximal end of the fiber to the left, which is protruding into the cuvette cavity. (B) A portion of the experimental set-up showing the LED, the 10X objective, and modified cuvette, in which green light is focused into the fiber.

The end of the hollow fiber was capped with the porous glass photosensitizer [3×10^{-7} mol sensitizer **1** was adsorbed onto 0.013 g pre-shaped PVG (dimensions: 3 mm^2 × 0.8 mm)]. The fiber acrylate coating was not removed so that the intensity of light was

the same at the source and at the fiber-PVG junction. The colorless PVG cap was converted to deep red or black on adsorption of **1**. About 0.5% of the cap surface was covered with photosensitizer, and the photosensitizer remained adhered to the cap in contact with water.[1,2] No desorption of **1** from PVG was observed at pH = 3, 7, and 10. Photobleaching of the fiber cap with the 5 mW laser was not evident up to 30 hours of irradiation. Cap samples could be grinded down to 0.6 mm, but any thinner led to cap leaking or cracking. A hole with the dimensions 2.38 mm × 0.38 mm was drilled length-wise into the sensitizer-coated porous silica cap (Figure 2). The fiber was inserted into the cylinder hole and glued into place at the hole entrance. As desired, water did not fill the cap hole nor did water fill the hollow fiber by capillary action. Excitation occurred by scattering of the light through the cap and absorption of the radiation by the sensitizer adsorbed to the surface. The sensitizer-coated surface faced the bulk solution and O_2 transport occurred by a pressure gradient, diffusing through the membrane cap; bubbles effused slowly. Parts per million oxygen delivered to a 100 μL water sample via the fiber-compressed oxygen tank system in Figure 2 was determined with a pO_2 micro-oxygen electrode (Table 1). The capped fiber flowed O_2 about twenty times slower than the uncapped fiber. Other researchers have also demonstrated the transportation of gases through porous Vycor glass.[14-17]

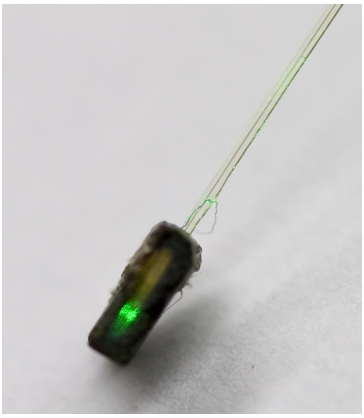

Figure 2. Image of the HC-580 fiber inserted into silica cap (length = 2.38 mm, bore diameter = 0.38 mm). Green light exited the distal end of the fiber. The absorption of light by the sensitizer occurs in the PVG cap.

Table 1. Quantities of oxygen delivered through a 30-cm segment of the HC-580 fiber into 100-μL H_2O from an oxygen tank at 40 PSI (room temperature)[1]

Uncapped Fiber		Capped Fiber	
Time (min.)	ppm/O_2 in H_2O	Time (min.)	ppm/O_2 in H_2O
5.0	8.59	34.0	8.75
10.0	9.03	64.0	8.95
21.0	9.59	129.0	9.32
30.0	9.99	184.0	9.48
50.0	10.35	214.0	9.57

[1] Porous Vycor glass cap (Dimensions: 3 mm^2 x 0.8 mm).

The experimental evidence suggested that singlet oxygen exited the distal end of the cap of the photosensitizer/fiber optic device and was trapped with *N*-benzoyl-DL-methionine anion (**2**, 0.02 M) in the surrounding aqueous solution (Figure 3). Only one

product was formed, *N*-benzoyl-DL-methionine S-oxide anion (**3**), which was monitored by ^{1}H NMR spectroscopy and is consistent with its literature assignment.[18,19] Methionine **2**, as the anion, does not adsorb onto the PVG, and no trace of methionine molecules pass through the PVG membrane. Dr. David Aebisher helped us to trap singlet oxygen by in H_2O and D_2O where *N*-benzoyl-DL-methionine S-oxide anion (**3**) used as chemical trap. The lifetime of $^1O_2$ increases by 20-fold in D_2O compared to H_2O;[20] however, the sulfoxidation reaction was found to be about two times faster in D_2O than H_2O (cf. 11% to 5%) after irradiation with the fiber device for 9 hours at pH 8. The 2-fold increase of sulfoxide in D_2O compared to H_2O was less than expected, and may relate to a surface effect (some singlet oxygen adsorption or quenching of singlet oxygen by anionic Si-O$^-$ sites). The exchange of Si-OH groups with D_2O to make Si-OD, potentially reducing surface physical quenching of singlet oxygen was not examined.[21]

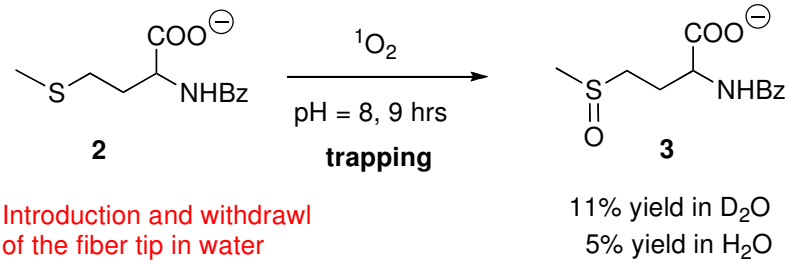

Figure 3. Photooxidation of *N*-benzoyl-DL-methionine anion 2 with the fiber device.

Steady-state (i)-(iv), control (v), and time-resolved experiments (vi) point to a singlet oxygen mechanism for the heterogeneous PVG sensitizer. (i) Quenching studies carried out with the singlet oxygen quencher sodium azide (2 mM) in D_2O, led to the reduced production of methionine S-oxide **3** (cf. 17% to 5%). (ii) Product yields were identical for the photooxidation of methionine **2** carried out in the presence of the radical scavenger *D*-mannitol (33 mM). (iii) Cumyl radical-derived products were not observed when using cumene radical scavenger in high concentrations, that is, when cumene was used as solvent. (iv) Previous studies[1] showed the photooxidation of *trans*-2-methyl-2-

pentenoate anion (**4**) afforded one main product, the hydroperoxide **5** from the singlet oxygen 'ene' reaction (^{1}H NMR spectra indicate 1-2% by-products derived from Type I reactions with oxygen radicals) (Figure 4). (v) Sulfoxidation of **2** did not take place in the dark. (vi) $^1O_2$ molecules were generated in aqueous media; in the absence of oxidizable reagents, $^1O_2$ was converted to $^3O_2$ physically, and was monitored by time-resolved $^1O_2$ ($^1\Delta_g$) phosphorescence at 1270 nm.[1] From studies of singlet oxygen diffusion, the square of distance (d) that an oxygen molecule travels during time (t) with the diffusion coefficient (D_o) is given by the equation $d^2 = 6D_o t$.[22-24] Thus, singlet oxygen is expected to diffuse a short distance (~150 nm) away from the silica cap into bulk H_2O.

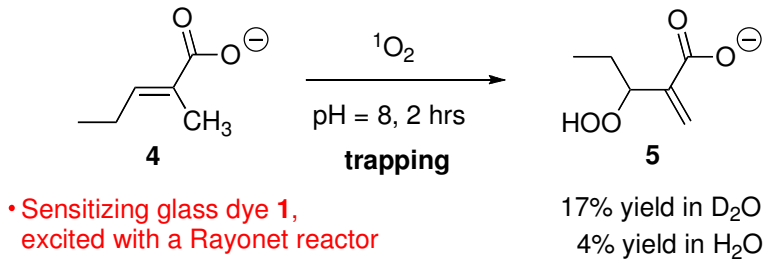

Figure 4. Photooxidation of *trans*-2-methyl-2-pentenoate anion 4 via "external" visible-light irradiation (Ref. 1).

3.3 Conclusion

This manuscript describes the development of a prototype (portable) singlet oxygen delivery device. The above data demonstrate that the oxygen-flowing fiber-capped configuration is suited for the heterogeneous generation of singlet oxygen in aqueous solution. The device is unique. Local concentrations of singlet oxygen can be delivered via introduction and withdrawal of the fiber tip.

3.4 Experimental Section

3.4.1 General Aspects. Porous Vycor glass (Corning 7930) was purchased from Advanced Glass and Ceramics (Holden, MA). *N*-Benzoyl-DL-methionine sodium salt (Aldrich), sodium azide (Aldrich), cumene (Aldrich), *D*-mannitol (Aldrich), *meso*-tetra(N-methyl-4-pyridyl)porphine tetratosylate (Frontier Scientific), and adipic acid (Monsanto Chemical Co.) were used as received. Deuterium oxide-d_2 (Aldrich), chloroform-d_1 (Aldrich), and acetonitrile-d_3 (Isotec, Inc.) were of spectrophotometric grade. Deionized H_2O was from a U.S. Filter Corporation deionization system (Palm Desert, CA). The 532-nm excitation source was either a AAA battery-powered green LED (5 mW, Astro Aimer II) or a New Wave Research Minilase-10 Hz Nd:YAG Q-switched laser (~4 ns FWHM, 3 mJ/pulse) (Fremont, CA). A hollow core photonic bandgap fiber HC-580 was used [core diameter of 4.9 μm, holey region diameter of 31 μm, silica cladding diameter of 89 μm, acrylate coating diameter of 220 μm, numerical aperture was 0.12 (Crystal Fibre Inc., Birkerød, Denmark)]. A Newport high-precision single-mode laser-to-fiber coupler (F-915) with an M-10X microscope objective focused the 532-nm light into the HC-580 fiber. The effective focal length of the M-10X microscope objective was 16.5 mm and its numerical aperture was 0.25. A Newport Teflon-lined fiber chuck (FPH-J) was used. The radiant power of the 532-nm light exiting the fiber was measured with a Nova energy meter (Ophir Optronics, Logan, UT). Fibers were cleaved with a 90° diamond wedge scribe, and the ends of the fibers were polished with diamond lapping polishing sheets (3 and 6 μm grain sizes) (Thor Labs, Newton, NJ). UV-visible spectra were collected on a Hitachi UV-VIS U-2001 instrument. NMR data were collected on a Brucker DPX400 NMR instrument. Mass spectrometry data were acquired on an Agilent Technologies 6890N GC/MS instrument with a 5973 Mass Selective Detector (MSD) and a HP-5MS column. A Rayonet photoreactor was used with Sylvania F8T5/CW 8 Watt bulbs that emit at ~425-650 nm.

Dissolved oxygen was measured with a pO_2 micro-oxygen electrode (2 mm tip) (Lazar Research Laboratories).

3.4.2 Fiber Modifications. A hole with the dimensions of 406 µm × 12.5 mm was drilled into one wall a polystyrene cuvette (10 mm path length, 4.5 mL, 12.5 mm^2×45 mm) (Fisherbrand). A diamond-head drill bit was used (UKAM Industrial Superhard Tools, Valencia, CA). Glued into this channel was a 0.25 mm ferrule (Valco Instruments, Houston, TX) so that the fiber could be threaded. The fiber protruded 2 mm beyond the ferrule collar and into the cuvette cavity. The cuvette was modified further by drilling a 3-mm hole into its PTFE cover and inserting a 200-µL Redi-tip (Fisherbrand). After gluing the cap and tip to the cuvette, the top of the cuvette was coupled to a 200 PSI compressed oxygen tank (gas regulator set to 40 PSI).

3.4.3 Cap Preparation, Adsorption and Desorption Studies. The sensitizer **1**-impregnated PVG cap was prepared for placement on the distal end of the hollow fiber. With silicon carbide sandpaper, PVG was sanded into a cylindrical shape (7.5 mm L × 3.5 mm diameter) or rectangular shape (3 mm^2 × 0.8 mm). The adsorption of **1** onto a 0.013 g rectangular piece of PVG was achieved by soaking the PVG cap in 15 mL of 3.3×10^{-5} M aqueous solution of **1** for 48 hours. A plateau was reached when there was 2.5×10^{-7} mol **1** adsorbed onto the PVG cap. The amount of **1** adsorbed onto PVG cap was calculated from the difference in absorbance of the solution before introduction of PVG and the absorbance of the same solution after the removal of PVG. The adsorption process was followed by monitoring the largest of the four Q-bands of **1-ads** at λ = 525 nm. The sensitizer-coated caps were rinsed with distilled water prior to use to remove any unbound **1**. A 2.38 mm x 0.38 mm core was drilled length-wise into the sensitizer-coated PVG cap. The 220 µm o.d. fiber was inserted into the cap hole and glued into place at the hole entrance. Desorption of **1** was not observed when sensitizer-coated PVG (7.5×10^{-7} mol **1** onto 1.5 g PVG) was placed into 2 mL of H_2O solution at pH = 3, 7, and 10 and stirred for 8 hours. No desorption of **1** was observed with Soxhlet

extraction, in which acetonitrile and methanol used as solvents; nor was desorption of **1** observed in a Soxhlet extractor with 2 N NaOH solution for 48 hours. Desorption of **1** (~70%) took place when the PVG cap was in a Soxhlet extractor in 2 N HCl over 48 hours.

3.4.4 Methionine Trapping Studies. Methionine trapping studies were conducted in 100 μL of H_2O and D_2O containing 0.02 M methionine **2**. The ratio of the void space inside the PVG cap to the 100 μL bulk solvent volume was ~1:300, in which ~0.3% of the solution volume resides in the cap relative to bulk solution. A sensitizer-coated PVG cap was immersed into H_2O and D_2O while connected to the fiber optic device. Oxygen flowed through the fiber during the irradiation of samples with the green LED for 9 hours. The long irradiation times were due to the low intensity of the radiation through the fiber cap. At less than 15% conversion, methionine S-oxide **3** was detected as the sole product based on ^{1}H NMR. Sulfone or cleavage products from *S*-hydroperoxysulfonium ylide chemistry were not observed.[25,26] The internal standard adipic acid (0.02 M) was added in order to determine the concentration of the photooxidation samples. The percent yield was determined by comparison of the sulfoxide with the methylene protons of adipic acid (internal standard) by ^{1}H NMR spectroscopy. The structure of *N*-benzoyl-DL-methionine S-oxide anion was elucidated by ^{1}H NMR (D_2O) δ 2.24 (m, 1H), 2.40 (m, 1H), 2.71 (s, 3H), 2.99 (m, 2H), 4.54 (m, 1H), 7.54 (m, 2H), 7.63 (m, 1H), 7.82 (m, 2H).

3.4.5 Further experiments included (1) a 1.0-mL D_2O solution containing methionine **2** (20 mM) and 2.5×10^{-7} mol **1** adsorbed onto 0.097 g PVG were placed in the dark for 10 hours, in which formation of methionine S-oxide **3** was not observed; (2) O_2 was bubbled into a 1.0-mL D_2O solution containing methionine **2** (20 mM) and 5×10^{-7} mol **1** adsorbed onto 0.34 g PVG, and into a 1.0-mL D_2O solution containing methionine **2** (20 mM), *D*-mannitol (33 mM), and 5×10^{-7} mol **1** adsorbed onto 0.34 g PVG; both solutions were irradiated with the Rayonet reactor for 4 hours, both led to methionine S-

oxide **3** in 21% yield; (3) O_2 was bubbled into a 2.0-mL D_2O solution containing methionine **2** (20 mM) and 5×10^{-7} mol **1** adsorbed onto 0.34 g PVG, and into a 2.0-mL D_2O solution containing methionine **2** (20 mM), sodium azide (2 mM), and 5×10^{-7} mol **1** adsorbed onto 0.34 g PVG; both solutions were irradiated with the Rayonet reactor for 4 hours, the formation of methionine S-oxide **3** was reduced in the latter case by 3-fold; and (4) O_2 was bubbled into a 2.0-mL cumene solution containing 5×10^{-7} mol **1** adsorbed onto 0.34 g PVG and was irradiated with the Rayonet reactor for 11 hours, in which formation of solvent radical-derived products, such as olefins were not observed.

3.5 References

1. Aebisher, D.; Azar, N. S.; Zamadar, M.; Gafney, H. D.; Gandra, N.; Gao, R.; Greer, A. *J. Phys. Chem. B* **2008**, *112*, 1913-1917.

2. Giaimuccio, J.; Zamadar, M.; Aebisher, D.; Meyer, G. J.; Greer, A. *J. Phys. Chem. B* **2008**, *112*, 15646-15650.

3. Peill, N. J.; Hoffmann, M. R. *Environ. Sci. Technol.* **1998**, *32*, 398-404.

4. Pradhan, A. R.; Uppili, S.; Shailaja, J.; Sivaguru, J.; Ramamurthy, V. *Chem. Comm.* **2002**, 596-597.

5. Matsuura, T.; Sato, H.; Suzuki, N.; Matsumoto, M. *J. Photoscience* **2002**, *9*, 409-411.

6. Podbielska, H.; Bindig, U.; Ulatowska-Jarza, A.; Holowacz, I.; Mueller, G.; Scheller, E. E. *Laser Physics* **2006**, *16*, 816-826.

7. Ollis, D. F.; Marinangeli, R. E. *AIChE J.* **1976**, *23*, 415-426.

8. Grandbois, M., Latch, D. E., McNeill, K. *Environ. Sci, Technol.* **2008**, *42*, 9184-9190.

9. Xiong, Z.; Xu, Y.; Zhu, L.; Zhao, J. *Environ. Sci. Technol.* **2005**, *39*, 651–657.

10. Borrelli, N. F. *Microoptic Technology* CRC Press, 2004, Cleveland, OH, pp. 389.

11. O'Shea, D. *Elements of Modern Optical Design*, Wiley Interscience, 1985, New York, NY; Ch. 7, pp. 257.

12. Henningsen, J.; Hald, J. *Appl. Optics* **2008**, *47*, 2790-2797.

13. Hoo, Y. L.; Ho, J. H. L.; Ju, J.; Wang, D. N. *Sensors Actuators B: Chem.* **2005**, *105*, 183-186.

14. Preethi, N.; Shinohara, H.; Nishide, H. *Bull. Chem. Soc. Jpn.* **2006**, *79*, 1308-1311.

15. Yang, J.; Čermáková, J.; Uchytil, P.; Hamel, C.; Seidel-M. A. *Catal. Today* **2005**, *104*, 344-351.

16. Uchytil, P.; Petrickovic, R.; Seidel-M. A. *J. Membrane Sci.* **2007**, *293*, 15-21.

17. Fernandes, N. E.; Gavalas, G. R. *Chem. Eng. Sci.* **1998**, *53*, 1049-1058.

18. Ranganathan, S.; Ranganathan, D.; Singh, S. K.; Bhattacharyya, D.; Shanthy, S.; Singh, G. P. *Tetrahedron* **1987**, *43*, 5363-5366.

19. Holland, H. L.; Brown, F. M. *Tetrahedron: Asymmetry* **1998**, *9*, 535-538.

20. Lindig, B. A.; Rodgers M. A. J. *J. Phys. Chem.* **1979**, *83*, 1683.

21. Iu, K.-K.; Thomas, J. K. *J. Photochem. Photobiol. A* **1993,** *71,* 55-60.

22. Wilkinson, F.; Helman, W. P.; Ross, A. B. *J. Phys. Chem. Ref. Data* **1995**, *24*, 663.

23. Schweitzer, C.; Schmidt, R. *Chem. Rev.* **2003**, *103*, 1685-1758.

24. Skovsen, E.; Snyder, J. W.; Lambert, J. D. C.; Ogilby, P. R. *J. Phys. Chem. B* **2005**, *109*, 8570-8573.

25. Clennan, E. L.; Pace, A. *Tetrahedron* **2005**, *61*, 6665.

26. Sawwan, N.; Greer, A. *Chem. Rev.* **2007**, *107*, 3247.

Chapter 4. Fiber Optic-Guided Photosensitizer Drug Delivery

4.1 Introduction

Only recently was a fiber-optic singlet oxygen (FOSG) device developed for the localized ‘‘delivery’’ of singlet oxygen.[1] The device consisted of a porous Vycor glass (PVG) cap coated with *meso*-tetra(N-methyl-4-pyridyl)porphine (**1**) fixed to the end of a hollow fiber-optic.[1] The hollow fiber flowed O_2 gas and guided 532 nm light from a continuous-wave or pulsed laser. The lifetime of photoexcited triplet-state adsorbed 1 was 57 μs and O_2 quenching at the water–PVG interface resulted in the formation of $^1O_2$ in aqueous solution.[2] Singlet oxygen is produced at the probe tip surface which is diffused out into the surrounding aqueous solution. But, singlet oxygen has lifetimes from microseconds to milliseconds and the corresponding diffusion distances of singlet oxygen range from nanometers to millimeters. To overcome the short diffusion distance of singlet oxygen from the cap, we have developed a fiber optic device with a maneuverable probe tip that sparges O_2 gas and photo-detaches pheophorbide (sensitizer) molecules. Among the *chlorophyll-a* family, the pheophorbide-a photosensitizer was chosen as a potential candidate for our study because of its lipophilicity. The major advantage is that pheophorbide will not strongly re-adsorb onto surface of the probe after photocleavage into surrounding solution. Additionally, it also present the selective accumulation in tumor, small toxicity and a photoxicity on tumor cells which can be 20-fold more efficient than hematoporphyrin derivatives, and the absorption around 660 nm and their monomeric state in organic solvents.[3] Singlet oxygen is produced at the probe tip surface which reacts with an alkene bridge causing the release of sensitizer upon fragmentation

of a dioxetane intermediate (Figure 1). Dioxetanes are 4-membered ring peroxides generated from singlet oxygen—alkene reactions, which readily cleave into carbonyl fragments. In 2008 Dolphin et al. reported a site-specific prodrug system, in which visible light was used to trigger drug release via facile cleavage of a dioxetane intermediate.[4] Thus, dioxetane cleavage is the basis of our research effort for releasing sensitizer from the probe into surrounding environment. The fiber optic device delivers pheophorbide molecules and singlet oxygen to discrete locations which may open the door to applications in tumor eradication in hydrophobic and hypoxic structures requiring cytotoxic control. In this chapter, we described the synthesis and charectiezation of ` pheophorbide sensitizer covalently attached with the probe (porous Vycor glass) by a photosensitive alkene spacer which behaves as a bridge between glass and photosensitizer. We also described their different loading onto the glass and how the different loading affects the photoclevage properties. We also presented the photocleavage properties depends on the medium, for example, photocleavage efficiency increases with lipophilicity of the medium.

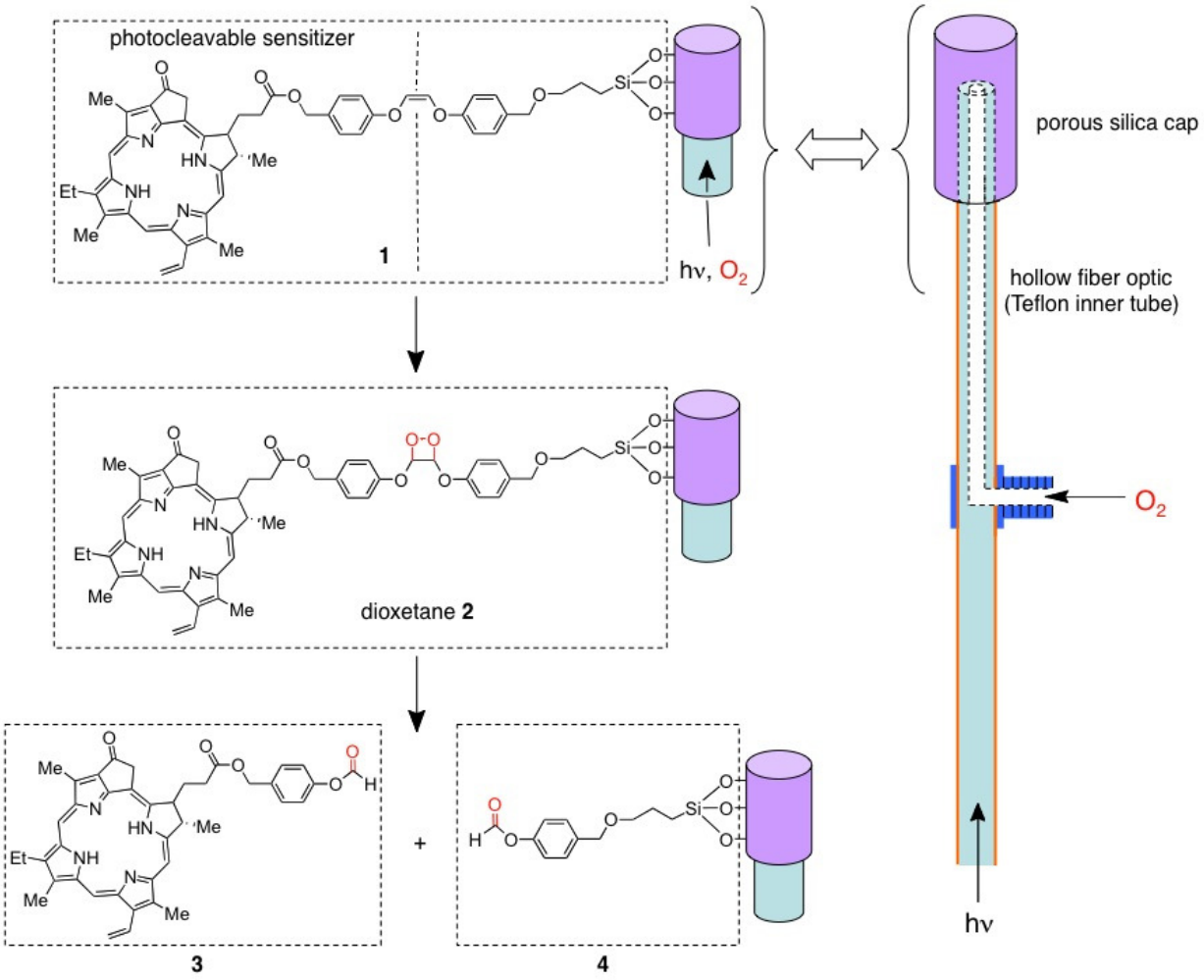

Figure 1. Concept of sensitizer photocleavage from the porous cap flowing oxygen and visible light through a hollow optical fiber. This graphic is adopted from Leda Lee.

4.2 Results and Discussion

4.2.1 Synthesis of the Sensitizer-Fiber Cap (Scheme 1). The conversion of 4-bromophenol (**5**) to *cis*-1,2-bis(4-bromophenoxy)ethene (**8**) was carried out in 3 steps using a known procedure.[5] *Meso*-**7** and *dl*-**7** were formed, and a separation of the *meso* was necessary to reach **8**, which reacted with *n*-BuLi and DMF to generate the bis-aldehyde (**9**) in 60% yield. Bis-aldehyde **9** reacted with sodium borohydride

quantitatively to give "spacer group" **10**. Spacer group **10** was prepared as a photocleavable group bridging the silica cap and the photosensitizer. Pyropheophorbide-*a* reacted with the **10**, EDC, and DMAP yielding pyropheophorbide monoester (**11**), which was purified and isolated in 60% yield.

Sensitizer **11** was converted to silane **12**, which was anchored to the fiber cap. Step vii covalently bonded silane **12** and 3-iodopropyltrimethoxy silane to the PVG cap. Ratios of the sensitizer to iodopropane to silanol sites were ~1:3:300 on cap **1**. Mn-Salen, and palladium silane catalysts have been loaded in 10-2000 μmol amounts onto silica particles, in which catalyst to iodosilane loading ratios were 1:3 to 1:200.[6] It is unlikely the covalently bonded iodosilane enhanced spin-orbit coupling and singlet oxygen production from increased population of triplet **1** because the loading was low compared to cases where enhancement was detected.[7]

Fiber cap **1** was stable in the dark, no sensitizer leaching was observed when the material was (i) repeatedly washed with toluene, THF, chloroform, ether, and hexane solvents, (ii) Soxhlet extracted with chloroform and ethanol, or (iii) immersed in solution at pH 2 or pH 12 for 4 h at room temperature. The filtrates of (i)-(iii) showed no photosensitizer activity. Since the fiber cap **1** showed no sensitizer released under these conditions, we concluded that **1** contained siloxane bonds where the sensitizer was chemically bound to the silica matrix. The FTIR data further bolstered the structural assignment of the saturated carbons of the spacer methylene groups of **1** (Figure 2).

The depth that the sensitizer penetrated into PVG was examined using a microscope equipped with a CCD camera. Figure 3 shows a sensitizer-attached PVG sample **1**, cut so that the depth of the sensitizer penetration into PVG could be viewed.

The sensitizer is localized on the outer surface of PVG reaching a depth of ~0.1 mm along the outer face of the cap. For comparison, $Ru(bpy)_3^{2+}$ penetrates 0.5 mm into PVG and *meso*-tetra(N-methyl-4-pyridyl)porphine penetrates 0.32 mm into PVG. Streptocyanine dyes also diffusives into silica gels and are influenced by the gel porosities.[8,2]

Scheme 1[a]. Synthesis of Sensitizer Functionalized Cap 1

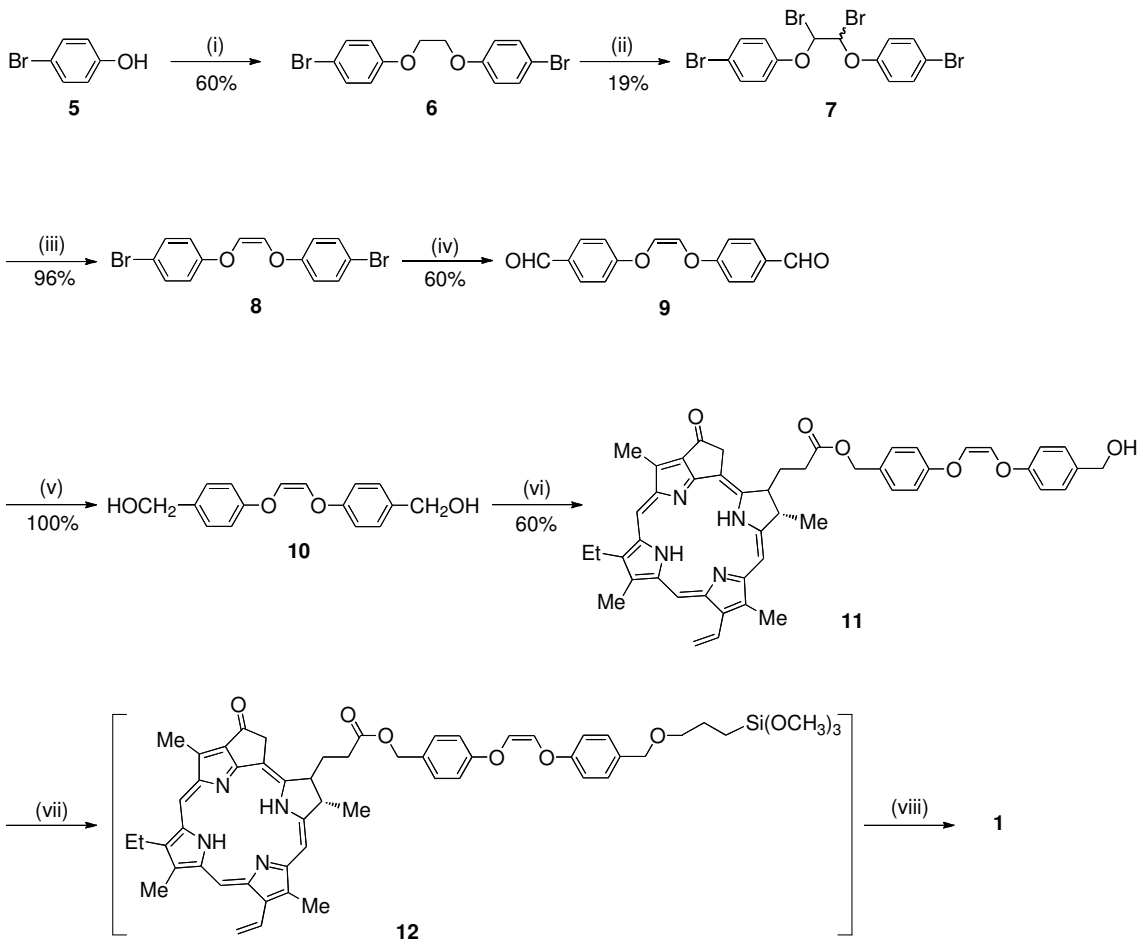

[a] Reagents and conditions: (i) $BrCH_2CH_2Br$, NaOH, 100 ^oC, 6 h; (ii) NBS, benzoyl peroxide, CCl_4, 80 ^oC, 6 h (*meso*-**7** was carried on to step iii); (iii) NaI, acetone, 25 °C, 2 h; (iv) *n*-BuLi, DMF, -78 °C, 3.5 h; (v) $NaBH_4$, CH_3OH, 25 °C, 14 h; (vi) pyropheophorbide-*a*, EDC, DMAP, CH_2Cl_2, 25 °C, 24 h; (vii) $(CH_3O)_3SiCH_2CH_2CH_2I$, NaI, THF, under N_2, 70 °C, 24 h; (viii) porous Vycor glass (pre-dried at 500 °C), toluene, reflux 110 °C, 24 h.

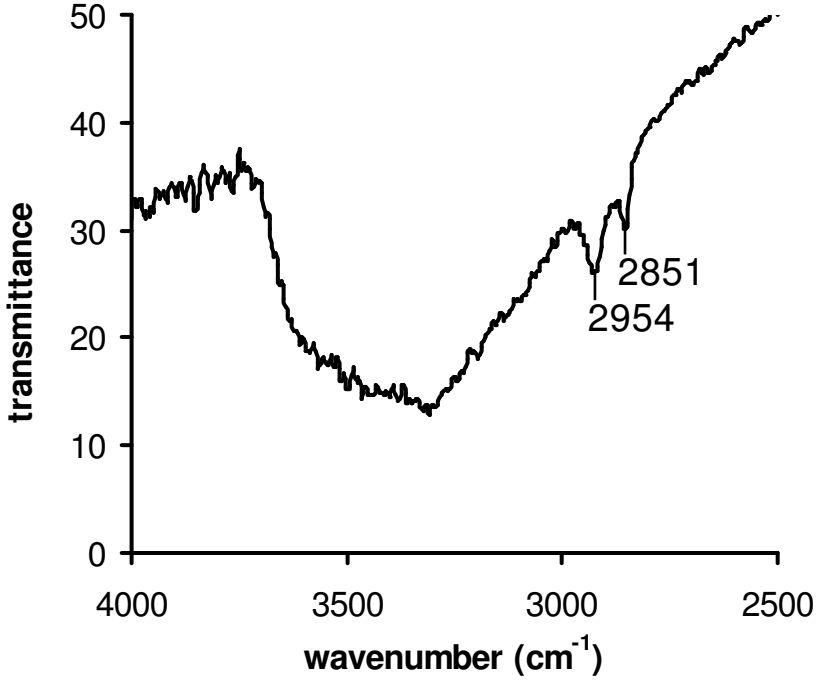

Figure 2. The FTIR spectrum of functionalized porous glass **1**, in which the C-H_x stretching modes observed at 2851 and 2954 cm^{-1} were assigned to saturated carbons of the spacer methylene groups indicating that **12** and $(CH_3O)_3SiCH_2CH_2CH_2I$ (1:3 ratio) were anchored to the porous Vycor glass surface. The FTIR spectrum of a clean piece of PVG was not identical, no C-H_x stretching modes were observed.

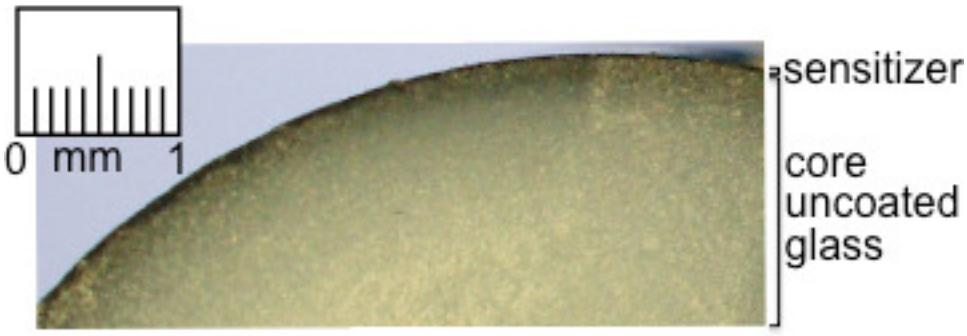

Figure 3. A low-magnification (10x) cross-sectional optical image. The dark green thin coating shows the depth of **1** accessed into PVG. The image shows ~0.1 mm penetration depth on the outer face of the cylinder-shaped PVG cap **1** (diameter 5.0 mm × length 8.0 mm).

4.2.2 Requirements for Sensitizer Loading Onto the Fiber Cap. Our goal was to maximize the amount of **3** that can be photocleaved from the probe tip (Figure 4). 0.06-1.1 µmol quantities of silane **12** were loaded onto porous Vycor glass per g, resulting in corresponding distances between the sensitizers of 8.9 to 38.4 nm (Table 1). We did not load mmol amounts of silane, even though this could be achieved due to the available silanol groups (1.66 mmol SiOH/g PVG).

The loading of 0.3 µmol (0.33%) sensitizer onto the fiber caps resulted in maximal photocleavage of **3**. Higher or lower sensitizer loadings reduced the photocleavage efficiency due to less available sensitizer and self-quenching, respectively (Figure 5). For example, a 3-fold mole increased loading of **12** resulted in an 11-fold decrease in sensitizer photocleavage (compare entries 2 and 5, Table 1). The results suggest that sensitizer molecules sufficiently isolated from each other (>17 nm) lead to more efficient cleavage, which agrees with self quenching by a neighboring sensitizer molecule by Förster resonance energy transfer (FRET), although congestion of sensitizer

molecules would also enhance unwanted $^1O_2$ physical quenching by the ground-state sensitizer. The next step was the attachment of the cap to the fiber optic and the ensuring oxygen flowed through the cap.

The cylinder-shaped cap **1** contains a hole (3.0 diameter × 2.0 mm length) to accommodate the fiber optic, which was glued to the end of the fiber optic. We found the transmission of oxygen gas through the pores of the water-saturated PVG membrane tip and into solution occurred at a rate of 0.19 ppm/min at 2 PSI, and 0.31 ppm/min at 10 PSI as measured by a dissolved oxygen meter (Table 2). In anaerobic conditions, the O_2 flow increased the photocleavage efficiency, but in air-saturated conditions the rate was too slow to have a significant impact on the photocleavage efficiency. Thus, a ~15 ppm egress of oxygen gas was observed over a 1-h period requiring about 40 min at 10 PSI for an anaerobic solution to become oxygen saturated. Oxygen gas is permeable and can pass through the connected pores of PVG, which is expected to reach the excited sensitizer sites of **1**, controlled by Knudsen diffusion, in which O_2 collides numerous times within the pore walls, eventually proceeding through the PVG channels.[9]

Table 1. Loading of Pheophorbide Silane 12 onto Porous Vycor Glass[a]

Entry	loaded,%[b]	ratio sens:SiOH	ave. sens-sens distance (nm)	photocleavage,%[c]
1	0.068	1:1470	38.4 nm	2.1
2	0.33	1:290	17.1 nm	6.06
3	0.48	1:210	14.5 nm	3.32
4	0.60	1:170	12.9 nm	1.42
5	0.99	1:100	10.0 nm	0.53
6	1.24	1:80	8.9 nm	0.39

[a] The sensitizer is thinly coated, it reaches a maximum depth of 0.1 mm into PVG. The percent of sensitizer loaded onto PVG was defined as the number of sensitizer molecules attached vs the number of silanol groups at a depth of 0.1 mm.
[b] The sensitizer loadings onto the PVG matrix were varied by the ratio of **12** and $(CH_3O)_3SiCH_2CH_2CH_2I$ added into the 50 mL THF reaction solution. The range was 0.06 to 1.1 µmol sensitizer silane **12** with concomitant decreases of iodosilane from 0.84 to 0.32 µmol. That is the range was **12** to iodosilane ranged from a ration of 1:14 to 1:0.3.
[c] White light from a Rayonet reactor was used to photocleave the sensitizer.

Table 2. Oxygen Permeability Through Porous Fiber Tip.

	ppm O_2 in H_2O[a]		increase, %	
time (min)	2 PSI	10 PSI	2 PSI	10 PSI
0	7.1	6.7	0	0
10	9.3	10.4	12	25
20	11.3	13.5	36	62
30	12.7	15.7	53	88

[a] Quantities of oxygen delivered through the hollow fiber optic cable (3-m) into 30.0 mL of H_2O from a compressed oxygen tank at room temperature and 760 torr. PVG fiber tip dimensions: cylinder shape with a length of 8.0 mm, diameter of 5.0 mm, and hole (3.0 diameter × 2.0 mm length).

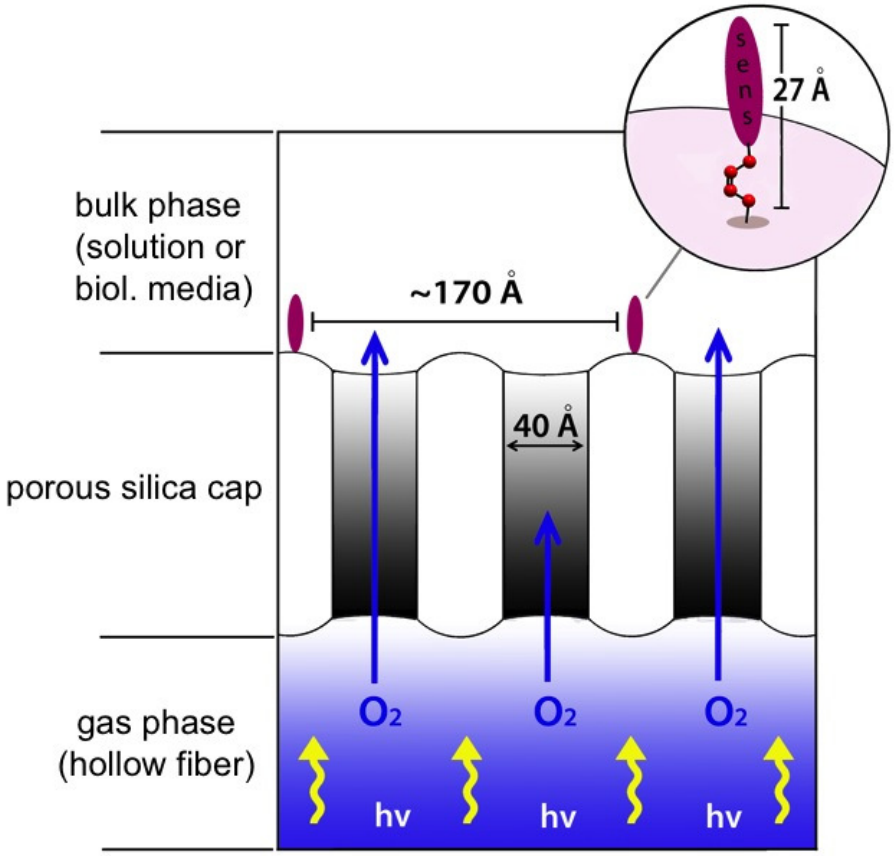

Figure 4. Schematic of the sensitizer functionalized porous cap **1** where oxygen and light come internally from the hollow optical fiber. Typically 0.3 μmol or 0.33% silane **12** was loaded per gram porous Vycor glass. The sensitizer may adopt various conformations on the isotropic PVG material. PVG is a transparent material with ~4 nm diameter pores and a ~200 m^2/g surface area. PVG has interconnected pores and the surface has "stalagmite-like" features that are ~3 nm in length and width. This graphic is adopted from Leda Lee.

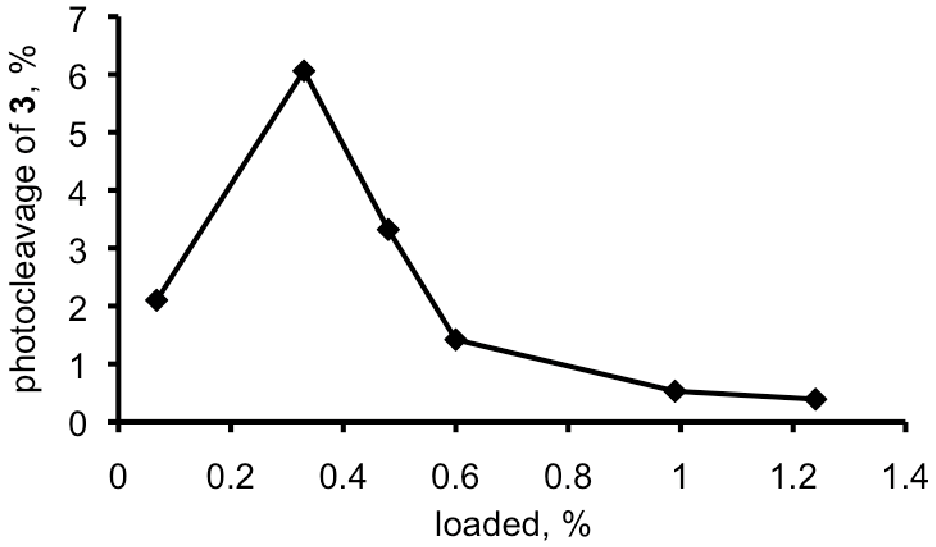

Figure 5. Percent photocleavage of **3** released into toluene-d_8 solution from the porous cap **1**. Silane **12** was loaded in 0.06 to 1.1 μmol amounts (0.068 to 1.24%) onto porous Vycor glass per gram and were exposed to visible light (xx mJ/cm^2).

4.2.3 Fiber Optic-Initiated Photocleavage of the Attached Sensitizer. We determined the performance of our fiber-optic probe and analyzed the dose released. These studies were performed with light from the 250-W illuminator coupled to the fiber optic that delivered visible light and oxygen to the sensitizer tip.

The amount of sensitizer molecules released from the probe tip depended on the medium in which the probe tip is placed (Figure 6). Quantitative sensitizer departure occurred in petrolatum in 4 h. The fluorescence intensity measured the diffusion distance of the sensitizer from the fiber-optic probe in the petroleum gel media (Figure 7). Bonnie I. Kruft and Dr. David Aebisher carried out petrolatum experiment.

Unlike petrolatum, sensitizer departure from the probe tip was not observed in agar. It was inefficient in toluene (5%) and water (<1%) due to poor solvation of the

hydrophobic sensitizer. Figure 8 shows the amount of sensitizer that results from photorelease into toluene-d_8 solution, it is a plot of sensitizer release, A vs time. The increase in A indicates the release into solution with a maximum at ~7300 nM. In the dark, the photoreleased product does adsorb back to surface via noncovalent association in toluene-d_8. After 12 h in the dark, all photoreleased **3** adsorbs onto the cap in solution. We found that adsorption plays a role in dampening photorelease. Soxhlet extraction of the photolyzed solid resulted in dissociation of **9** into the surrounding solution. In the latter cases, sensitizer **3** remained adsorbed onto the probe tip even though the alkene bridging the sensitizer and glass was destroyed. PVG contains hydrophilic silanol groups in an otherwise hydrophobic matrix.

The sensitizer payload release showed an extreme affinity of **3** into the hydrophobic petrolatum medium. Petrolatum (soft paraffin, a semi-solid mixture of hydrocarbons). These observations show that the nonpolar **3/4** adsorbate is influenced to depart based on the medium. Hydrophobic sensitizers can be delivered across plasma membranes.[10] Due to its hydrophobic character, pheophorbide **3** desorbs away from the probe surface.

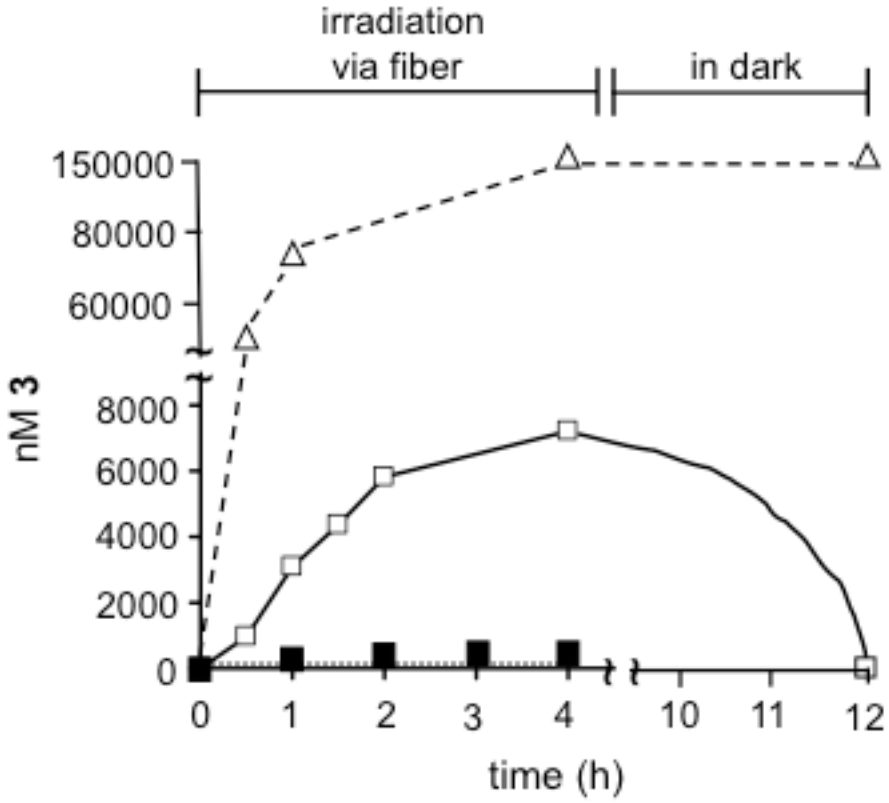

Figure 6. Plot of nanomolarity of **3** arising from fiber tip **1** upon photooxidation over time. Photocleavage of **3** away from the sensitizer device cap **1** into in petrolatum (open diamonds) at 65 °C and into D_2O (solid squares) and toluene-d_8 (open squares) at room temperature.

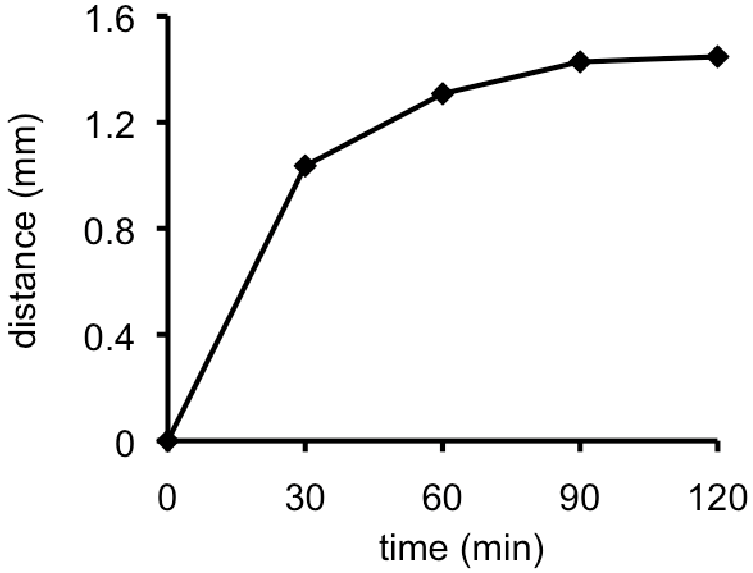

Figure 7. Time course of photorelease of **3** into petrolatum at 65 °C and the diffusion of the sensitizer away from the probe tip.

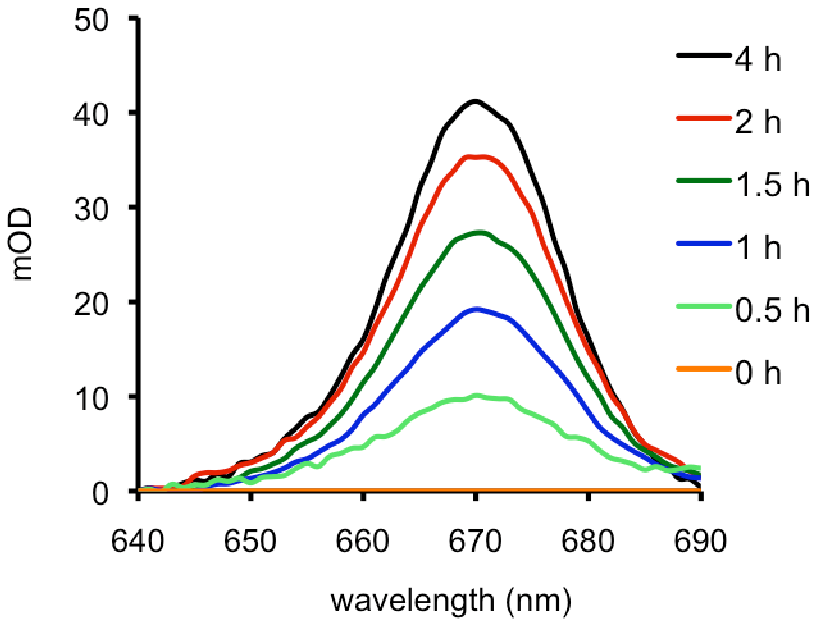

Figure 8. Time course of photorelease of **3** into toluene-d_8 solution arising from photooxidative cleavage *and* departure from the fiber optic device tip. The absorption spectra show the fourth Q-band of **3** and were normalized at 640 nm: (a) orange, (b) turquoise 0.5 h, (c) blue 1.0 h, (d) green 1.5 h, (e) red 2.0 h, and (f) black 4.0 h.

4.3 Conclusion

A porous fiber optic cap with a photo-detachable pheophorbide sensitizer was prepared. No leaching of the photosensitizer was observed in the dark. The loading of 0.33% sensitizer **11** onto the porous caps resulted in maximal photocleavage. Higher or lower sensitizer loadings reduced the photocleavage efficiency due to less available sensitizer and self-quenching, respectively. The probe tip sparges O_2 gas to hypoxic sites at a rate of ~15 ppm O_2 per hour in water. Visible light and O_2 gas were co-administered through the porous fiber optic tip. Singlet oxygen peroxidation of the alkene spacer group of the probe tip surface led to dioxetane formation. Rapid dioxetane cleavage provided

the means to break the alkene bond. The amount of sensitizer molecules released from the probe tip depends on the medium in which the probe tip is placed. Quantitative sensitizer departure occurred in petrolatum, but this was less efficient in other media (5% in toluene, 0% in water, 0% in agar, and 0% in acrylamide) due to the permeability of the pheophorbide compound in lipophilic. In the latter cases, sensitizer **3** remained adsorbed onto the probe tip even though the alkene bridging the sensitizer and glass was destroyed.

Optimization of the photoclevage reaction in different solvent medium, under different temperature, studies on biological system, and trapping of dioxetanes intermediate on the glass surface experiment will be presented in future.

4.4 Experimental Section

4.4.1 Materials and Instrumentation. Corning 7930 porous vycor glass was purchased from Advanced Glass and Ceramics, Holden, MA. Pyropheophorbide-a was purchased from Frontier Scientific and was used as received. Spectrophotometric grade toluene-d_8, deuterium oxide-d_2, chloroform-d_1 were purchased from Sigma Aldrich or Cambridge Isotope Laboratories and were used as received. Acetonitrile-d_3 was purchased from Isotec, Inc. Deionized water was purified using a U.S. Filter Corporation deionization system. Reagents and solvents such as NaOH, 4-bromophenol, 1,2-dibromoethane, CH_2Cl_2, CCl_4, benzoyl peroxide, acetone, NaI, sodium thiosulfate, ethanol, *n*-BuLi, DMF, NH_4Cl, anhydrous Na_2SO_4, MeOH, $NaBH_4$, DMAP, EDC, NaH, 3-iodopropyltrimethoxysilane, toluene, and THF were purchased from Sigma Aldrich and used without further purification. Column chromatography was carried out on silica gel

40-60 Å particles. TLC was conducted on silica gel 60F 254 TLC-plates. The radiant power of the visible light exiting the fiber was measured with a Nova energy meter from Ophir Optronics, Logan, UT. Dissolved oxygen was measured with a Hach sens-ION6 dissolved oxygen meter. Proton NMR spectra were acquired at 400 MHz and ^{13}C NMR spectra were acquired at 100.6 MHz on a Bruker DPX400 MHz instrument. HRMS data were obtained on Agilent 6220-TOF coupled with 1200 series LC. GC/MS data were acquired on Agilent 6890N coupled with 5973 MSD. HPLC data were obtained on a Perkin-Elemer 200 series instrument equipped with bondclone 10 C18 column at 254 nm and FTIR spectra were collected on a Perkin-Elmer Spotlight Imaging System. The melting points were obtained on a MEL-TEMP apparatus. UV-visible spectra were collected on a Hitachi UV-VIS U-2001 instrument. Fluorescence spectra were collected on a Nikon Eclipse TE 200 inverted epifluorescence microscope. Elemental analyses were conducted by Atlantic Microlab, Inc. (Norcross, GA). A Rayonet photoreactor fitted with Sylvania visible light bulbs was used.

4.4.2 Construction of the Fiber Optic Apparatus. The portable system consisted of a 250-W quartz-halogen illuminator (Fiberoptic Systems, Inc., Simi Valley, CA), a custom-made fiber-optic cable, a compressed oxygen gas tank, and a porous Vycor glass tip. CUT OFF FILTER TOO An integral dichroic reflector was used to focus the light of the illuminator into the proximal end of the optical fiber. The 3 ft 0.55 NA borosilicate fiber optic used had an external diameter of 1.4 mm including the jacket black PVC and consisted of a 1.1 mm diameter Teflon gas flow tube running from the distal end to a T valve surrounded by ~350 excitation fibers (diameter 300 μm) randomized in a ring around it capable of delivering 2-5 W out of the end of the fiber

bundle. The T value of the fiber was connected to a 200 PSI compressed oxygen tank with the gas regulator set at 2-10 PSI. The PVG cap had a hole drilled into it and was inserted at the end of the fiber that received the excitation light and oxygen gas. Because the o.d. of the fiber optic was often just slightly larger than that of the cap, gluing the two together was not always necessary, which made withdrawal and reuse of the cap easy. Oxygen was delivered through the Teflon gas-flowing tube of the fiber optic to the porous cap then into solution. An adapter for other end of the fiber fit to the illuminator (secured by a socket cap screw). PVG caps were shaped into rectangular pieces with a Buehler IsoMet Low Speed Saw (Model 11-1280-160). Holes were drilled with a Buehler ultrasonic disc cutter (Model 170) and drill dremel (Model 200). Finally, pieces were shaped into a cylindrical shape using a Buehler variable speed grinder-polisher. The dimensions of the caps were 7.5 mm × 4 mm × 1 mm.

4.4.3 Synthesis and Characterization

1,2-Bis(4-bromophenoxy)ethane (6). Yield 32.7 grams (57 %). To a solution of sodium hydroxide (12.4 g, 0.31 mol) in water (50 mL) was added 4-bromophenol (51.7 g, 0.3 mol). The mixture was stirred at 60-70 °C for 0.5 h followed by addition of 1,2-dibromoethane (26.3 g, 0.14 mol). The resulting mixture was then heated at reflux for 6 h. After cooling, the white solid was separated from the reaction mixture by filtration at room temperature. The solid was purified by recrystallization from ethanol and dried in vacuo. mp 130-132 °C; ^{1}H NMR (400 MHz, $CDCl_3$) δ 7.38 (d, J = 9.20 Hz, 4H), 6.82 (d, J = 9.20 Hz, 4H), 4.27 (s, 4H); ^{13}C NMR (400 MHz, $CDCl_3$) δ 157.68, 132.35, 116.50, 113.43, 66.70 (lit. data for **6**, ref 5); mp 130-132 °C; ^{1}H NMR (250 MHz, $CDCl_3$) δ 7.37(d, J = 6.85 Hz, 4H), 6.81 (d, J = 6.85 Hz, 4H), 4.25 (s, 4H); ^{13}C NMR (250 MHz, $CDCl_3$) δ 157.45, 132.33, 116.48, 113.41, 66.68.

***meso*-1,2-Dibromo-1,2-bis(4-bromophenoxy)-ethane (*meso*-7).** Yield *meso*-**7**, 0.82 g (17%). In 50 mL of carbon tetrachloride was dissolved 3.37 g (9.06 mmol) **6**, 3.95 g (22.19 mmol) of *N*-bromosuccinimide, and 0.54 g (2.23 mmol) of benzoyl peroxide. The resulting solution was heated at reflux for 6 h. After being cooled to room temperature, the mixture was filtered and the crude products obtained from the filtrate by evaporating the solvent. The crude product was purified by silica gel chromatography (230-400 mesh; 6:1 hexane/ dichloromethane) yielded pure *meso*- and *dl*-**7**. mp (*meso*-**7**) 140-142 °C; ^{1}H NMR (400 MHz, $CDCl_3$) δ 7.51 (d, J = 9.04 Hz, 4H), 7.08 (d, J = 9.04 Hz, 4H), 6.50 (s, 2H); ^{13}C NMR (400 MHz, $CDCl_3$) δ 154.25, 132.91, 118.89, 117.37, 85.31 (lit. data for **7**, ref 5); mp 140-142 °C; ^{1}H NMR (500 MHz, $CDCl_3$) δ 7.51 (dd, J = 8.95, 1.25 Hz, 4H), 7.08 (dd, J = 8.95, 1.25 Hz, 4H), 6.51 (s, J = 6.2 Hz, 2H); ^{13}C NMR (250 MHz, $CDCl_3$) δ 153.72, 132.89, 118.87, 116.97, 85.31.

***cis*-1,2-Bis(4-bromophenoxy)ethene (*cis*-8)**. Yield 0.35g (95%). The *meso*-**7** (0.54 g, 1.02 mmol) was dissolved in 20 mL of acetone. Sodium iodide (0.45 g, 3 mmol) was then added to this solution. The reaction mixture was stirred for 2 h at room temperature. A deep red color of the solution was developed. Solvent was evaporated in rotary vap. Water (25 mL) and dichloromethane (100 mL) were added to the flask with continuous stirring. A saturated aqueous solution of sodium thiosulfate was added until the solution became colorless. The organic layer was then separated, dried over anhydrous $NaSO_4$, and evaporated to get a small amount of a solid. The solid was purified by recrystallization from ethanol to obtain *cis*-**8** (mp: 102-105 °C) ^{1}H NMR (400 MHz, $CDCl_3$) δ 7.42 (d, J = 9.04 Hz, 4H), 6.97 (d, J = 9.04, 4H), 6.11 (s, 2H); ^{13}C NMR

(400 MHz, $CDCl_3$) δ 156.33, 132.56, 128.49, 117.97, 115.42 (lit. data for **8**, ref 5); mp 102-104 °C; ^{1}H NMR (500 MHz, $CDCl_3$) δ 7.42 (d, J = 9.04 Hz, 4H), 6.97 (d, J = 9.04, 4H), 6.11 (s, 2H); ^{13}C NMR (250 MHz, $CDCl_3$) δ 156.30, 132.54, 128.46, 117.94, 115.40.

(*Z*)-4,4'-(Ethene-1,2-diylbis(oxy))dibenzaldehyde (9). Yield 0.30 g (60%). To the 0.5 g of arylbromide **8** in 5 mL THF, 1.6 mL of (0.003 mol) *n*-BuLi was added and the solution stirred at -78 °C for 0.5 h. DMF (0.0058 mol, 0.5 mL) was added to the reaction mixture and stirred for 20 min at -78 °C. The solution was warmed up to the room temperature and stirred for another 3.5 h. The reaction mixture was quenched with 20 mL cold saturated aqueous NH_4Cl and then 25 mL of CH_2Cl_2 was added to that solution. Organic layer was washed with saturated sodium chloride solution dried with Na_2SO_4. Evaporation of organic layer resulted crude liquid, which was purified by column chromatography (3:1 hexane and ethyl acetate) to yield **9** (mp 108-110°C). R_f = 0.15; ^{1}H NMR (400 MHz, $CDCl_3$) δ 9.93 (s, 2H), 7.88 (d, J = 8.80 Hz, 4H), 7.20 (d, J = 8.68 Hz, 4H), 6.34 (s, 2H). ^{13}C NMR (100 MHz, $CDCl_3$) δ 116.2, 128.4, 131.8, 131.9, 161.5, 190.5. HRMS calcd for $C_{16}H_{12}O_4$ $(M + H)^+$ 268.0736, found: 268.0736.

(*Z*)-(4,4'-(Ethene-1,2-diylbis(oxy))bis(4,1-phenylene))dimethanol (10). Yield 97 mg (100%). To the 100 mg (0.37 mmol) of **9** in 2.5 mL MeOH, 0.140g (1.86 mmol) $NaBH_4$ was added in small portions. The reaction mixture was stirred for 14 h. Methanol solvent was evaporated out from the reaction mixture and quenched with saturated aqueous NH_4Cl solution Ethyl acetate was added to the solution mixture. Organic layer was separated and dried over Na_2SO_4. After the evaporation of organic solvent to give a pure solid 5 (mp: 150-153 °C). ^{1}H NMR (400 MHz, $CDCl_3$) δ 7.33 (d, J = 8.52 Hz, 4H),

7.09 (d, J = 8.52 Hz, 4H), 6.15 (s, 2H), 4.66 (d, J = 5.52, 4H). ^{13}C NMR (100 MHz, $CDCl_3$) δ 64.3, 116.1, 128.3, 128.4, 135.5, 156.8. HRMS calcd for $C_{16}H_{16}O_4$ $(M + H)^+$ 272.1049, found: 272.1047. To determine the acid stability of the alkene linkage of bis-alcohol **10**, 0.02 M of **10** with 0.02 M dilute hydrochloric acid (pH 2) with 1.1x10-4 M 1-pentanol as the internal standard with stirring in 2 mL $CDCl_3$. The solution was stirred and monitored by ^{1}H NMR after 0, 60, and 120 min with no degradation or loss of the alkene peaks observed.

(*Z*)-4-[2-(4-Hydroxymethyl-phenoxy)-vinyloxy]benzyl-pyropheophorbide (11). Yield 6 mg (60%). 10 mg (0.018 mmol) of commercially available pyrpheophorbide, 5.0 mg (0.018 mmol) of bis alcohol **10**, 2.28 mg (0.018 mmol) of DMAP, and 5.37 mg (6.9 mmol) of EDC dissolved in 3 mL of DCM solution. After stirring overnight at room temperature, DCM was evaporated from the reaction mixture and the crude product was purified on the column (1% methanol in $CHCl_3$) yielding a black solid. R_f = 0.48. ^{1}H NMR (400 MHz, $CDCl_3$ δ 9.51 (s, 1H), 9.40 (s, 1H), 8.54 (s, 1H), 8.01 (dd, J = 17.8, 11.52 Hz, 1H), 7.29 (d, J = 8.48 Hz, 2H), 7.14 (d, J = 8.48 Hz, 2H), 7.03 (d, J = 8.48 Hz, 2H), 6.64 (d, J = 8.48 Hz, 2H), 6.28 (d, J = 17.86 Hz, 1H), 6.17 (d, J = 11.52 Hz, 1H), 6.08 (dd, J = 17.05 Hz, 3.36, 2H), 5.24 (d, J = 19.80 Hz, 1H), 5.06 (d, J = 19.85 Hz, 1H), 4.94 (dd, J = 29.73 Hz, 12.12 Hz, 2H), 4.61 (s, 2H), 4.46 (d, J = 7.08 Hz, 1H), 4.28 (d, J = 8.32 Hz, 1H), 3.70 (q, J = 7.18 Hz, 4H), 3.40 (s, 3H), 3.24 (s, 3H), 2.61 (m, J = 8.04 Hz, 2H), 2.31 (m, J = 5.85 Hz, 2H), 1.78 (d, J = 7.24 Hz, 3H), 1.70 (t, J = 7.62 Hz, 3H), -1.68 (s, 1H). ^{13}C NMR (100 MHz, $CDCl_3$) δ 11.2, 12.0, 17.4, 19.5, 23.1, 29.7, 29.8, 31.1, 48.0, 49.9, 51.6, 64.8, 65.9, 93.0, 97.2, 104.1, 106.1, 116.1, 116.3, 122.5, 128.1, 128.3, 128.5, 128.6, 129.2, 130.0, 130.1, 130.5, 130.6, 131.5, 135.4, 135.9,

136.1, 136.2, 137.9, 141.5, 145.0, 149.0, 150.8, 155.2, 156.9, 157.3, 160.2, 171.3, 172.8, 196.1. HRMS calcd for $C_{49}H_{48}N_4O_6$ $(M + H)^+$ 788.3573, found: 788.3563.

Pheophorbide-Modified Glass (1). Covalent bonding of the sensitizer to the PVG was achieved by adding pyropheophorbide monoester **11** (10 mg, 0.0126 mmol) to 3-iodopropyltrimethoxysilane (0.250 mmol) and NaI (0.302 mg, 0.0126 mmol) in 5 mL dry THF, and refluxing the mixture at 70 °C for 24 h. THF was evaporated under N_2 leaving the pyropheophorbide–trimethoxysilane **12** residue, which was added to 100 mL dry toluene and porous Vycor glass (3.2 g pre-dried at 500 °C in a muffle furnace) and refluxed at 110 °C for 24 h. After the synthesis of **1**, no leaching of the photosensitizer was observed. Control experiments were carried out in order to establish that the sensitizer molecules derived from **12** were anchored and not adsorbed to the silanol groups of PVG. Any silanes that were not covalently attached to the PVG surface were washed away with toluene, THF, chloroform, ether, and hexane, followed by Soxhlet extraction with methanol for 24 h. In the absence of 3-iodopropyltrimethoxysilane and NaI a weaker non-covalent interaction exists between **11** molecules and PVG that were readily carried off the surface by solvent washing and Soxhlet extraction. The heterogeneous sensitizer **1** was recovered by drying under vacuum at rt for 12 h. UV (air) λ: 415 (Soret band), 510, 539, 612, and 659 nm; FT-IR: 2851 and 2954 cm^{-1}.

Colorless porous glass tips were converted to a deep maroon color when silane **12** was anchored on the cylinder shaped

4.4.4 Sensitizer Coverage Measurements. Goutam Ghosh, a graduate student in our lab helped us in determining the loading of sensitizer onto glass surface and how photoclevage efficiency is affected with different loading of sensitizers onto the glass.

The sensitizer was exposed from the PVG surfaces by dipping **1** into a 26% hydrofluoric acid solution for 30 min adapted from a procedure developed previously.[11] Amount of photosensitizer bonded onto PVG was calculated from the difference in absorbance of the solution before introduction of PVG and the absorbance of the same solution after the PVG's removal and the absorbance of the solution after Soxhlet extraction [at the λ_{max} value of pyropheophorbide-derivative (415 nm)].

For instance, 50% adsorption of **10** took place in 2.5 h. After 24 h, all photoreleased **10** adsorbs onto the cap in solution.

Porous Vycor glass was pre-dried at 500 °C with a muffle furnace for 24 hours prior to use. 3-iodopropyltrimethoxysilane (0.501 g, 1.72 mmol) was added dropwise onto porous Vycor glass suspended in anhydrous toluene solution (50 mL) under Ar. The solution was refluxed for 24 hours. The functionalized porous glass was taken off from the solution, thoroughly washed with toluene, hexane, ethanol, diethyl ether and Soxhlet extracted methanol for 24 hours, and dried under vacuum at room temperature. The functionalization of the solid was estimated from the carbon content: 1.03% C, 0.215 mmol of C_4H_9I per gram PVG. (Elemental analysis report %C=1.03, % H= 0.33, %I= 2.54).

4.4.5 Oxygen Flow Measurements. Dr. David Aebisher measured the rate of oxygen flow through the porous vycor cap using a Hach sensION6 Dissolved Oxygen Meter. 30mL of distilled H_2O was added to a glass container. The oxygen meter and the fiber optic cable attached to the glass tip were placed simultaneously inside of the water sample. Oxygen flowed through the fiber optic cable at 10 psi and 2 psi. Measurements were taken from the oxygen meter at one minute intervals for a total of thirty minutes.

For example, after 30 min at 2 PSI an increase in oxygen concentration of 53% beyond the starting air-saturated concentration (2.6×10^{-4} M). The rate of O_2 flow is 4.0×10^{-9} mL/min (0.19 ppm/min) at 2 PSI, and 7×10^{-9} mL/min (0.31 ppm/min) at 10 PSI respectively.

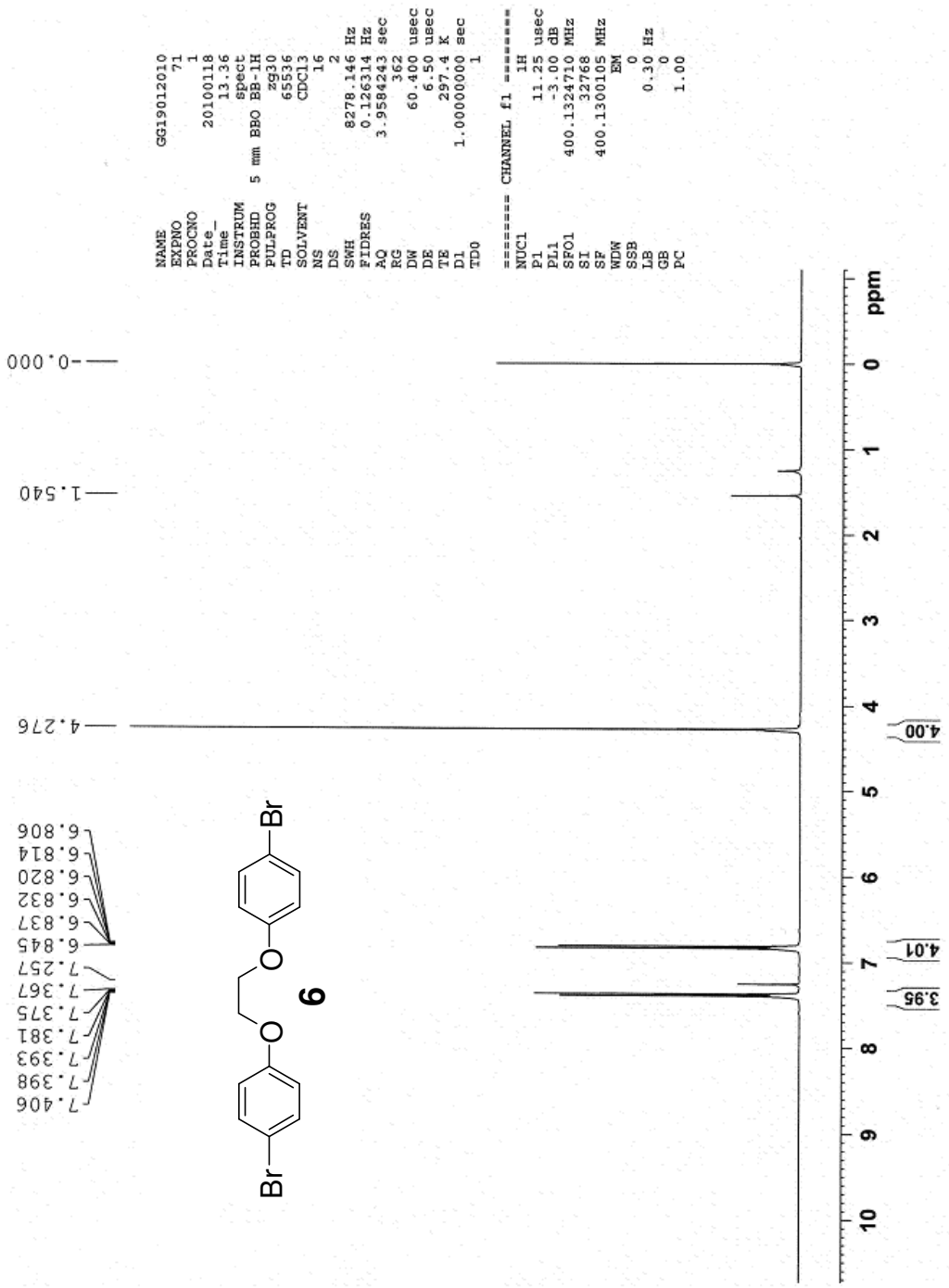

Figure 9. ^{1}H NMR of 1,2-Bis(4-bromophenoxy)ethane (**6**) in $CDCl_3$.

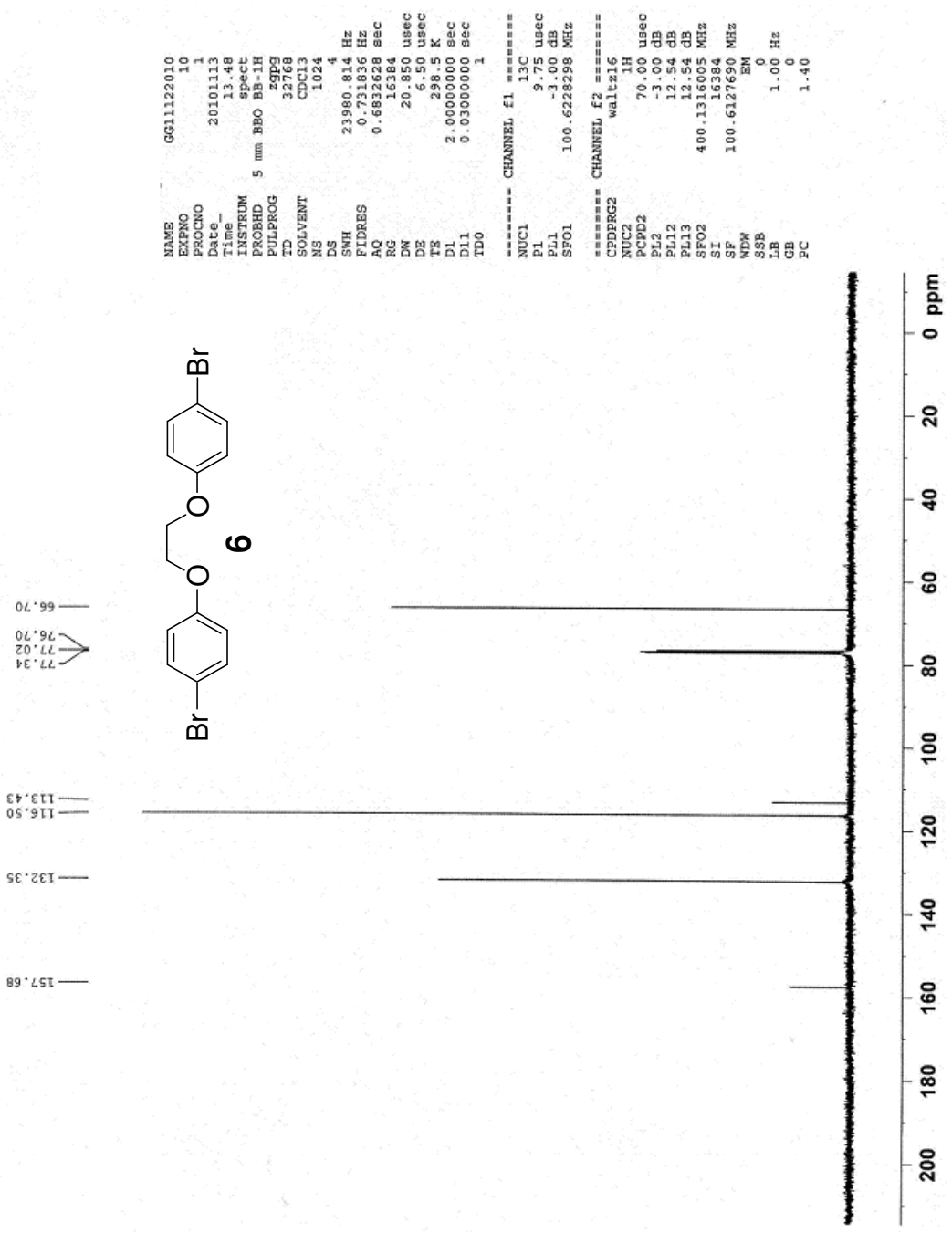

Figure 10. ^{13}C NMR of 1,2-Bis(4-bromophenoxy)ethane (**6**) in $CDCl_3$.

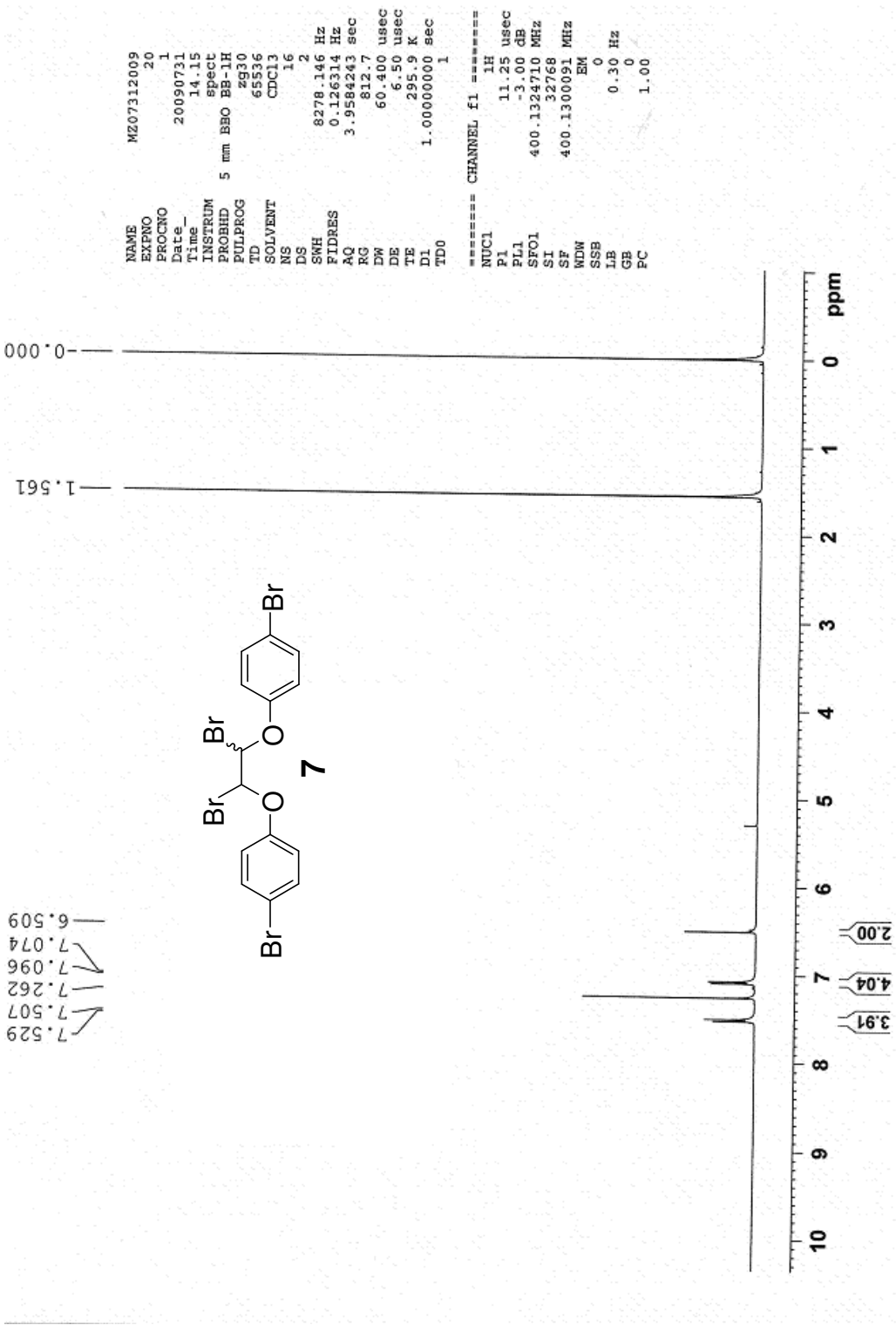

Figure 11. ^{1}H NMR of *meso-* and *dl*-1,2-Dibromo-1,2-bis(4-bromophenoxy)-ethane (**7**) in $CDCl_3$.

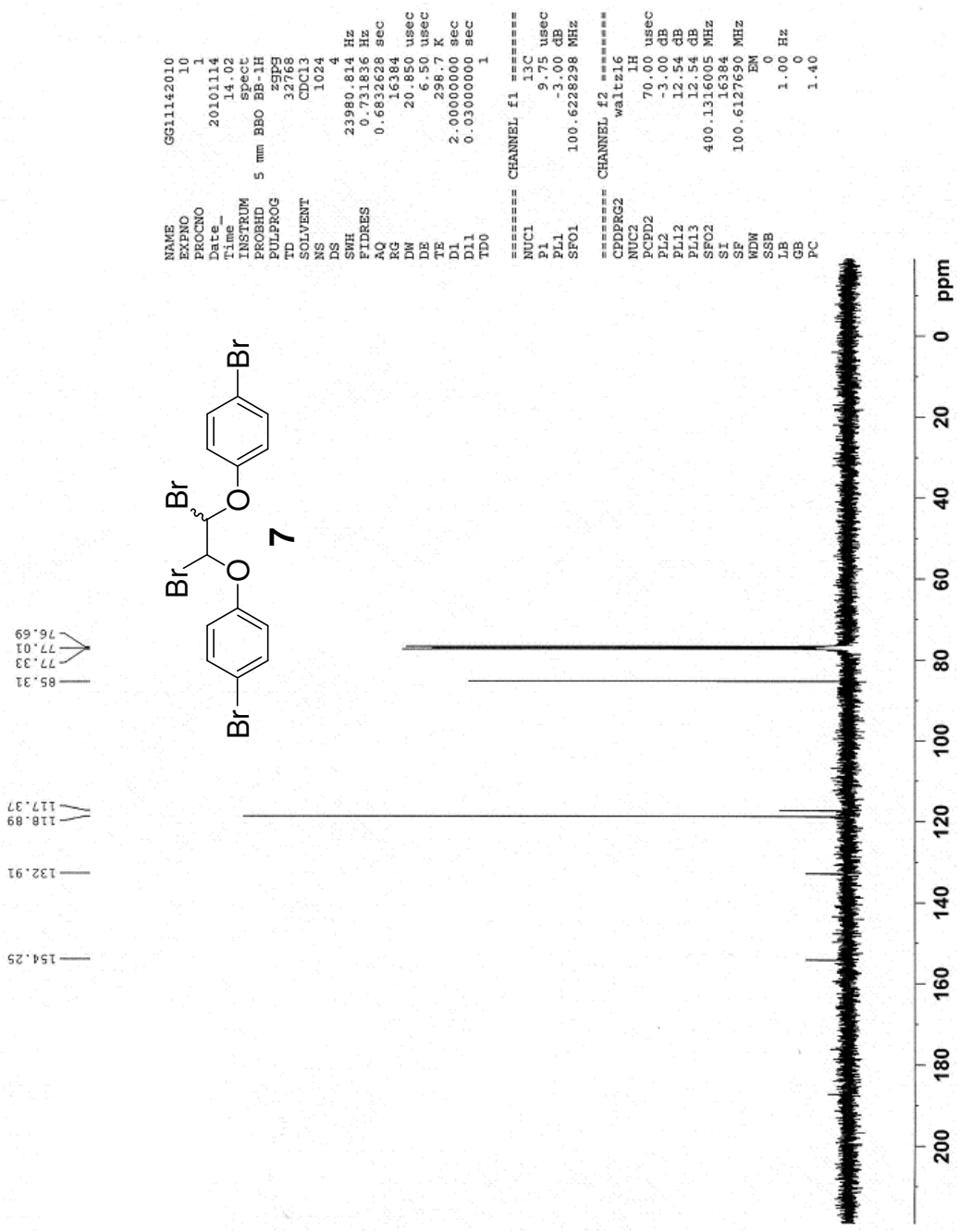

Figure 12. ^{13}C NMR of *meso-* and *dl*-1,2-Dibromo-1,2-bis(4-bromophenoxy)-ethane (**7**) in $CDCl_3$.

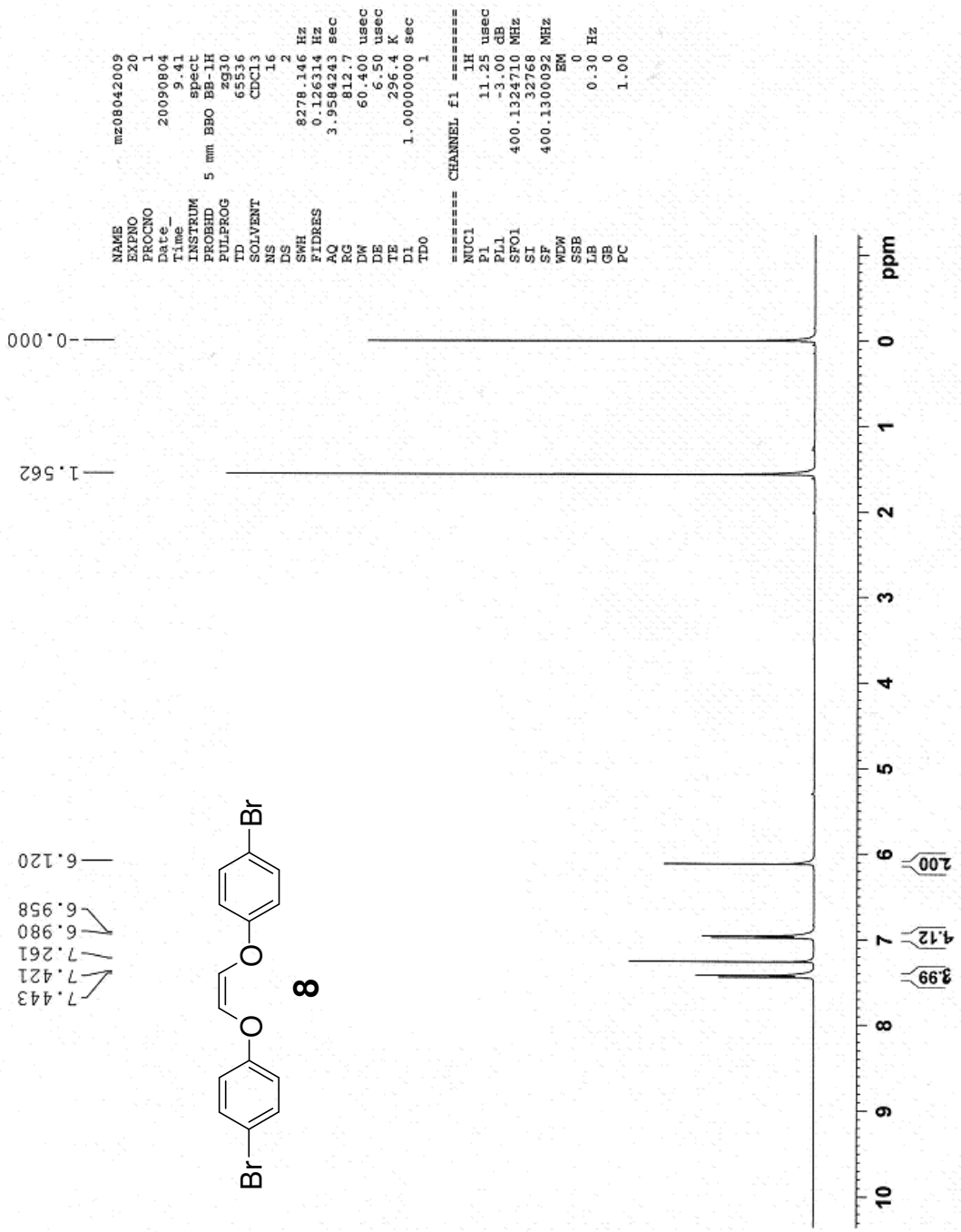

Figure 13. ^{1}H NMR of *cis*-1,2-Bis(4-bromophenoxy)ethene (**8**) in $CDCl_3$.

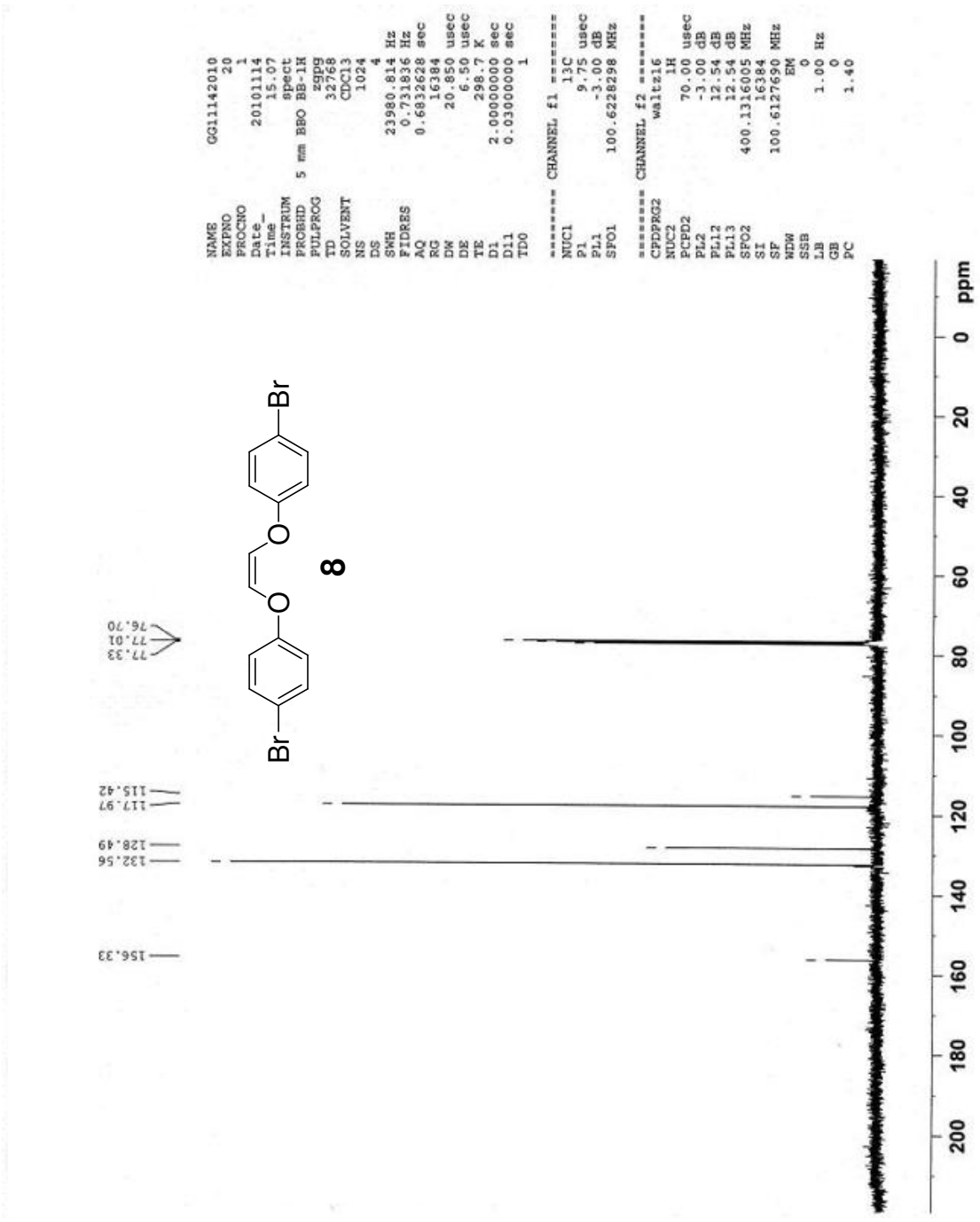

Figure 14. ^{13}C NMR of *cis*-1,2-Bis(4-bromophenoxy)ethene (**8**) in $CDCl_3$.

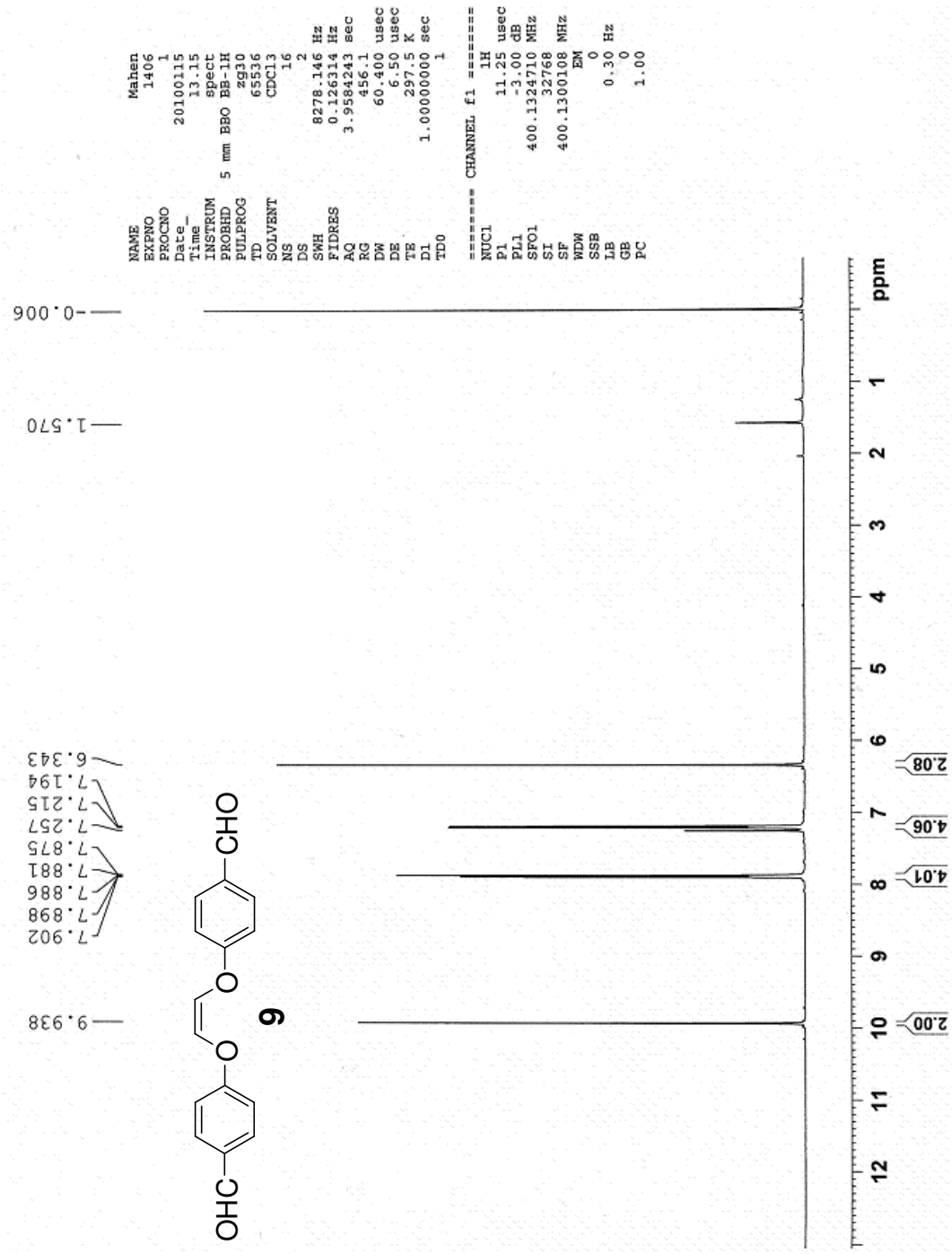

Figure 15. ^{1}H NMR of (Z)-4,4'-(ethene-1,2-diylbis(oxy))dibenzaldehyde (**9**) in $CDCl_3$.

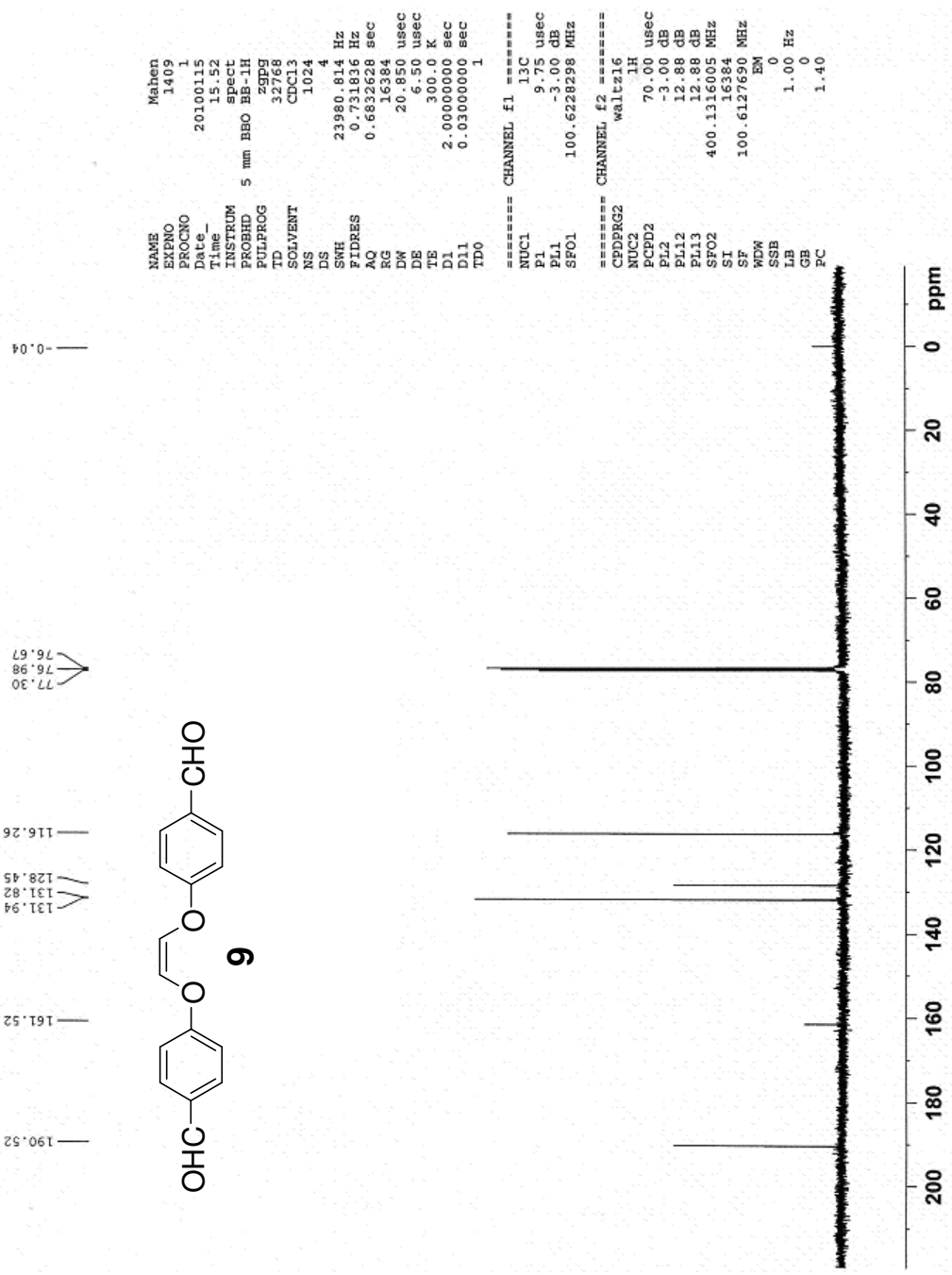

Figure 16. ^{13}C NMR of (Z)-4,4'-(ethene-1,2-diylbis(oxy))dibenzaldehyde (**9**) in $CDCl_3$.

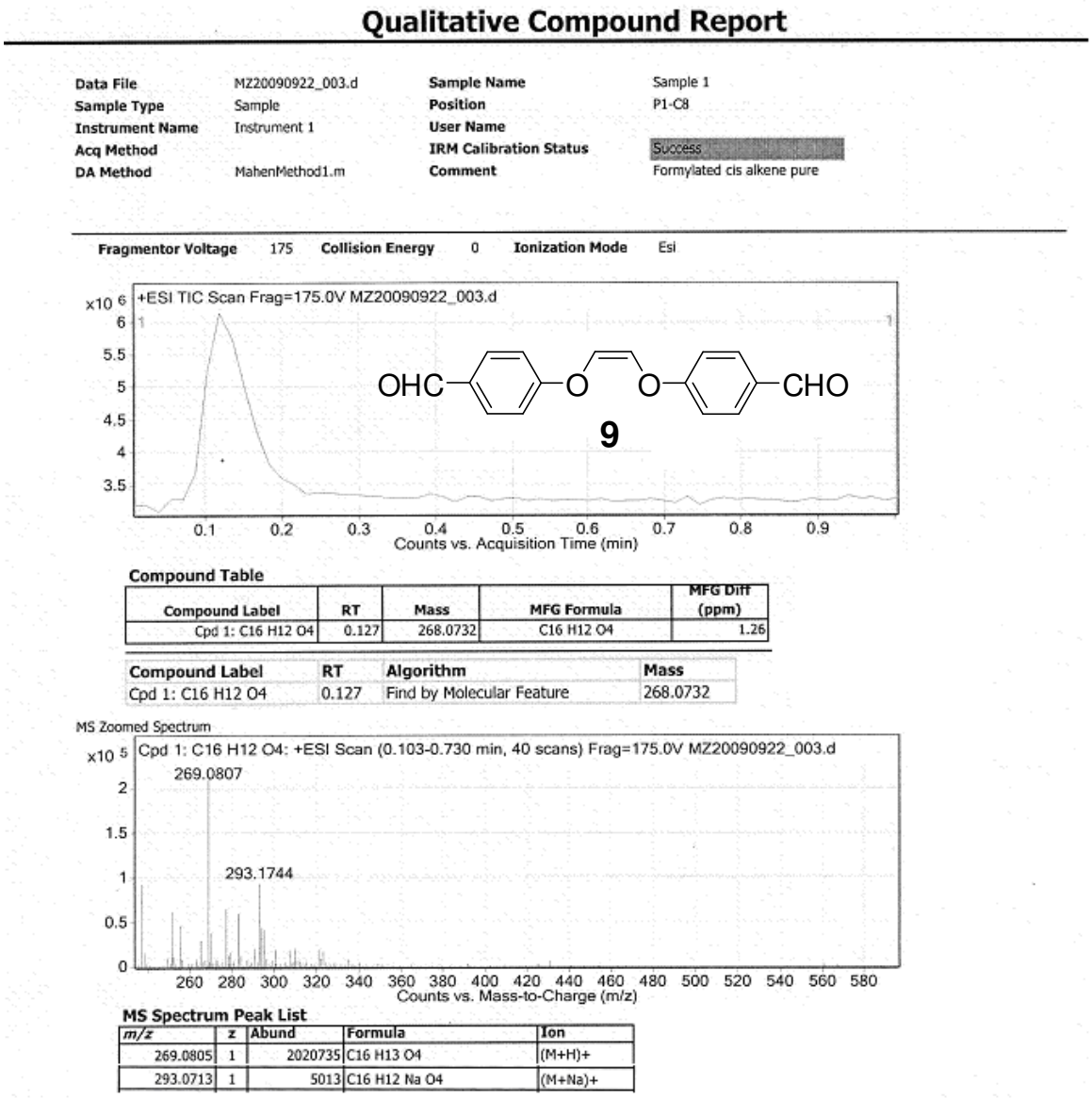

Figure 17. HRMS of (Z)-4,4'-(ethene-1,2-diylbis(oxy))dibenzaldehyde (**9**).

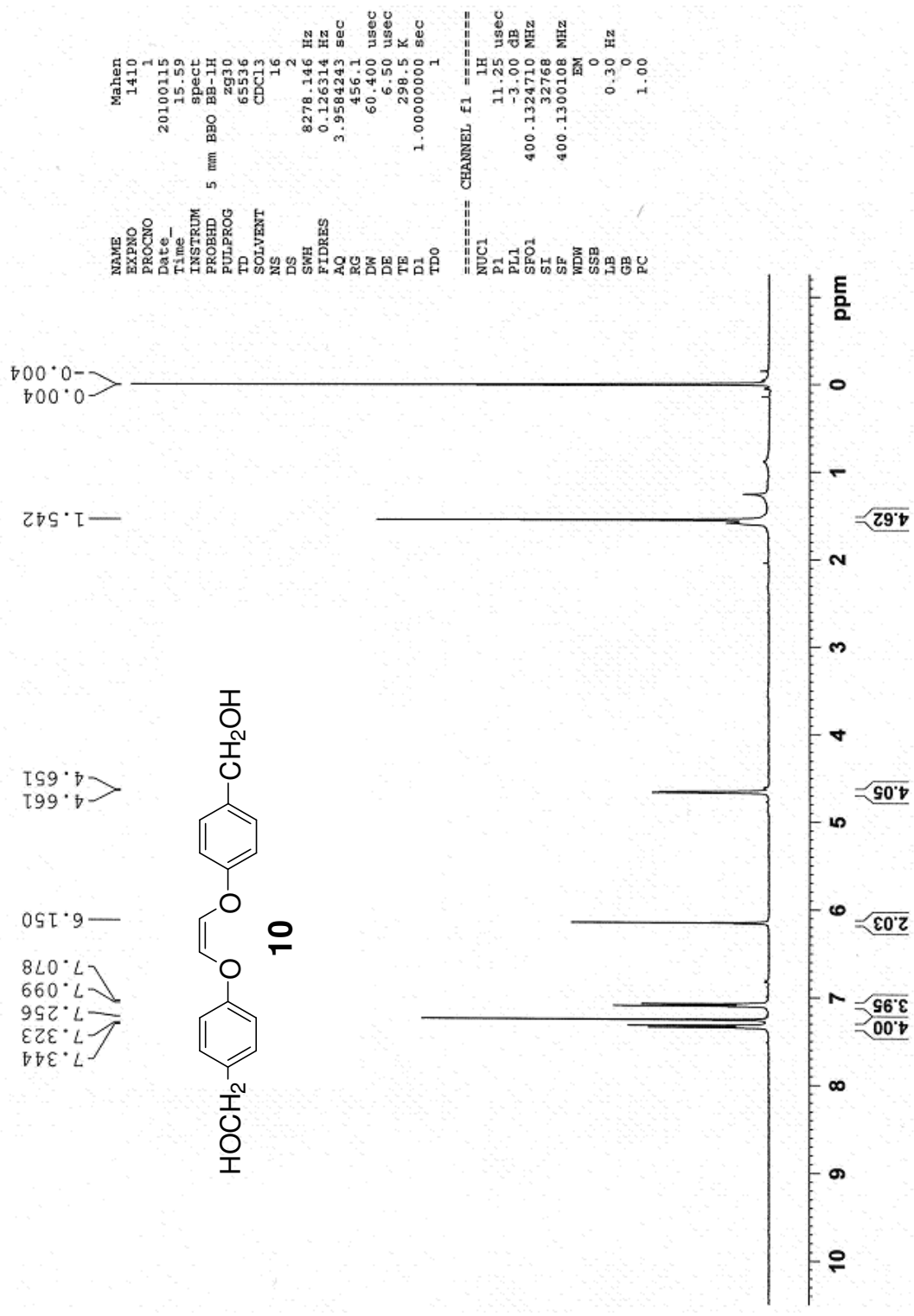

Figure 18. ^{1}H NMR of (Z)-(4,4'-(ethene-1,2-diylbis(oxy))bis(4,1-phenylene))- dimethanol (**10**) in $CDCl_3$.

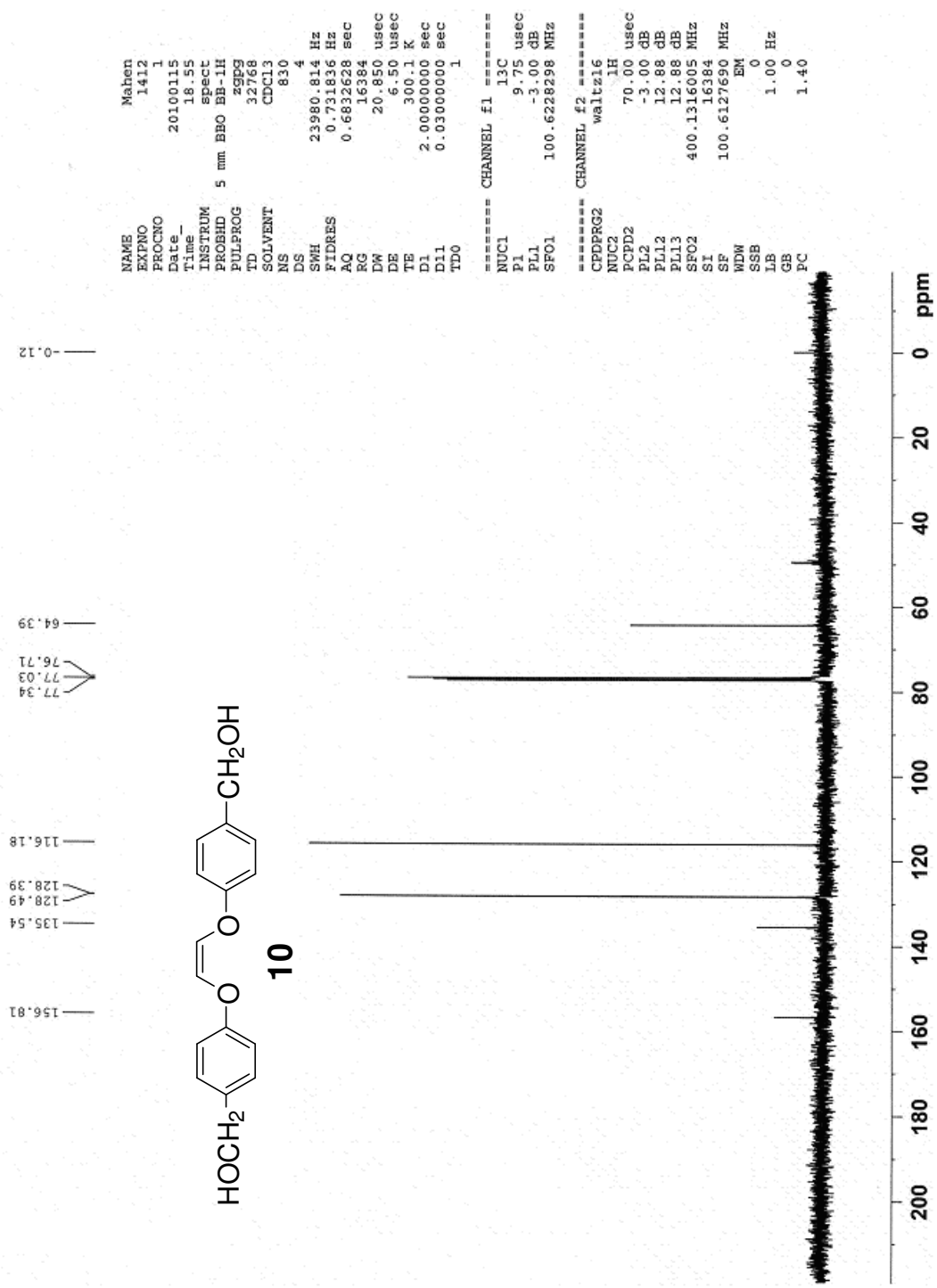

Figure 19. ^{13}C NMR of (Z)-(4,4'-(ethene-1,2-diylbis(oxy))bis(4,1-phenylene))- dimethanol (**10**) in $CDCl_3$.

Qualitative Compound Report

Data File	MZ20091105_004.d	**Sample Name**	Sample 3 (10 mg scale)
Sample Type	Sample	**Position**	P1-F3
Instrument Name	Instrument 1	**User Name**	
Acq Method		**IRM Calibration Status**	Success
DA Method	Default.m	**Comment**	EM=272.10 CF=C16H16O4

Fragmentor Voltage 175 **Collision Energy** 0 **Ionization Mode** Esi

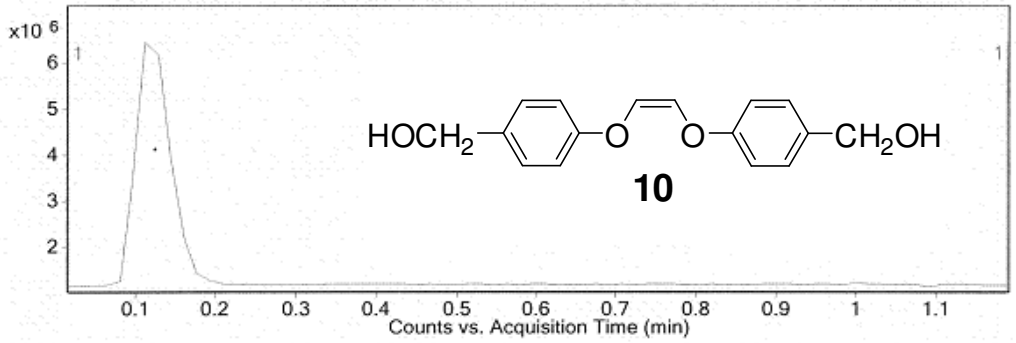

Compound Table

Compound Label	RT	Mass	Abund	Formula	Tgt Mass	Diff (ppm)
Cpd 1: C16 H16 O4	0.1	272.10474	1881770	C16 H16 O4	272.10486	-0.43

Compound Label	RT	Algorithm	Mass
Cpd 1: C16 H16 O4	0.1	Find By Formula	272.10474

MS Zoomed Spectrum

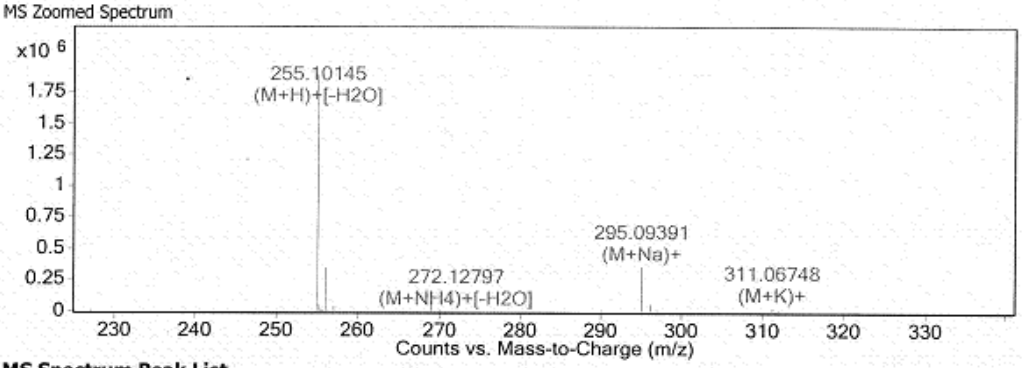

MS Spectrum Peak List

m/z	*Calc m/z*	Diff(ppm)	z	Abund	Formula	Ion
255.10145	255.10157	-0.46		1881770	C16 H15 O3	(M+H)+[-H2O]
255.24356				55872		
255.30133				21580		
256.1049	256.10496	-0.23		347501	C16 H15 O3	(M+H)+[-H2O]
257.10814	257.1076	2.1		43492	C16 H15 O3	(M+H)+[-H2O]
272.12797	272.12812	-0.55	1	1081	C16 H18 N O3	(M+NH4)+[-H2O]
290.13822	290.13868	-1.61	1	12161	C16 H20 N O4	(M+NH4)+
295.09391	295.09408	-0.57	1	360920	C16 H16 Na O4	(M+Na)+
296.09698	296.09747	-1.66	1	62600	C16 H16 Na O4	(M+Na)+
311.06748	311.06802	-1.72	1	31090	C16 H16 K O4	(M+K)+

--- End Of Report ---

Figure 20. HRMS of (Z)-(4,4'-(ethene-1,2-diylbis(oxy))bis(4,1-phenylene))-dimethanol (**10**).

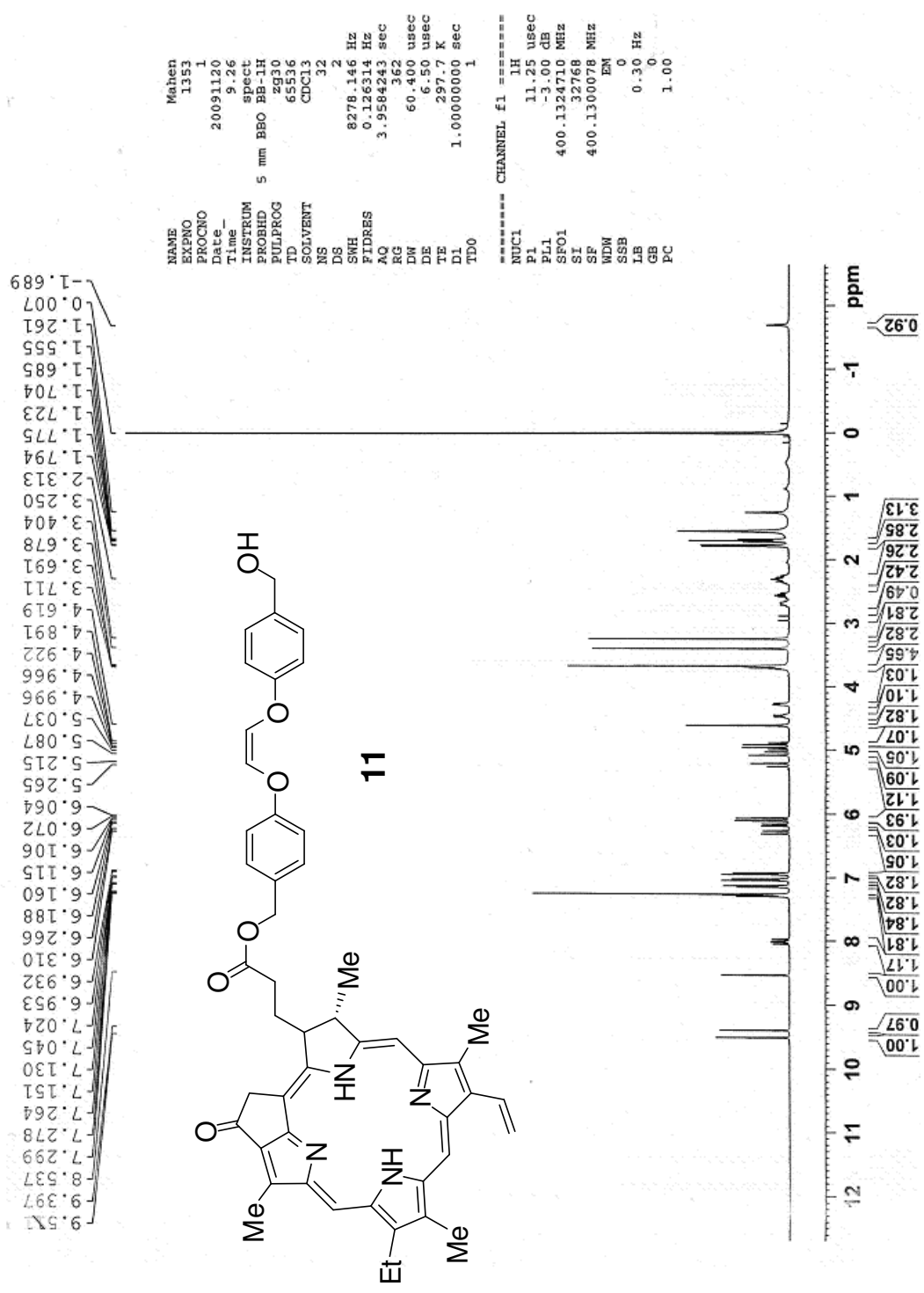

Figure 21. ^{1}H NMR of (Z)-4-[2-(4-hydroxymethyl-phenoxy)-vinyloxy]-benzyl-pyropheophorbide-a (**11**) in $CDCl_3$.

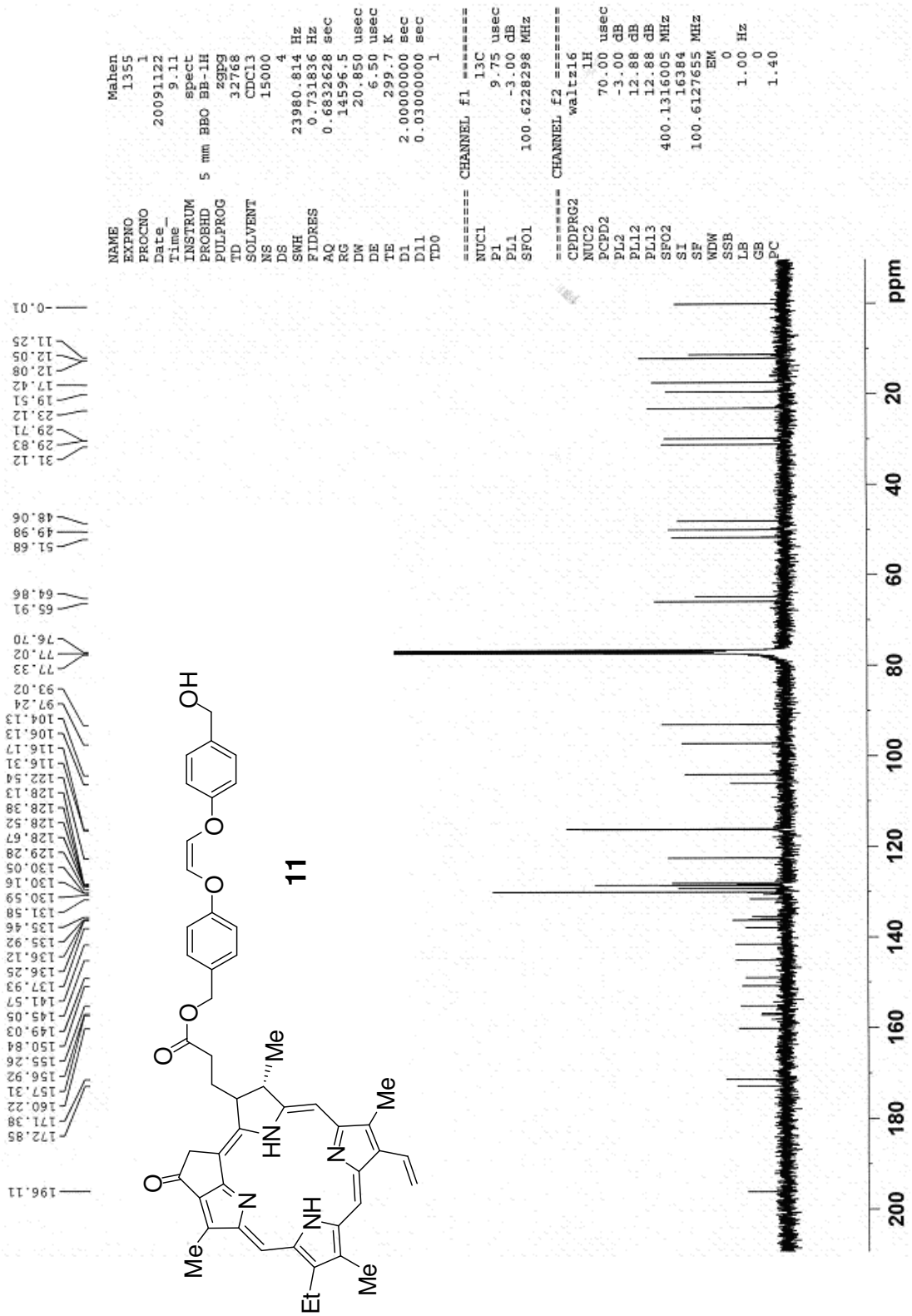

Figure 22. ^{13}C NMR of (Z)-4-[2-(4-hydroxymethyl-phenoxy)-vinyloxy]-benzyl-pyropheophorbide-a (**11**) in $CDCl_3$.

Qualitative Compound Report

Data File	MZ20091105_003.d	**Sample Name**	Sample 2 (10 mg scale)
Sample Type	Sample	**Position**	P1-F2
Instrument Name	Instrument 1	**User Name**	
Acq Method		**IRM Calibration Status**	Success
DA Method	Default.m	**Comment**	EM=788.3574 CF=C49H48N4O6

Fragmentor Voltage 175 **Collision Energy** 0 **Ionization Mode** Esi

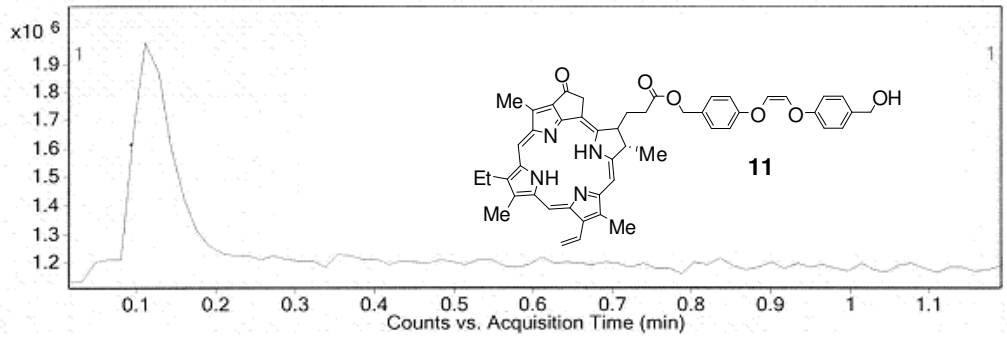

Compound Table

Compound Label	RT	Mass	Abund	Formula	Tgt Mass	Diff (ppm)
Cpd 1: C49 H48 N4 O6	0.1	788.35616	35578	C49 H48 N4 O6	788.35739	-1.55

Compound Label	RT	Algorithm	Mass
Cpd 1: C49 H48 N4 O6	0.1	Find By Formula	788.35616

MS Zoomed Spectrum

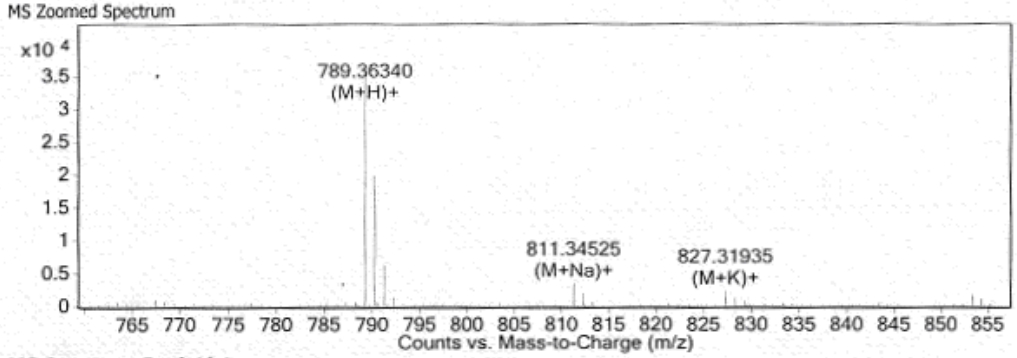

MS Spectrum Peak List

m/z	*Calc m/z*	Diff(ppm)	z	Abund	Formula	Ion
787.38112				669		
789.3634	789.36466	-1.6		35578	C49 H49 N4 O6	(M+H)+
790.36687	790.36788	-1.29		19757	C49 H49 N4 O6	(M+H)+
791.3704	791.37093	-0.67		6178	C49 H49 N4 O6	(M+H)+
792.37633	792.37387	3.1		1377	C49 H49 N4 O6	(M+H)+
811.34525	811.34661	-1.68	1	3380	C49 H48 N4 Na O6	(M+Na)+
812.34956	812.34983	-0.33	1	1986	C49 H48 N4 Na O6	(M+Na)+
827.31935	827.32054	-1.44	1	2256	C49 H48 K N4 O6	(M+K)+
828.32549	828.32376	2.09	1	1141	C49 H48 K N4 O6	(M+K)+
829.32356	829.3243	-0.89	1	799	C49 H48 K N4 O6	(M+K)+

--- End Of Report ---

Figure 23. HRMS of (Z)-4-[2-(4-hydroxymethyl-phenoxy)-vinyloxy]-benzyl-pyropheophorbide-a (**11**).

Qualitative Compound Report

Data File	AM20101101_013.d	**Sample Name**			
Sample Type	Sample	**Position**	P1-F1		
Instrument Name	Instrument 1	**User Name**			
Acq Method		**IRM Calibration Status**	Success		
DA Method		**Comment**	CF =	EM =	

Compound Table

Compound Label	RT	Mass	Abund	Formula	Tgt Mass	Diff (ppm)
Cpd 1: C41 H40 N4 O5; 2.26	2.26	668.29972	3235	C41 H40 N4 O5	668.29987	-0.22
Cpd 2: C40 H40 N4 O4; 2.08	2.08	640.30482	5088	C40 H40 N4 O4	640.30496	-0.22

Compound Label	RT	Algorithm	Mass
Cpd 1: C41 H40 N4 O5; 2.26	2.26	Find By Formula	668.29972

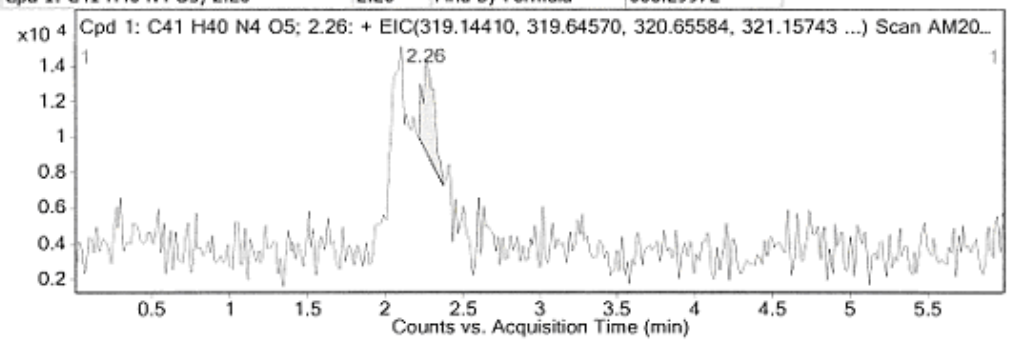

MS Spectrum

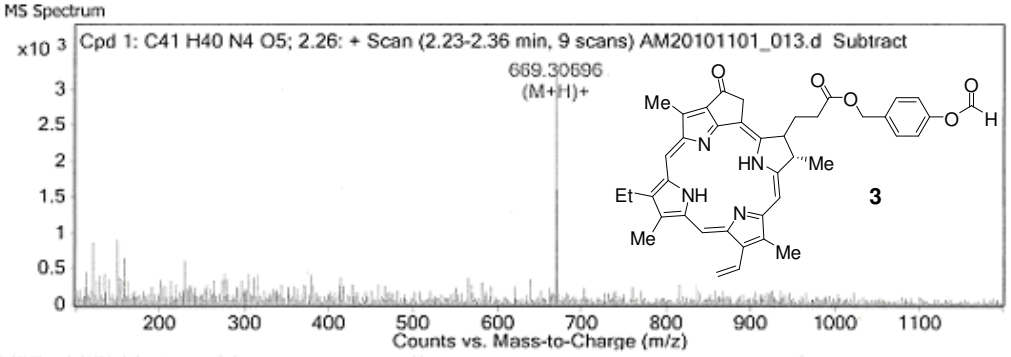

MS Zoomed Spectrum

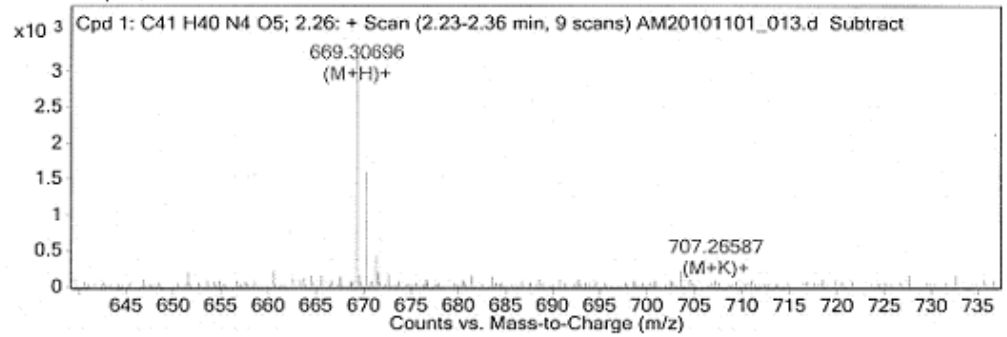

Figure 24. HRMS of pheophorbide (**3**).

Qualitative Compound Report

MS Spectrum Peak List

m/z	*Calc m/z*	Diff(ppm)	z	Abund	Formula	Ion
664.50646				161		
665.51901				157		
667.59961				146		
669.30696	669.30715	-0.29		3235	C41 H41 N4 O5	(M+H)+
669.60066				175		
670.3105	670.31034	0.25		1592	C41 H41 N4 O5	(M+H)+
671.31476	671.31333	2.13		442	C41 H41 N4 O5	(M+H)+
671.53912				203		
672.59577				160		
707.26587	707.26303	4.02	1	81	C41 H40 K N4 O5	(M+K)+

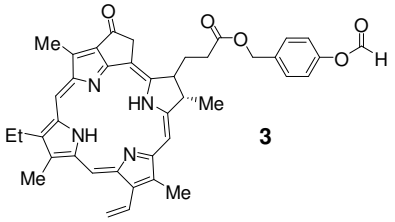

3

Figure 24 cont.. HRMS of of pheophorbide (**3**).

4.5 References

1. Zamadar, M.; Aebisher, D.; Greer, A. *J. Phys. Chem. B* **2009**, *113*, 15803.

2. Giaimuccio, J.; Zamadar, M.; Aebisher, D.; Meyer, G. J.; Greer, A. *J. Phys. Chem. B* **2009**, *112*, 15646.

3. Krasnovsky, A. A. J.; Neverov, K. V. S.; Egorov, Y.; Roeder, B.; Levald, T. *J. Photochem. Photobiol. Biol. B* **1990**, *5*, 245.

4. Jiang, M. Y.; Dolphin, D. *J. Am. Chem. Soc*., **2008**, *130*, 4236–4237.

5. Yang, J.; Bauld, N. L. *J. Org. Chem.* **1999**, *64*, 9251

6. (a) Luts, T.; Suprun, W.; Hofmannb, D.; Klepel, O.; Papp, H. *J. Mol. Catal. A: Chem.* **2007**, *261*, 16. (b) Yu, K.; Sommer, W.; Weck, M.; Jones, C. W. *J. Catal.* **2004**, *226*, 101.

7. Kim, S.; Ohulchanskyy, T. Y.; Bharali, D.; Chen, Y.; Pandey, R. K.; Prasad, P. N. *J. Phys. Chem. C* **2009**, *113*, 12641.

8. (a) Gafney, H. D.; Wolfgang, S. *J. Phys. Chem.* **1983**, *87*, 5395. (b) Hellriegel, C.; Kirstein, J.; Braeuchle, C.; Latour, V.; Pigot, T.; Olivier, R.; Lacombe, S.; Brown, R.; Guieu, V.; Payrastre, C.; Izquierdo, A.; Mocho, P. *J. Phys. Chem. B* **2004**, *108*, 14699.

9. Preethi, N.; Shinohara, H.; Nishide, H. *Bull. Chem. Soc. Jpn.* **2006**, *79*, 1308.

10. Lovell, J. F.; Liu, T. W. B.; Chen, J.; Zheng, G. *Chem. Rev.* **2010**, *110*, 2839.

11. Houghten, R. A.; Yu, Y. *J. Am. Chem. Soc.* **2005**, *127*, 8582.

Chapter 5: Singlet Oxygen as a Reagent in Organic Synthesis

5.1 Introduction

In this chapter we review the synthesis of organic peroxides from singlet molecular oxygen [$^1O_2$ ($^1\Delta_g$)] via dye-sensitized photooxygenations. This chapter comprises four sections which describe the synthesis of dioxetanes from [2 + 2]-cycloadditions, endoperoxides from [2 + 4]-cycloadditions, hydroperoxides from 'ene' reactions, and tandem combinations there of (Scheme 1). Examples include endoperoxides and bisperoxides that rearrange to spiro compounds.

Scheme 1

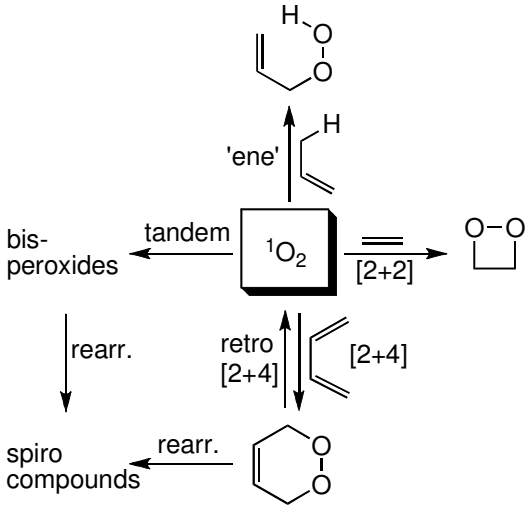

Whilst this chapter is not comprehensive, attention is focused on those reports of photooxygenation where peroxide yields approached or exceeded 50%. The isolation of peroxides involves meticulous and potential dangerous work.[1] Thus, percentage yields are not always reported in the same way, and may relate to the feasibility of purification and safety and, perhaps because of this issue, safety information is often incomplete.

Analytical methods such as low-temperature nuclear magnetic resonance (NMR) spectroscopy has allowed the characterization of unstable peroxides in reaction mixtures. Some peroxides have been isolated in traps under vacuum or by low-temperature silica gel chromatography, while others were recrystallized at room temperature.[2-4]

Singlet oxygen is conveniently generated by sensitization and, in view of the low energy of this species, dye are effective and can be used in low concentrations due to the high absorptivity.

$$\text{Dye} + h\nu \longrightarrow \text{Dye}^* \qquad \text{Dye}^* + {}^3O_2 \longrightarrow \text{Dye} + {}^1O_2$$

Suitable light sources for exciting the sensitizer include halogen or mercury lamps equipped with a 400 nm cut-off filter to transmit visible light. The sensitizers methylene blue (MB), *meso*-tetraphenylporphyrine (TPP), sulfonated aluminium phthalocyanine, and Rose Bengal (RB) are widly used in homogeneous solutions. The mail appeal of heterogeneous sensitizers is that they are easy to separate from solution after reaction; examples include, polymer-supported RB or seco-porphyrazine, MB-doped zeolites, and fullerene-supported silica gel.[5-6]

The lifetime of singlet oxygen is critically dependent on the solvent used.[7-9] The longer lifetime of singlet oxygen in halogenated solvents than organic or aqueous solvents is well known, e.g., carbon tetrachloride (59 ms) compared to benzene (30 μs), water (3.5 μs), and deuterium oxide (65 μs). The use of halogenated solvents also comes about in response to the need for low-temperature solvents in view of the instability of peroxide products. The combination of halogenated solvents with low-temperature conditions is seen often in peroxide synthesis with singlet oxygen.[10,11] Whether intended or not, low temperature conditions offer another advantage, enhancing reaction rates

since entropy-controlled reactivity often accompanies singlet oxygen chemistry.[12] Peroxides are formed also through mechanisms that do not involve singlet oxygen, in particular via an electron transfer (see Section 5.3.3), although preparative examples are limited in number.

5.2 Dioxetanes

5.2.1 Background Information

1,2-Dioxetanes are 4-membered ring peroxides, which have been synthesized from singlet oxygen—alkene reactions as pure compounds (e.g., **18**-**33**, Schemes 2 and 3). The rosette of Scheme 3 shows reported examples of dioxetanes formed in good yield from the corresponding alkenes displayed in Scheme 2. The sensitized photooxidation of alkenes **1**-**17** proceeded rapidly with visible light, but stopped after the uptake of 1 equivalent of oxygen.

Scheme 2

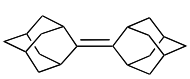

1

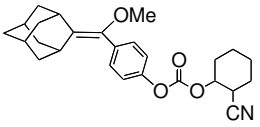

2

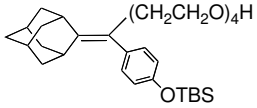

3

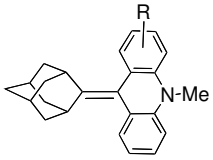

4 (R = m-OMe)
5 (R = m-OSi^{t}BuMe)

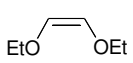

6

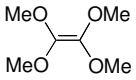

7

8 (R = Ph)
9 (R = anthracene)

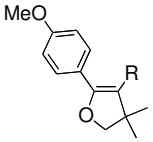

11 (R = Me)
12 (R = ^{i}Pr)
13 (R = ^{t}Bu)

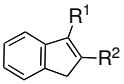

14 (R^1 = OTBS, R^2 = H)
15 (R^1 = R^2 = Ph)

16 (R = Me)
17 (R = Ph)

Scheme 3

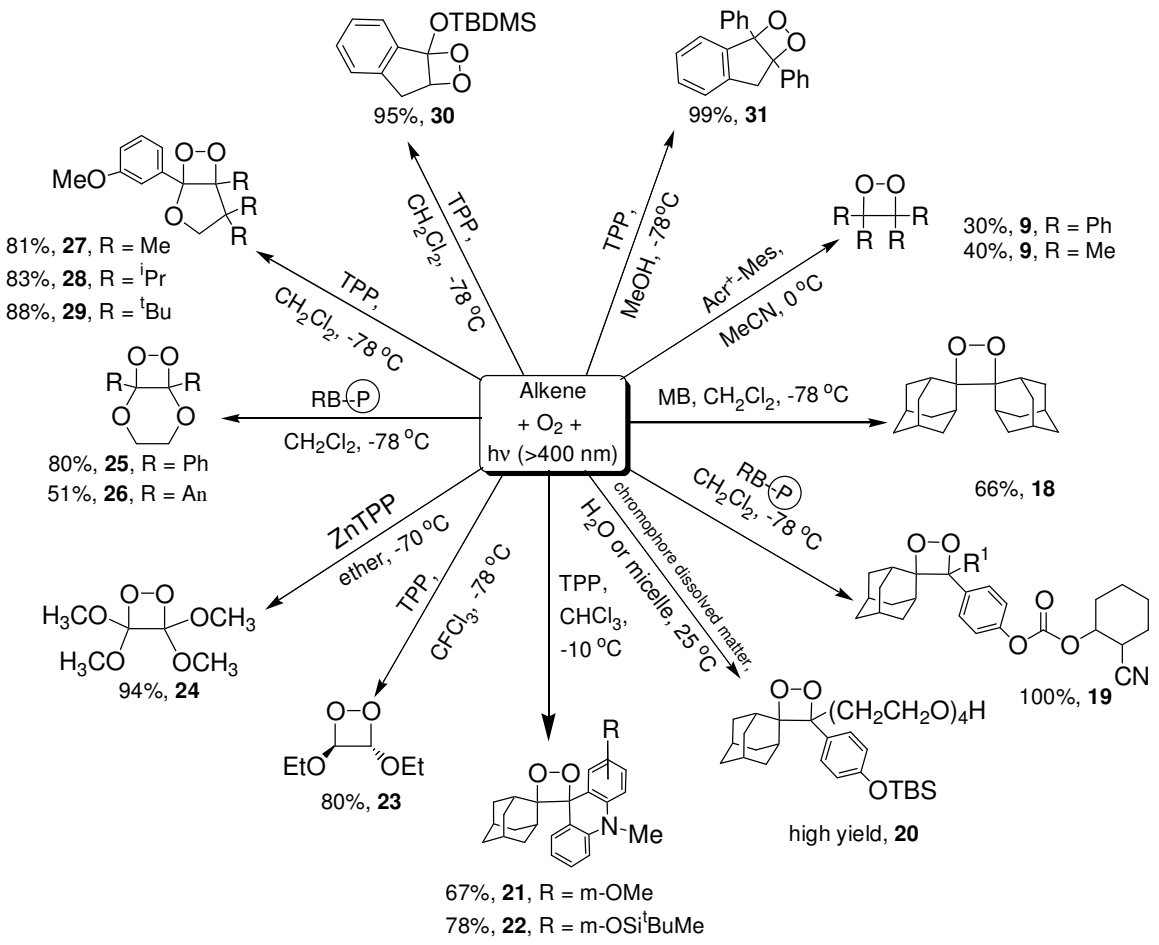

5.2.2 Adamantyl-Substituted Alkenes

In 1975, adamantylideneadamantane-1,2-dioxetane (**18**) was prepared from an MB-sensitized reaction of biadamantylidene (**1**) with singlet oxygen in CH_2Cl_2 at -78 °C in good yield (66%) after recrystallization.[13] The scope of the singlet oxygen reaction include monospiroadamantyl-dioxetanes, which were also stable toward isolation and characterization.[14] For example, in 1998, singlet oxygenation of *cis*-2-cyanocyclohexyl carbonate **2** with polymer-supported RB in O_2-saturated CH_2Cl_2 at -78 °C provided dioxetane **19** quantitatively (100% yield).[15] In 2006, the formation of spiroadamantane dioxetane **20** was reported from a tetraglycol-substituted alkene **3** in environmental water

samples containing chromophoric dissolved organic matter (CDOM) as the photosensitizer.[16,17] CDOM was not characterized structurally, but was proposed to contain amphiphilic macromolecular species with micelle-like properties. Dioxetane **20** served as a hydrophobic trap-and-trigger chemiluminescent probe to validate singlet oxygen concentrations in natural waters.[16,17] In 1997, photooxygenations of methoxy- and siloxy-substituted adamantylideneacridanes (**4** and **5**) produced the corresponding dioxetanes **21** and **22**.[14] The reaction was conducted with TPP as the photosensitizer in $CHCl_3$ at -10 °C. To avoid decomposition, dioxetanes **21** and **22** were isolated at reduced temperature (-10 °C) during silica-gel chromatography, and were obtained in 67% and 78% yield, respectively.

5.2.3 Alkoxy-Substituted Alkenes

Electron-rich olefins also react with singlet oxygen and form dioxetanes. In 1970, the formation of *cis*-1,2-dioxetane **23** was achieved stereospecifically in greater than 80% yield in a photooxidation reaction with *cis*-diethoxyethylene **6** (Scheme 3).[18] The photolysis of **6** was carried out in O_2-saturated TPP-sensitized $CFCl_3$ at -78 °C, where no *trans*-1,2-dioxetane was obtained. *Trans*-1,2-dioxetane can be prepared itself stereospecifically from the singlet oxygenation of *trans*-diethoxyethylene.[18] In 1970, irradiation of tetramethoxyethylene (**7**) sensitized by zinc tetraphenylporphine or dinaphthalenethiophene in an O_2-saturated ether solution at -70 °C produced dioxetane **24**.[19] Purification was conducted by evaporation of the solvent at -78 °C, and distillation of the residue at 25 °C, which gave **24** as a liquid in 94% yield.

In 1978, the photooxidation of 2,3-diphenyl-1,4-dioxene (**8**) was reported in CH_2Cl_2 solution at -78 °C.[3,20] Compound **8** reacted with singlet oxygen from irradiation of polymer-bound RB afforded the corresponding dioxetane (1,6-diphenyl-2,5,7,8-tetraoxabicyclo[4.2.0]octane, **25**) in ~80% yield. Bicyclic dioxetane **25** was insufficiently stable for combustion analysis. On the basis of ^{13}C-NMR spectroscopy, the dioxetane structure was assigned.[20] 2,3-Di(2-anthryl)-1,4-dioxene (**9**) was also photooxidized in CH_2Cl_2 solution at -78 °C, and dioxetane **26** was obtained in 51% yield.[21] An enhanced chemiluminescence from silica gel was observed with the catalytic decomposition of **26**.[21] In 1997, dioxetanes **27**-**29** were synthesized in 81-88% yields from singlet oxygenation of the corresponding 4-alkyl-3-dimethyl-2,3-dihydrofurans (**11**-**13**) in CH_2Cl_2 at -78 °C.[22] This reaction has been conducted with a variety of dihydrofuran derivatives to generate similar dioxetanes. In 1999, an excellent yield of dioxetane **30** was obtained (95%) in the photooxidation of silyl enol ether **14**.[23] Dioxetane **30** was characterized at low-temperature, it was unstable at room temperature. ^{13}C NMR signals at δ_{C1} (~113 ppm) and δ_{C2} (~92 ppm) where characteristic of the dioxetane ring indicating and were the basis for the structure assignment.

Singlet oxygen reactions involving rearrangements of initially formed endoperoxides to dioxetanes have been reported.[24,25] For example, 2-(2'-anthryl)-1,4-dioxene **9** initially formed an endoperoxide by a [2 + 4] cycloaddition reaction, and later rearranged to a dioxetane when separated on silica gel with *o*-xylene.[24]

5.2.4 Phenyl- or Methyl Substituted Alkenes

5.2.4.1 Diphenylindene Photooxidation. In 1979, an interesting effect on the dioxetane/diendoperoxide product ratio was observed upon addition of methanol to acetone. The photooxidation of 2,3-diphenylindene **15** afforded its dioxetane **31** in methanol at -78 °C.[26] The addition of methanol increased the dioxetane/diendoperoxide ratio. On the basis of LC and NMR spectroscopy, dioxetane **31** formed in high yields in methanol or methanol-acetone (3:7) mixtures. But there was the formation of a diendoperoxide with the solvents Freon-11 and acetone-d_6. The topic of bisperoxides will be discussed in Section 5.5.2.1. The synthesis of benzofuran dioxetanes has also been accomplished from a TPP-sensitized photooxidation of benzofurans.[27,28]

5.2.4.2 Electron-Transfer Photooxidation. Despite the fact singlet oxygen oxidizes tetramethylethylene (**16**) via the 'ene' pathway with abstraction of one of the twelve α protons, under electron-transfer photooxidation conditions, dioxetane **32** (R=Me) has been generated.[29] The electron-deficient sensitizer 9-mesityl-10-methylacridinium ion (Acr^+-Mes) in its excited state $Acr^{\bullet}$-$Mes^{\bullet+}$ was generated, in which the alkene radical cation and the superoxide ion ($O_2^{\bullet-}$) were proposed, coupling to the dioxetane. Similar results were observed in the electron-transfer photosensitized oxidation of tetraphenylethylene (**17**).

5.2.5 Summary

Reports of photooxidations giving dioxetanes is quite extensive.[30,31] Steric and polar factors have a profound influence in activating alkenes to react with singlet oxygen. Isolable dioxetanes from singlet oxygen have been restricted to adamantyl-, alkoxy-, and

phenyl-substituted alkenes. The [2 + 2] cycloaddition of singlet oxygen to alkenes that bear α protons have little success in dioxetane synthesis in view of the hydroperoxide formation from the singlet oxygen 'ene' reaction. But an electron-transfer photooxidation reaction to dioxetanes offers a possible way around the structural restrictions of singlet oxygen;[29] for example, alkene radical cation arose from tetramethylethylene coupling to $O_2^{\bullet-}$, and formation of the dioxetane, but the broader synthetic utility has not yet been established.[29,32]

Dioxetanes vary in their stability toward decomposition to excited carbonyl products. Some require heating to induce decomposition to carbonyl compounds with chemiluminescence (e.g., **18**-**22**). Base-catalyzed β-elimination of the *cis*-2-cyanocyclohexylcarbonate protecting group of dioxetane **19** produced the corresponding phenoxide ion dioxetane, a structure that facilitated the molecule's fragmentation into ketones and subsequent chemically initiated electron exchange luminescence (CIEEL). Upon treatment with fluoride ions, dioxetanes **21** and **22** underwent fragmentation into ketones via CIEEL. The thermolytic stability of dioxetanes has been reviewed.[33] Dioxetanes can also catalytically decompose from trace impurities in solvents, such as transition metal ions,[34] or can decompose upon silica-gel chromatography workup (e.g., **26**).[14,21] Treatment of dioxetanes with phosphines led to phosphorane intermediates, and subsequently phosphine oxides and epoxides.[35-37]

5.3 Endoperoxides

5.3.1 Background Information

Endoperoxides (sometimes called 1,4-epiperoxides or dioxapaddlanes) are 6-membered ring peroxides, which arise from singlet oxygenations of arene and diene compounds and have been synthesized as pure compounds (e.g., **43**-**52** and **62**-**72**; Scheme 4 to 8). Many endoperoxide structures have been reported.[38-41] The rosettes of Schemes 5 and 7 show examples where endoperoxides were formed in good yield.

Scheme 4

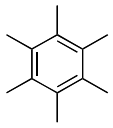

34

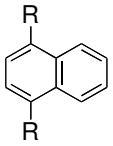

35 (R = Me)
36 (R = $CH_2CH[CONHCH_2CH(OH)CH_2OH]_2$

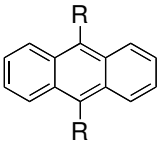

37 (R = Ph)
38 (R = Me)

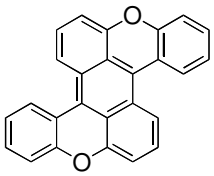

39

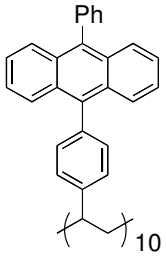

40

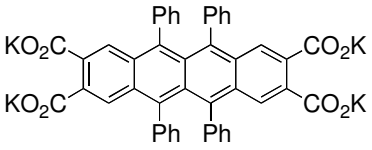

41

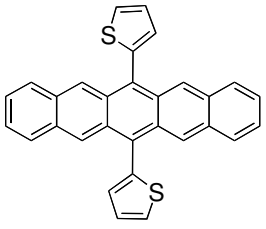

42

Scheme 5

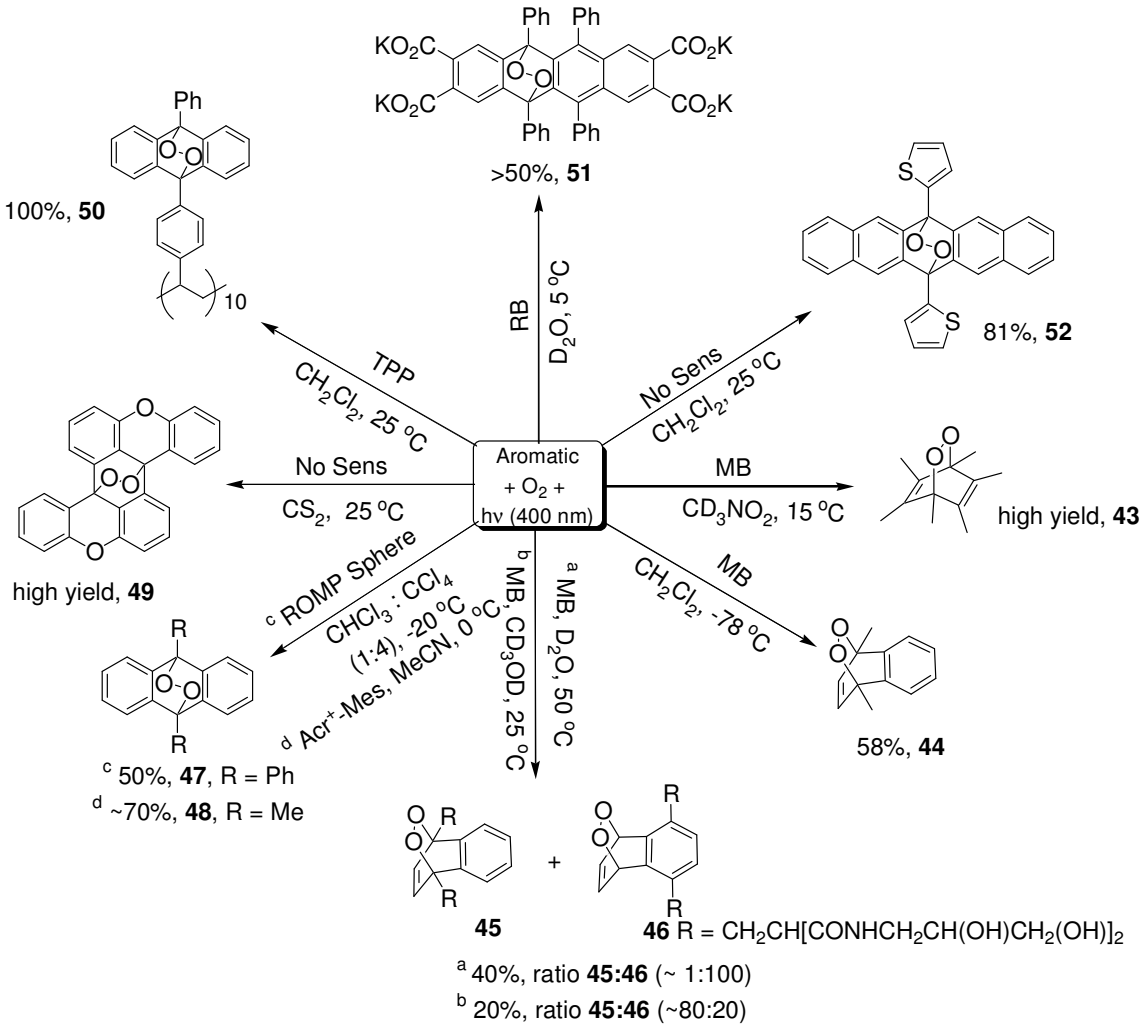
Ph Ph
KO2C
CO2K
KO2C
CO2K
Ph Ph
>50%, 51
Ph
100%, 50
10
RB
D2O, 5 °C
TPP
CH2Cl2, 25 °C
No Sens
CH2Cl2, 25 °C
S
S
81%, 52
Aromatic
+ O2 +
hv (400 nm)
No Sens
CS2, 25 °C
MB
CD3NO2, 15 °C
high yield, 43
high yield, 49
c ROMP Sphere
CHCl3 : CCl4
(1:4), -20 °C
d Acr+-Mes, MeCN, 0 °C
b MB, CD3OD, 25 °C
a MB, D2O, 50 °C
MB
CH2Cl2, -78 °C
R
R
c 50%, 47, R = Ph
d ~70%, 48, R = Me
58%, 44
45
+
46 R = CH2CH[CONHCH2CH(OH)CH2(OH)]2
a 40%, ratio 45:46 (~ 1:100)
b 20%, ratio 45:46 (~80:20)

Scheme 6

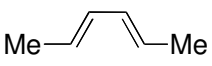

53

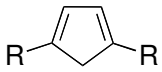

54 (R = Ph)
55 (R = p-FC_6H_4)

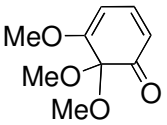

56

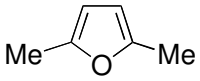

57

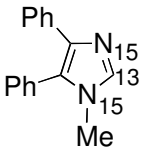

58

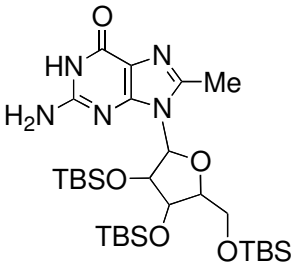

59

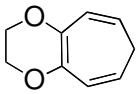

60

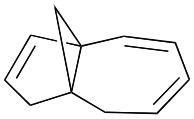

61

Scheme 7

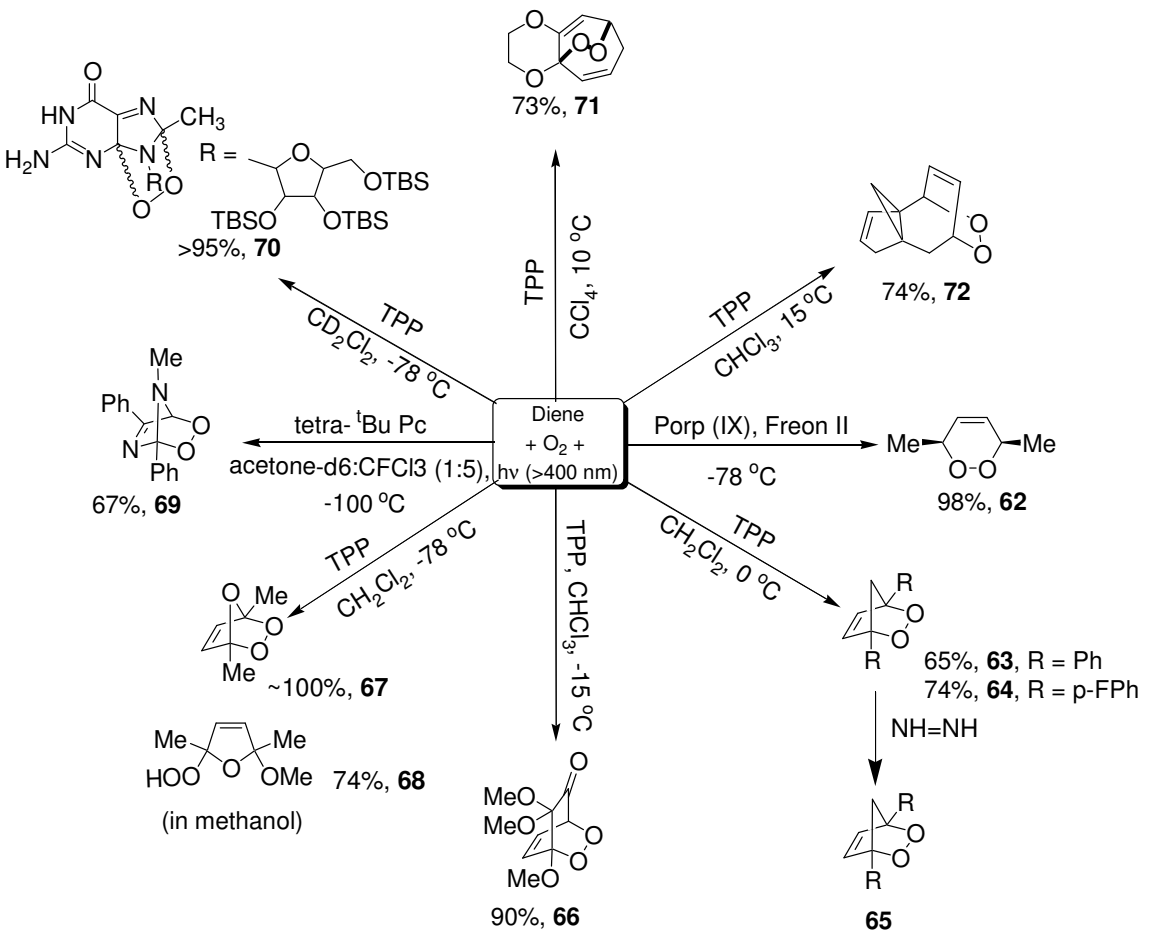

5.3.2 Arenes

The rosette of Scheme 5 shows the endoperoxidation of the corresponding arene compounds in Scheme 4.

5.3.2.1 Benzenes. Benzene, toluene, and xylenes do not chemically react with singlet oxygen. However, hexamethylbenzene (**34**) is sufficiently electron rich to react with singlet oxygen.[42] Hexamethylbenzene-1,4-endoperoxide (**43**) formed in a MB-sensitized reaction in CD_3NO_2 at 15 °C and, over time, endoperoxy-hydroperoxide **43'**

arose from a secondary singlet oxygenation in 90% yield (not isolated, quantitated from the NMR spectrum with an added internal standard) (Scheme 8). The second equivalent of oxygen added, interestingly, by a singlet oxygen 'ene' reaction on the initially formed endoperoxide **43**. Bisperoxides that were formed from the addition of two singlet oxygen molecules are the subject of Section 5.5.2. Heating the primary endoperoxide product **43** at 40 °C for one hour led to oxygen evolution and the regeneration of hexamethylbenzene **34**. Singlet oxygen also reacted with pentamethylbenzene except much more slowly than hexamethylbenzene.[42,43] The reaction of phenol with singlet oxygen led to *p*-catechol and *p*-quinone products in near quantitative yield, although the proposed endoperoxide intermediate was not directly observed (Scheme 9).[44,45]

Scheme 8

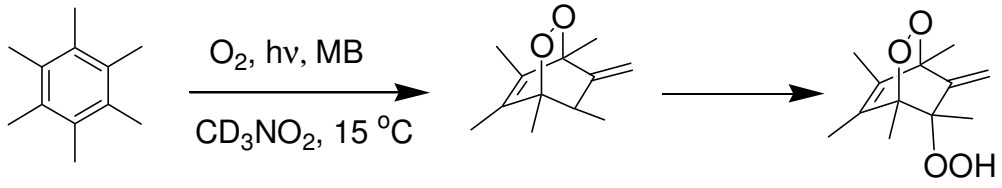

34 **43** 90%, **43'**

Scheme 9

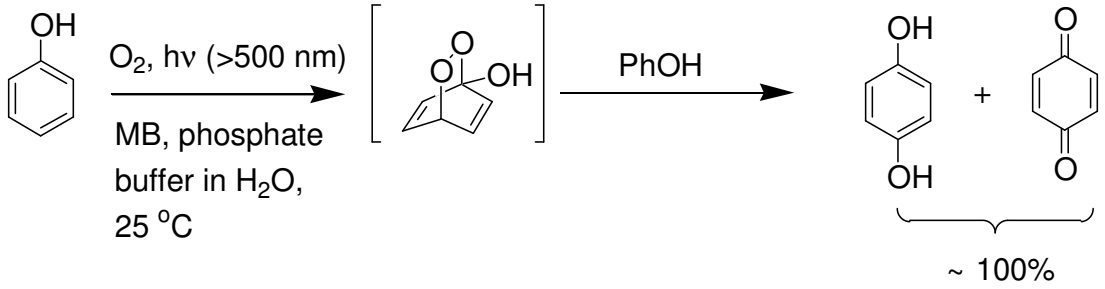

5.3.2.2 Naphthalenes. Many naphthalene endoperoxides have been prepared.[46-49] In 1972, the singlet oxygenation of 1,4-dimethylnaphthalene (**35**), in which MB served as sensitizer in O_2-saturated CH_2Cl_2 at -78 °C gave regioselectively 1,4-dimethylnaphthalene-1,4-endoperoxide **44** in 58% yield after column chromatography at 0 °C.[47] Compound **35** reversibly binds singlet oxygen. It forms endoperoxide **44** and gradually decomposes back to **35** by dissociation of singlet oxygen.[47] With enriched $^{18}O_2$ gas used in the photooxidation, an ^{18}O-^{18}O labeled naphthalene endoperoxide has also been synthesized.[50] Bulky substituents at the 1,4-positions of naphthalene slowed the rate of singlet oxygen addition to **45** and competitive binding of singlet oxygen at the 5,8-positions, **46**.[51,52] The maloamide substitutents exerted steric interactions that slowed binding of $^1O_2$ at the 1,4-positions. Instead, binding of $^1O_2$ at the 5,8-positions was favored in D_2O at 50 °C (ratio of **45**:**46** was ~1:100), in which the stability of **46** ($t_{1/2}$ = 5 h) was greater than **45** ($t_{1/2}$ = 0.5 h) at 25 °C due to higher crowding at the dioxapaddlane core of **45**. The maloamide chains are not themselves oxidized; for example, no side-chain hydroperoxides were formed. Solvent effects on the singlet oxygen endoperoxidation have been studied.[51-53] Binding of singlet oxygen at the 1,4-positions was favored in CD_3OD at 25 °C (ratio of **45**:**46** was 80:20).[51] Studies of solvent effects of singlet oxygen [2 + 4] cycloadditions point to exciplex formation preceding the endoperoxide product in view of the dependence on solvent parameters π^* and σ_H.[53]

Naphthalene endoperoxides have been synthesized with methyl groups located at the 1,4-, 1,8-, 1,2,4-, 1,4,5-, 1,2,3,4-positions, and 1,2,3,4,5,6,7,8-positions in good yield after recrystallization 58%, 88%, 93%, 54%, 83%, and 69%, respectively.[48,49] The C-O bond formation preferably takes place at aryl sites bonded by the methyl groups.

Stabilities of the endoperoxides were greater with increased numbers of methyl groups on naphthalene [at 25 °C in $CDCl_3$, compare 1,2,4-trimethylnaphthalene-1,4-endoperoxide ($t_{1/2}$ = 70 h) with 1,2,3,4-tetramethylnaphthalene-1,4-endoperoxide ($t_{1/2}$ = indefinite)], and where *peri* methyl-methyl interactions increased stability [at 25 °C in $CDCl_3$, compare **44** ($t_{1/2}$ = 5 h) with 1,8-dimethylnaphthalene-1,4-endoperoxide ($t_{1/2}$ = 30 h)].[48]

5.3.2.3 Anthracenes, Polyacenes, and Carbon Nanotubes. In 2006, the singlet oxygenation of 9,10-diphenylanthracene (**37**) led to 9,10-diphenylanthracene-9,10-endoperoxide (**47**) in O_2-purged $CHCl_3$-CCl_4 (1:4) at -20 °C.[5] The photosensitizer *seco*-porphyrazine was immobilized in a ring-opening metathesis sphere (ROMP-sphere) in a heterogeneous reaction.[5,55] In 1982, the photooxidation of anthracene derivative **39** in CS_2 at 25 °C gave selectively endoperoxide **49** in high yield.[56,57] Here, sunlight was used as the light source and the substrate **39** served as its own sensitizer. Oligomeric anthracene endoperoxide (**50**) was prepared from singlet oxygenation of thin anthracene films of **40** mixed with TPP or MB, which produced the polyendoperoxide **50**.[58] Thermolysis of **50** led to the release of singlet oxygen molecules and gave back the starting anthracene **40**.

Singlet oxygenation of a tetraphenyltetracene compound bearing four carboxylate groups (**41**) gave endoperoxide **51** in high yield in D_2O.[46,59] Here, singlet oxygen reacted with **41** regioselectivity at one of the two center rings.[60] Photooxidation experiments showed that parent tetracene (naphthacene, $C_{18}H_{12}$) gave the 5,12-endoperoxide not the 1,4-endoperoxide.[60,61] In $CDCl_3$, the ^1H NMR absorptions at δ_{H5} (6.15 ppm) and δ_{H6} (7.84 ppm) where characteristic of the 5,12-endoperoxide.[62] In 2008, singlet oxygen was found to add to 5,12-diamide substituted tetracene **73** crystals at the 6,11-positions (**75**,

Scheme 10).[62] However, the singlet oxygen addition in chloroform afforded the 5,12-endoperoxide **74**. The product distribution was apparently distinguished by a H-bond-mediated $^1O_2$ endoperoxidation. The regioselectivity derives from an *anti* diamide conformation in the solid state give the opposite regioselectivity to that in chloroform. Hydroxyl substitutents are also known to assist singlet oxygen binding with facial selectivity in endoperoxidation reactions.[60]

Scheme 10

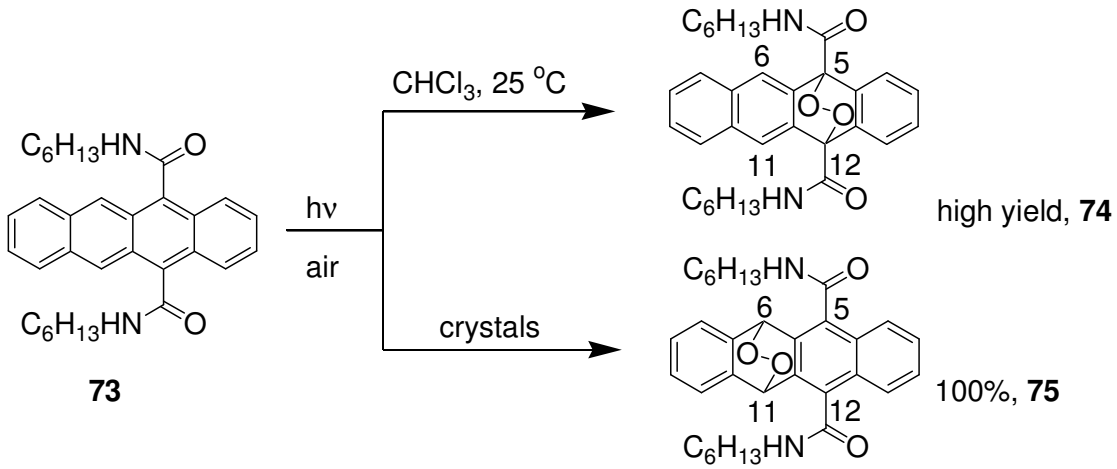

An investigation of a pentacene—$^1O_2$ reaction appeared in 2007.[63] 6,13-Thienylpentacene-6,13-endoperoxide (**52**) was synthesized in 81% yield in the reaction of 6,13-thienyl-substituted pentacene **42** with singlet oxygen in CH_2Cl_2 at 25 °C.[63] Compound **42** served as its own sensitizer. On the basis of ^{13}C-NMR spectroscopy and X-ray crystallography, endoperoxide structure **52** was assigned. The X-ray structure displayed an intramolecular through space 1,4-sulfur-oxygen (S--O) interactions in the crystal structure.[63] Photooxidation of the parent pentacene $C_{22}H_{14}$ molecule followed similar chemistry yielding the 6,13-endoperoxide, but neither the 1,4- nor 5,14-endoperoxide.[64,65] Pentacene-6,13-endoperoxide decomposed to pentacenequinone.[64,65]

Reports on higher polyacene—$^1O_2$ reactions are scarce because of ground state $^3O_2$ reactions which preferentially take place.

In 2007, a paper on single-walled carbon nanotubes (SWCNs) reported the reaction with singlet oxygen.[66] Purification became easy due to contrasting solubility properties of unfunctionalized and oxyfunctionalized SWCNs, but it was uncertain whether the SWCN peroxides formed from a [2 + 2], a [2 + 4] cycloaddition, or both.[66] A subsequent report found SWCNs to be of very low chemical reactivity with $^1O_2$.[67,68] Instead, SWCNs were proposed to physically quench singlet oxygen (convert $^1O_2$ to $^3O_2$) with rate constants on the order of 10^8 M^{-1} s^{-1}.

5.3.3 Electron Transfer Photooxidation

In 2004, a report appeared that 9,10-dimethylanthracene-9,10-endoperoxide **(48**) arose from an electron-transfer photooxidation of 9,10-dimethylanthracene (**38**) with the use of the sensitizer Acr^+-Mes in O_2-saturated CH_3CN at 0 °C.[32] Subsequent coupling of the anthrecene radical cation and the superoxide ion generated endoperoxide **48**. Endoperoxide **48** was detected during the initial stage of the photooxidation, it was not isolated, and over time the reaction yielded 10-hydroxanthrone, anthraquinone, and H_2O_2.

5.3.4 Conjugated Dienes

The rosette of Scheme 7 shows the endoperoxidation of the corresponding diene compounds in Scheme 6. In some cases, solvent addition adducts are formed.

5.3.4.1 Acyclic Dienes. In 1989, the irradiation of (*E,E*)-2,4-hexadiene **53** sensitized by *meso*-porphyrin IX dimethyl ester led to the formation of *cis*-3,6-dimethyl-

1,2-dioxene (**62**), which was the major product detected at -78 °C in Freon 11.[69] Endoperoxide **62** was purified under vacuum at 0.75 mmHg, passing and collecting it in a trap (98% isolated yield). Dienes that can adopt *cisoid* conformation, such as **53** or (*E,E*)-1,4-diphenylbutadiene (**53'**) were photooxidized the corresponding endoperoxides in high or quantitative yield in a suprafacial Diels-Alder reaction.[60,70] Dienes that cannot readily adopt *cisoid* conformations, such as (*E,Z*)-2,4-hexadienes and (*Z,Z*)-2,4-hexadienes lose stereochemistry in the singlet oxygen [2 + 4] cycloaddition.[60] (*E,Z*)- and (*Z,Z*)-dienes give a complex mixture of hydroperoxides and aldehydes suggesting the intervention of intermediate zwittersions or 1,4-diradicals.[71]

5.3.4.2 Cyclopentadienes and Cyclohexadienes. Singlet oxygen reactions have been conducted with many cyclopentadiene and cyclohexadiene compounds as a means to generate bicyclic endoperoxides.[72] The synthesis of an endoperoxide from the parent cyclopentadiene in O_2-purged $CHCl_3$-CCl_4 (1:4) at -20 °C has been reported in 93% yield, in which the photosensitizer was a ring-opening metathesis sphere (ROMP-sphere)—supported *seco*-porphyrazine.[5] In 2005, endoperoxides **63** and **64** were synthesized, in 65% and 74% yields in CH_2Cl_2 at 0 °C, from TPP-sensitized photooxygenations of dienes **54** and **55**.[73]. Diimide (HN=NH) from potassium azodicarboxylate and acetic acid selectively reduced the carbon-carbon double bond of endoperoxide **63** to give **65**.[39,74] The reaction of endoperoxide **63** with thiourea leads to *cis*-2-cyclopenten-1,4-diol.[39] In 2008, the singlet oxygenation of diene **56** afforded endoperoxide **64** in good yield (90%), from a TPP-sensitized photooxygenation reaction in $CHCl_3$ at -15 °C.[75] The photooxidation of dienes similar to **56** in methanol gave 4-hydroxy-2-cyclopentenones via ring contraction reactions upon addition of thiourea.[75]

5.3.4.3 Heterocycles and Cyclohexatriene. Furans have been employed to generate ozonides via photooxidations. The formation of ozonide **67** resulted from the TPP-sensitized photooxygenation of 2,5-dimethylfuran (**57**) in CH_2Cl_2 at -78 °C.[72] Low-temperature NMR spectra were recorded and the reaction can presumably be taken to 100% yield, although the endoperoxide was not isolated. Spectral data showed the existence of the monomeric furan endoperoxide **67**. Low temperatures were maintained to prevent dimerization of endoperoxide **67**.[76] Results similar to **57** were observed in the photosensitized oxidation of a ^{13}C,^{15}N-labeled *N*-methyl-4,5-diphenylimidazole (**58**).[77] The sensitizer used was 2,9,16,23-tetra-*tert*-butyl-29*H*,31*H*-phthalocyanine (tetra-^{t}BuPc) and the solvent was acetone-d_6 and fluorotrichloromethane in a 1:5 ratio. Singlet oxygen reacted with **58** via a [2 + 4] cycloaddition forming the 2,5-endoperoxide **69** (67%, NMR spectrum of the reaction mixture), which was stable at -100 °C, but upon warming decomposed to a hydroperoxide. In 1993, diasteromeric endoperoxides **70** were characterized in the low-temperature photooxidation of 2',3',5'-*O*-(*tert*-butyldimethylsilyl)-8-methylguanosine (**59**).[78] The OTBS groups provided solubility for low-temperature characterization in CD_2Cl_2, and the 8-methyl group prevented the facile rearrangement that rapidly occurs in guanine peroxides bearing an 8-H substituent. On the basis of -20 °C ^1H and ^{13}C NMR and low-temperature FAB mass spectrometry, endoperoxides **70** were assigned in greater than 95% NMR yield.[78] Unlike CD_2Cl_2, in methanol the photooxidation of **59** gave endoperoxide **70** in low yields. In methanol, a methoxy-hydroperoxide intermediate (**68**) was formed in 74% from the photooxygenation of **57**.[79,80] Formation of 1,2- and 1,4-methanol adducts had been

observed previously, for example the photooxidation of 2,5-dimethyl-2,4-hexadiene in methanol produced such solvent adducts.[71]

Butenolides arise from the reaction of furans, such as **76** with singlet oxygen in the presence of alkyl amine bases.[81] Scheme 11 shows an intermediate endoperoxide (**77**) converting to diasteromeric γ-hydroxyacrylbutenolides **78** in 88% yield after column chromatography. Singlet oxygenation of **76** was conducted in the presence of Hünig's base in CH_2Cl_2 at -78 °C. Scheme 11.12 shows the proposed conversion of intermediate endoperoxide **77** to diasteromeric butenolides **78**. The absence of Hünig's base in the photooxidation of **76** resulted in a complex mixture of compounds.

Scheme 11

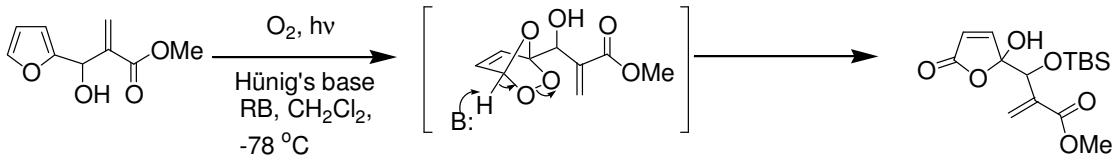

76 **77** 88%, **78**

Two examples are presented in which intramolecular nucleophilic attack of adjacent alcohol groups led to the formation of spiro compounds (Scheme 12 and 13). In 2008, spirolactone **80** was synthesized in CH_2Cl_2 from an MB-sensitized photooxygenation of furan **79.**[82] A possible mechanism, with an endoperoxide intermediate converting and setting up an intramolecular alcohol attack at the γ-ring site. Acetic anhydride and pyridine were added to the reaction, which provided **80** in 57% yield over the two steps. In 2006, the singlet oxygenation of 2-substituted furan **81** led to [6,5,6]-bis-spiroketal (**82**) in an MB-sensitized reaction followed by the addition of dimethylsulfide and *p*-TsOH.[83] In 1991, the singlet oxygenation of 2-carboxy-4-methoxy-5-(methoxycarbonyl)-1-methylpyrrole (**83**), in which RB served as the

sensitizer in O_2-saturated CH_3CN-H_2O (3:1) at 22 °C gave 5-hydroxy-4-methoxy-5-(methoxycarbonyl)-2-methyl-3-pyrrolin-2-one (**85**) in 92% yield after silica gel chromatography (Scheme 11.15).[84] The reaction likely produced the endoperoxide intermediate **84** prior to decarboxylation and formation of pyrrolin-2-one **85**.[84] The reported examples in Schemes 11-14 did not yield isolable endoperoxides, and revealed the potential for endoperoxide decomposition in the presence of a base or internal alcohol.

Scheme 12

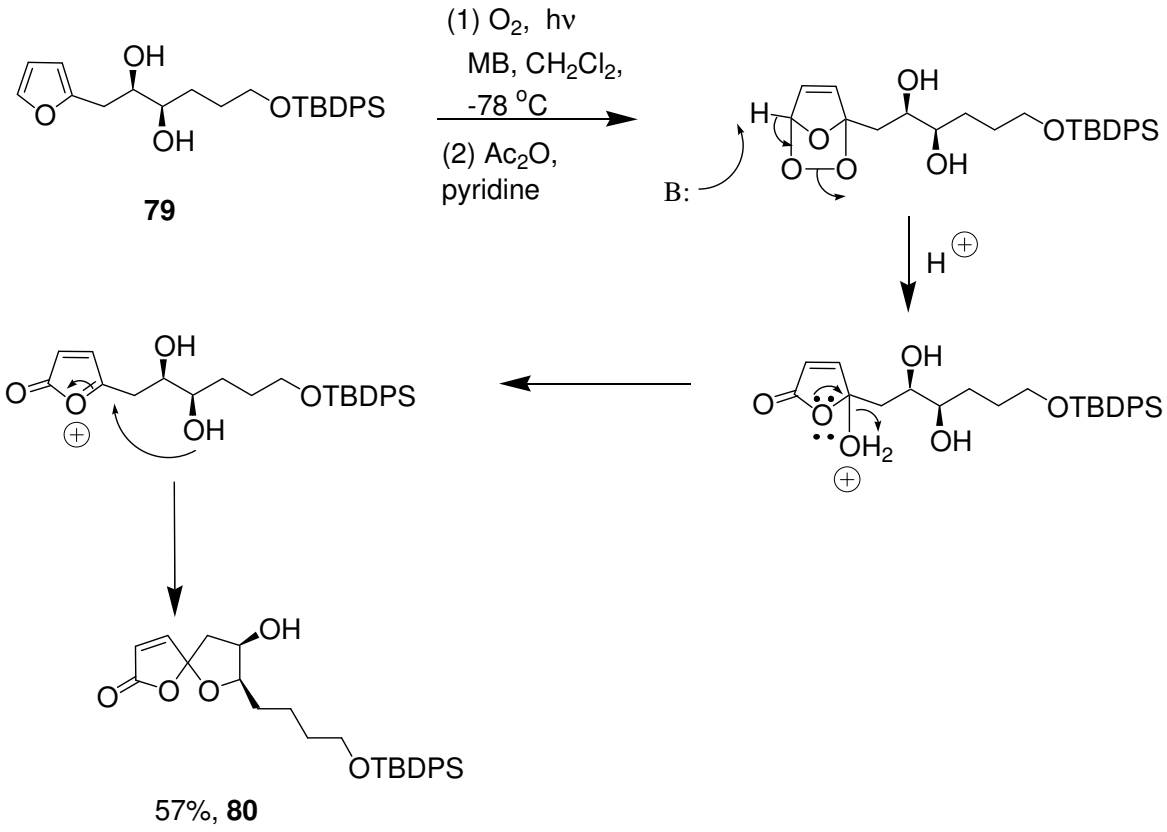

Scheme 13

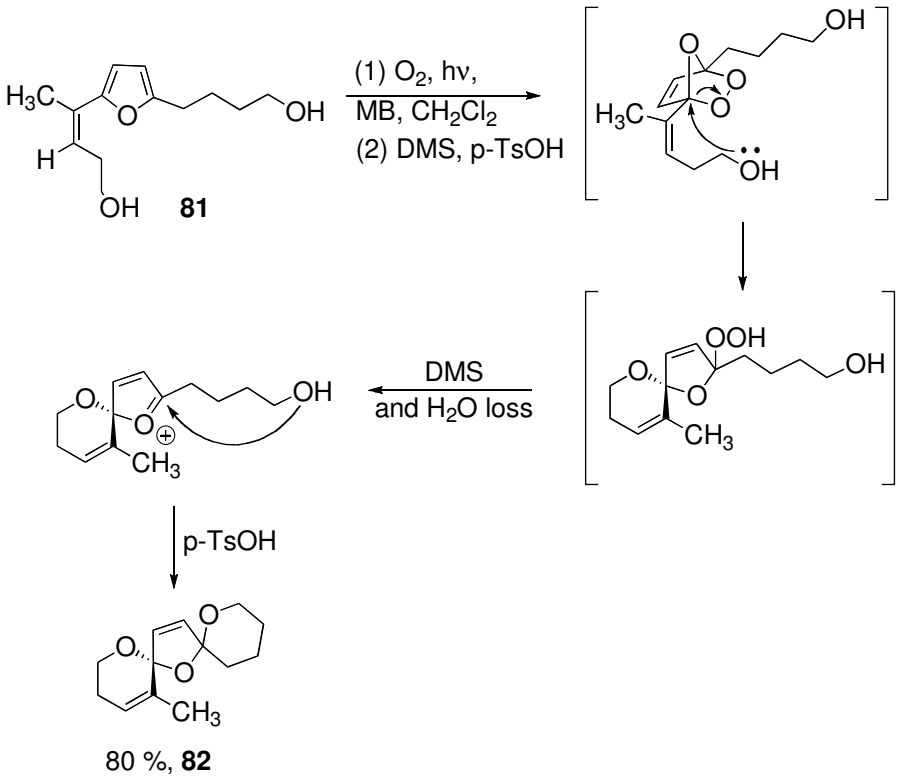

Scheme 14

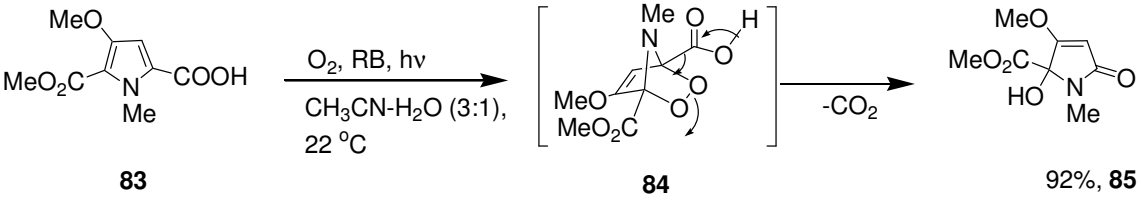

In 2006, the TPP-sensitized photooxidation of a cycloheptatriene derivative (**60**) led to a tricyclic endoperoxide (**71**) as the major product in O_2-purged CCl_4 at 10 °C (Scheme 15).[85] Treatment of **71** with triethylamine in CH_2Cl_2 at -30 °C led to O-O bond cleavage and the generation of tropolone **86**. On the other hand, heating **71** at 160°C resulted in the formation of epoxyketal **87**. In 1982, the photooxidation of

tricyclo[5.3.1.0]undeca-2,4,9-triene (**61**) in $CHCl_3$ at 10 °C gave selectively endoperoxide **72** in high yield (see Schemes 6 and 7).[86] After removing solvent, the residue was chromatorgraphed on silica gel at 0 °C, and the endoperoxide (**72**) was obtained in 74% yield as an oil that crystallized in the refrigerator.

Scheme 15

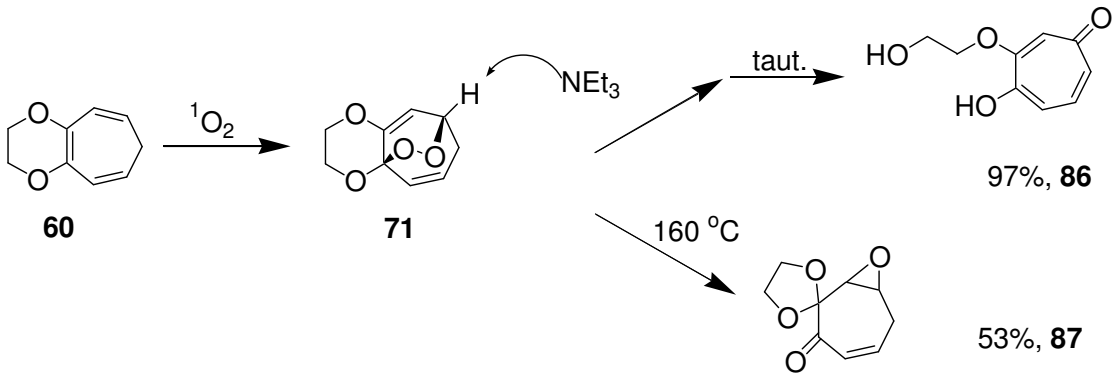

5.3.5 Summary

Reported of photooxidations giving endoperoxides has been published in several reviews.[2,38-41] The clean production of endoperoxides has been achieved, and many of these endoperoxides have been isolated pure and in high yields. Endoperoxides have been generated in organic and aqueous media, but some are unstable above 0 °C. Decomposition of endoperoxides can lead to the dissociation of oxygen.[46-48] Endoperoxide decomposition also occurs by O-O bond cleavage, which results in the formation of bisepoxides (e.g., spiro[2.4]hepta-4,6-diene endoperoxide)[39] or ketones (such as the conversion of the natural product kalasinamide via its endoperoxide to the corresponding quinone, marcanine A).[87] Endoperoxides are not known to rearrange to dioxetanes. For example, vinyl dioxetanes do not rearrange to the corresponding

endoperoxides. Endoperoxides have been trapped with phosphines. Insertion of phosphines into the O-O bond of unsaturated endoperoxide **61** and other bicyclic endoperoxides have been conducted, and point to a biphilic insertion mechanism with varying degrees of nucleophilic and electrophilic contributions in the transition states giving the bicyclic dioxaphosphoranes.[88] Alcohol solvents can lead to trapping and addition of the solvent giving hydroperoxy alcohols.

5.4 Allylic Hydroperoxides

5.4.1 Background Information

Singlet oxygen chemistry has been employed in the synthesis of allylic hydroperoxides.[89,90] The $^1O_2$ 'ene' reaction of alkenes gives allylic hydroperoxides, where the double bond has shifted. Scheme 8 presented one example (*vide supra,* Section 5.3.2.1).[42,43] Schemes 16 to 19 demonstrate several reported examples of hydroperoxides formed in good to high yields. Singlet oxygen reacts rapidly with allylic alkenes in solution or confined within zeolites. Zeolites have been used to affect the regio- and stereochemical outcome of the hydroperoxide products.[91,92]

5.4.2 Simple Alkenes

An example of a singlet oxygen 'ene' reaction was provided in 2006, where hydroperoxide **89** was prepared from C_{60}-supported silica gel in a solvent-free reaction of tetramethylethylene (**88**) at 25 °C (Scheme 16).[93] Purification was conducted by washing the silica gel with chloroform or ethyl acetate, and obtaining **89** after evaporating the solvent. The scope of the solvent-free $^1O_2$ reaction in the work included mono-alkenes,

dienes, and diethylsulfide.[93] Singlet oxygen 'ene' reactions of allylic alcohols have also been performed by solid-state photooxygenations in dye-crosslinked polystyrene and gave diastereomeric hydroperoxides.[94,95]

Scheme 16

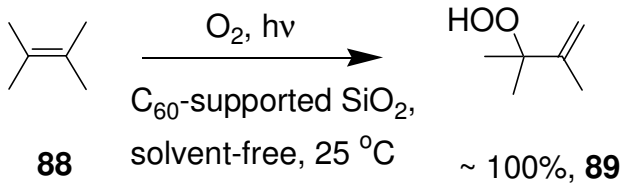

In 2004, excellent yields of hydroperoxides **91** and **92** were obtained (>95%) in the photooxidation of racemic acid **90** (Scheme 17).[96] The diastereoselectivity of the photooxidation favored the *trans* configurated products due to the *anti* directing effect of the protonated carboxylic acid group. Low regioselectivity was observed for **92** compared to **91**. Pyridine helped accelerate the deprotonation of the CH next to COOH of **90** affording **92**, and also suppressed the formation of aromatic compounds, which would otherwise take place in the absence of pyridine. A great many studies of 'ene' reactions have been conducted in organic solvents.[97-101] or aqueous media.[102-106] One report appeared which used a fluorous biphasic solution.[107]

Scheme 17

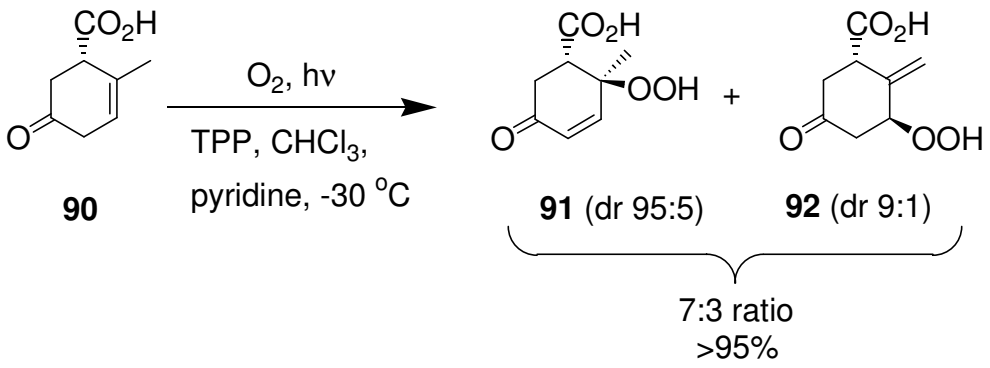

In 1996, the photooxidation of alkene **93** was reported in a fluorous biphasic solution (C_6F_{14}/CD_3CN) at 0 °C (Scheme 18).[107] Compound **93** reacted with $^1O_2$ produced from irradiation of 5,10,15,20-tetrakis(heptafluoropropyl)porphyrin (TPFPP), and **94** was obtained in 57% yield where a shift in the double bond took place. Acetonitrile was chosen as the co-solvent due to a favorable partition coefficient of the TPFPP sensitizer, which was important. Over time sensitizers eventually decompose, but TPFPP proved to be more chemically stable compared to TPP in the presence of singlet oxygen, which was attributed to the physical segregation of TPFPP from **93** and **94**. A three-phase solid-gas-liquid experiment also noted enhanced sensitizer stability when is had become distanced from the reagents.[108] In 2007, a report appeared on photooxidations of alkenes within fluorinated zeolite media, which due to an enhanced lifetime of $^1O_2$ proved useful for 'ene' reactions. Zeolites will be the subject of the next subsection.[109]

Scheme 18

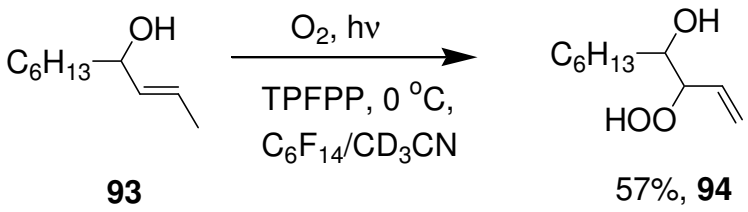

93 57%, **94**

5.4.3 'Ene' Reactions Confined in Zeolites

In recent years, singlet oxygen hydroperoxidations have been conducted in zeolites because different product distributions are observed.[91,92,110,111] Diastereoselection in singlet oxygen 'ene' reactions of chiral alkenes has been observed due to zeolite confinement.[111] Trisubtituted alkenes gave different diastereoselectivity in solution than when carried out within zeolite NaY, the latter was attributed to a synergistic effect of sterics and cation-π interactions. In 1996, a thionin-supported cation-exchanged zeolite reaction was reported for the $^1O_2$ 'ene' reaction with 2-methyl-2-pentene (**95**) (Scheme 19).[112] The interior of the cavity helped to control the direction of attack by singlet oxygen on **95**. Singlet oxygen adds –OOH selectively to the 3-position of **95** within the zeolite. In acetonitrile solution, singlet oxygen adds to **95**, yielding the 3- and 2-hydroperoxides (**96** and **97**, respectively).

Scheme 19

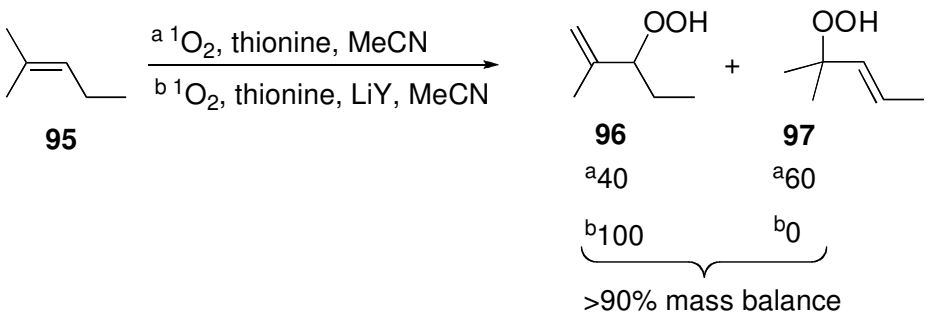

5.4.4 Summary

Allylic hydroperoxides have been synthesized as pure compounds in high yield. The sensitized photooxidation of the allylic alkenes proceeded rapidly with visible light, and ceased after uptake of 1 equivalent of oxygen. Researchers have studied singlet oxygen 'ene' reactions extensively and recent reviews have appeared on the subject.[89,90] Allylic alkenes not only react readily with singlet oxygen to afford hydroperoxide products, but also provide synthetic routes to asymmetric hydroperoxides. Zeolite-mediated asymmetric hydroperoxidations have been of recent interest. In 2003, a theoretical study concluded that the perepoxide is not a minimum on the potential energy surface in reactions of *cis*-2-butene or tetramethylethylene with $^1O_2$.[113]

5.5 Tandem Singlet Oxygen Reactions

5.5.1 Background Information

The bisperoxides described in this section represent compounds that have taken up 2 equivalents of singlet oxygen. Sections 5.3.2.1 and 5.3.2.3 have mentioned the formation of a bisperoxide **43'** and a polyendoperoxide **50**. Schemes 20 to 25 demonstrate reported examples of bisperoxides formed from tandem singlet oxygen

reactions in good to high yields (Section 5.5.2). A degree of correlation among furan and guanine photooxidations is mentioned, in both cases spiro compounds form.

5.5.2 Bisperoxides

5.5.2.1 Phenyl-Substituted Alkenes. In 1978, a bisdioxetane (**99**) was prepared from a double [2 + 2] cycloaddition reaction of two molecules of singlet oxygen with bisdioxene **98**. The reaction used polymer-supported RB in O_2-saturated CH_2Cl_2 at -78 °C and formed **99** in good yield (70%, Scheme 20).[114] Another example is the tandem [2 + 4]/[2 + 4] singlet oxygenations of 2,3-diphenylindene **15**, which was reported in 1979 (Scheme 21). The reaction afforded a diendperoxide (**100**) in Freon-11 or acetone-d_6 at -78 °C (100% NMR yield, not isolated).[26] The initially formed monoendoperoxide was not characterized structurally. The second mole of $^1O_2$ was proposed to add rapidly on the opposite side (on the 6-membered ring portion) thereby forming **100**. Interestingly, evidence showed that the photooxidation of **15** in methanol or in methanol-acetone solvent mixtures produced a dioxetane (*vide supra*, Section 5.2.4). In 1972 and 1973, the photooxidation of benzhydrylidene-cyclobutane (**101**) in chloroform and 0.5% ethanol at -60 °C was reported to lead to diendoperoxide **102** (63% yield), a compound which exploded above 130 °C (Scheme 22).[115,116]

Scheme 20

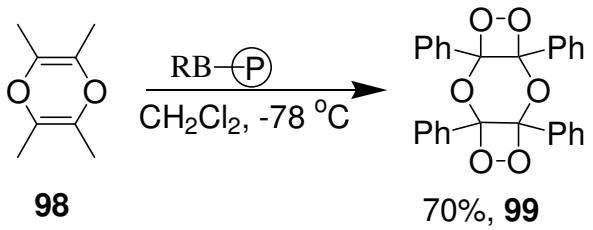

98 70%, **99**

Scheme 21

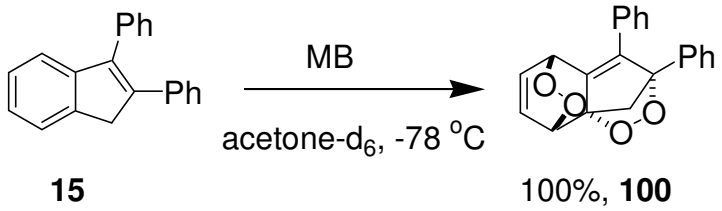

15 100%, **100**

Scheme 22

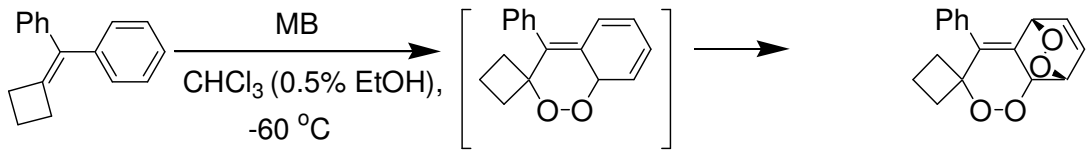

101 63%, **102**

5.5.2.2 Cyclic Alkenes. In 1995, the RB-sensitized photooxygenation of 6,6-diethoxyfulvene (**103**) in acetone-d_6 at -78 °C afforded diethoxyfulvene endoperoxide (**104**) as a primary product (Scheme 23).[117] On the basis of ^{1}H-NMR spectroscopy at -50 °C, the initial endoperoxide **104** was assigned, the dioxetane, **105**, was not observed. Further photooxygenation resulted in the formation of bisperoxides *syn*-**106** and the *anti*-**106** in a 9:1 ratio. Peroxides **104** and **106** were not stable and were not isolated. Above -30 °C, endoperoxide **104** relased oxygen and gave back fulvene **103**, the bisperoxides **106** decomposed to *cis*-butenedial, diethylcarbonate, and carbon monoxide.

Scheme 23

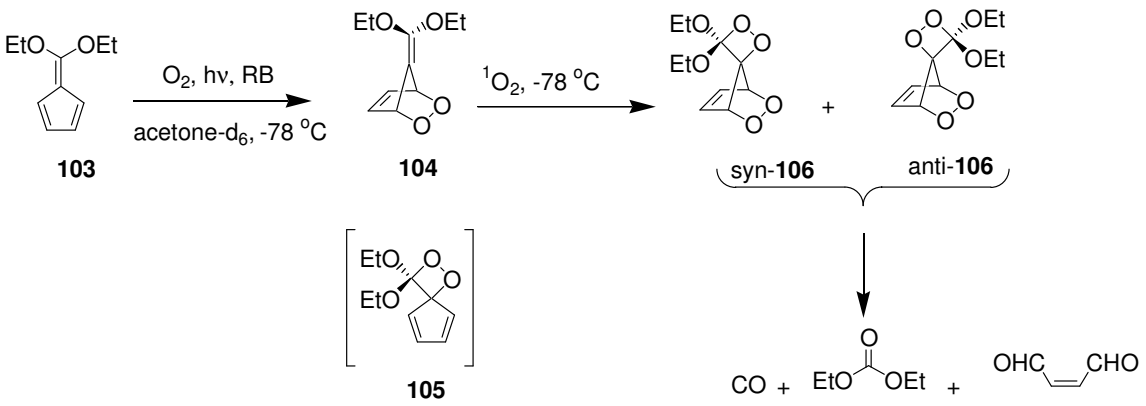

The TPP-sensitized photooxidation of 1,4-cyclohexadiene (**107**) yielded several peroxide products, **109**-**112** (Scheme 24).[118-120] Once the primary 'ene' product formed (**108**), endoperoxy-hydroperoxides **109** and **110** arose by secondary [2 + 4] cycloadditions in 87% and 9% yield, respectively, and bishydroperoxides **111** and **112** arose by secondary 'ene' reactions in less than 4% yield combined. The purification of peroxides **109**-**112** was accomplished by silica gel chromatography at low temperature. *cis*-Hydroperoxide **112** was recrystallized. In 2006, a hydroperoxy-endoperoxide (**114**) was isolated in 80% chromatographed yield from a TPP-sensitized oxygenation of tetrahydronaphthalene (**113**) in CH_2Cl_2 at 15 °C (Scheme 25).[121] The primary singlet oxygen 'ene' product was not observed, but its formation produced a diene unit capable of adding the second equivalent of singlet oxygen. The configuration of hydroperoxy-endoperoxide **114** was determined indirectly based on the X-ray structure of **116** produced from the bromination of **114** via intermediate **115**.

Scheme 24

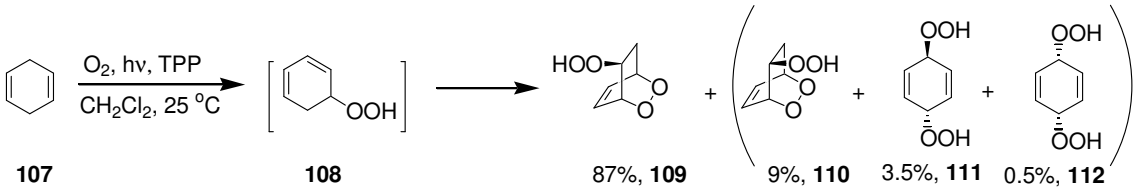

Scheme 25

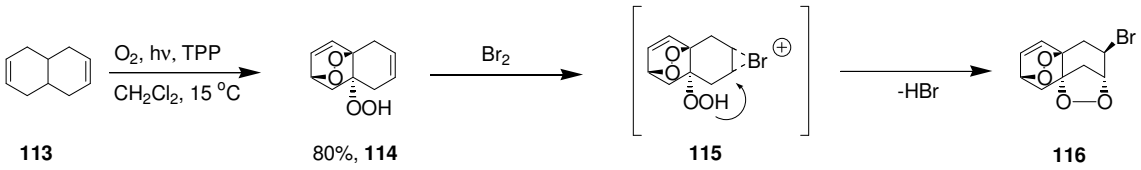

In 2005, 4α-hydroxy peroxyguaienes *anti*-**118** and *syn*-**118** were formed from the photooxidation of diene **117** in CH_2Cl_2 upon reduction of the hydroperoxide group with triphenylphosphine (Scheme 26).[122] The first addition of singlet oxygen was found to be stereoselective. The second addition of singlet oxygen was less selective, presumably forming endoperoxy-hydroperoxides prior to reduction by the triphenylphosphine to give mixtures of endoperoxy-alcohols **118** in 56% combined yield.

Scheme 26

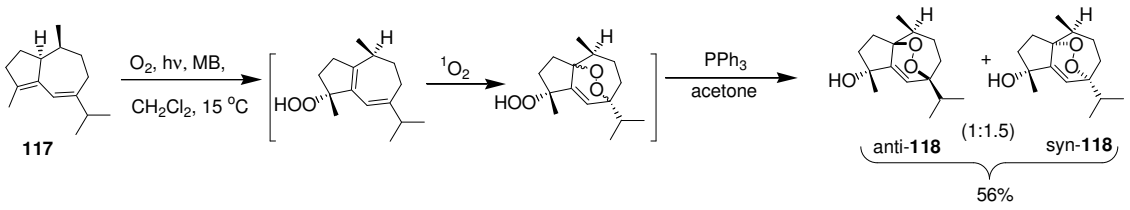

5.5.3 Rearrangment to a Hemiketal Hydroperoxide

In 1998, the singlet oxygenation of biphenylene (**119**) with TPP in O_2-saturated acetone at -40 °C yielded a hemiketal hydroperoxide (**122**) in 56% yield after silica gel chromatography (Scheme 27).[123] On the basis of ^{1}H-NMR spectroscopy, the primary product was assigned to the monoendoperoxide (**120**), which underwent fragmentation into a dicarbonyl product **121**. After further cyclization and tautomerization steps, a furanone derivative added a second singlet oxygen molecule by the 'ene' reaction to reach the hemiketal hydroperoxide, **122**.

Scheme 27

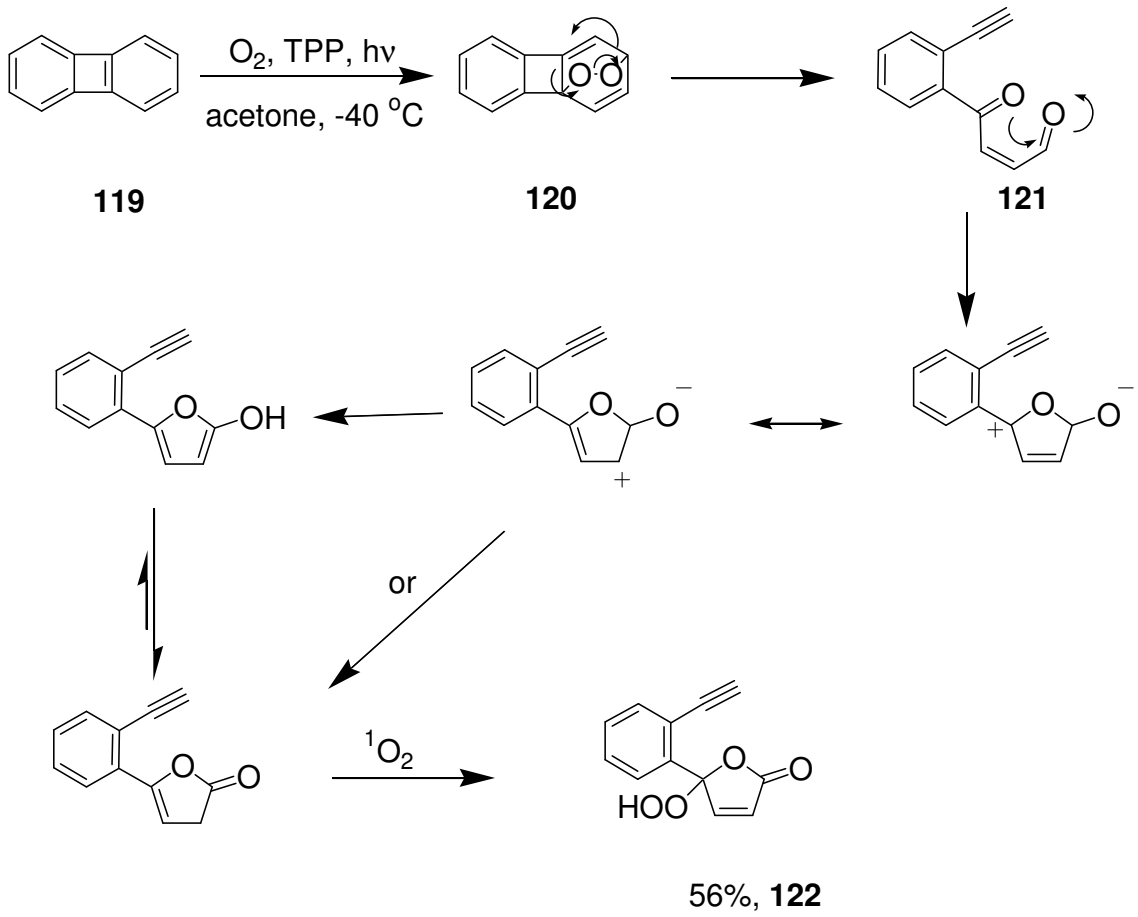

5.5.4 Rearrangements to Spiro Compounds

In 2005, a tandem singlet oxygen reaction with *Z*- or *E*-silylated furan **123** was studied, which gave diastereomeric bis-4-hydroxybutenolides **124** as the initial products (Scheme 28). [82,124] After workup with mild acid from silica gel chromatography or *p*-TsOH, spiroketals **125** were isolated in good yield (80%). The spiroketal moiety of *cis*- and *trans*-**125** represents the core structure of the natural product prunolide C. Replacement of the $SiMe_3$ group for H in unsubstituted furans has been shown to be synthetically useful.[125] A mechanism for the singlet oxygenation of 2-methyl-5-trimethylsilylfuran (**126**) proposed silyl migration and methanolysis to give γ-hydroxy-γ-lactone **127** (Scheme 29).[125]

Scheme 28

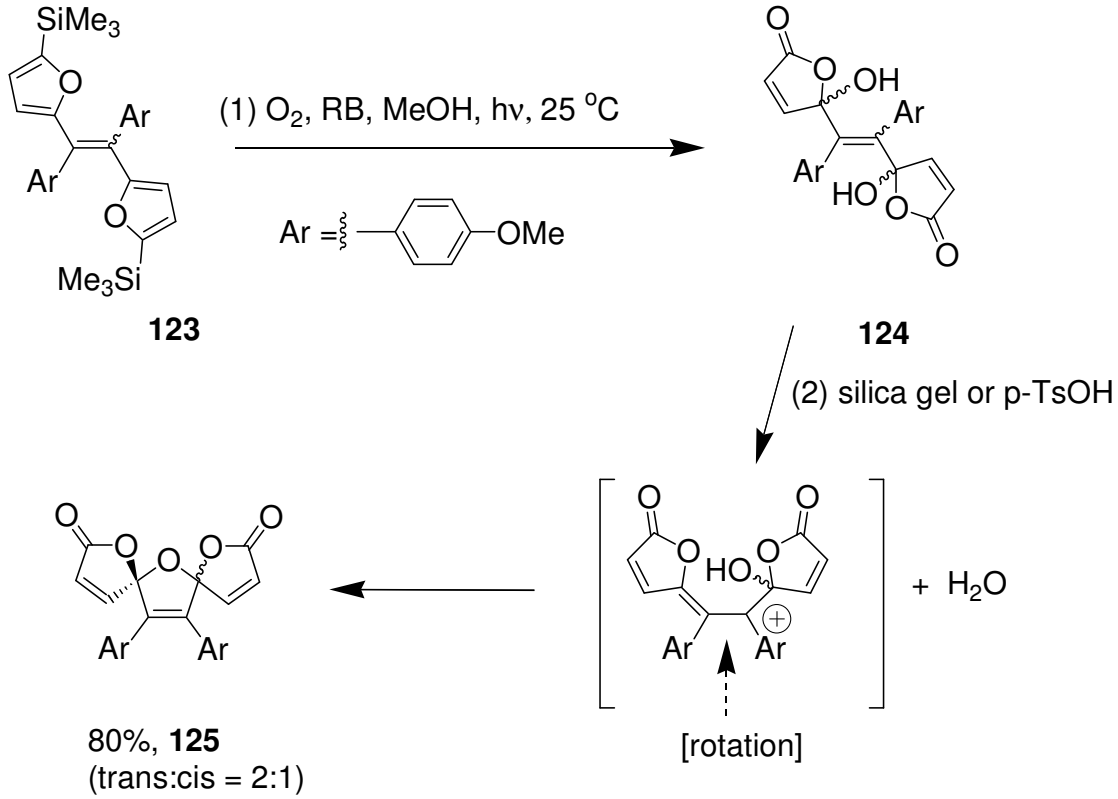

Scheme 29

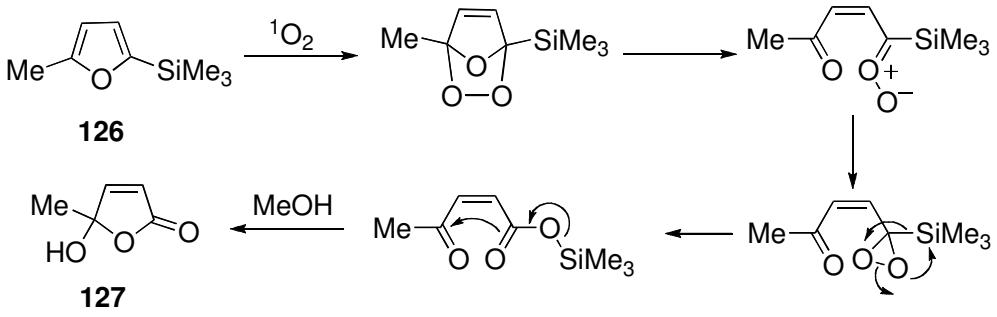

In 2007, a tandem singlet oxygen [2 + 4] cycloaddition and 'ene' reaction and ketalization was reported for **128** (Scheme 30).[126] The reaction was conducted with MB as the photosensitizer in $CDCl_3$ at 8 °C. The overall yield of 8-epi and (+)-premnalane was 62% (ratio **129**:**130** was 2:1), and they could be separated by column chromatography. In addition to the NMR spectroscopy evidence for **129** and **130**, X-ray crystal data was obtained for one of the diastereomers of (+)-premnalane **130**.

Scheme 30

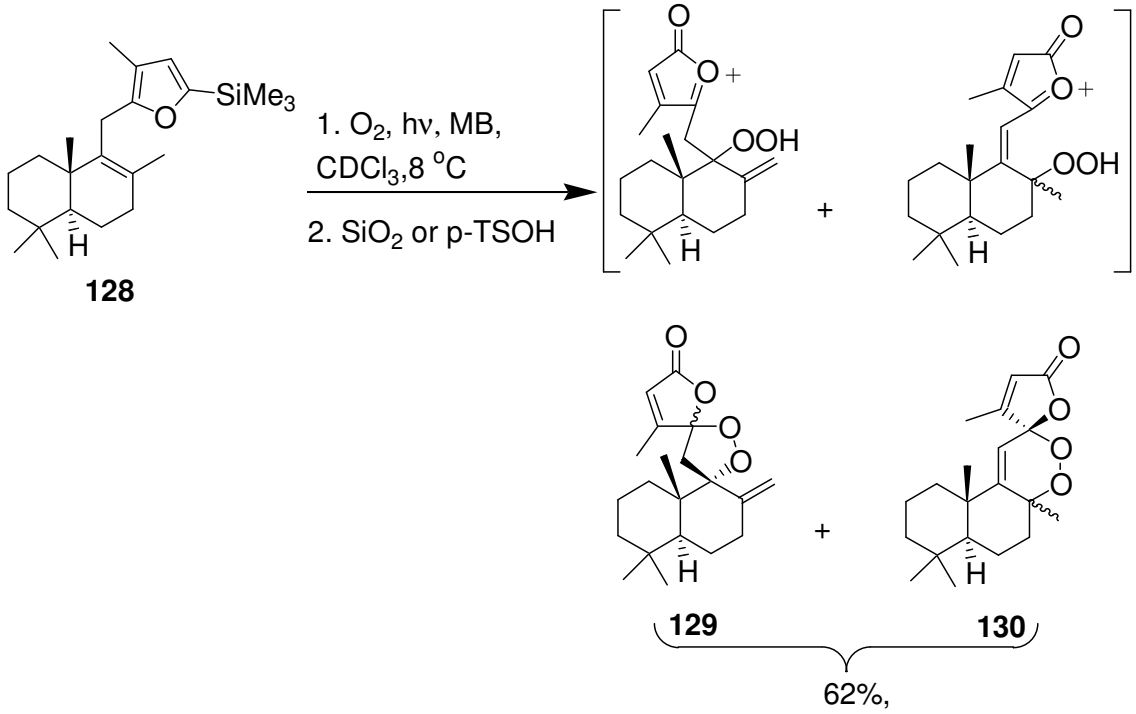

Unlike guanosine **59** described in Section 5.3.4.3 [78], the reaction of singlet oxygen with 2',3',5'-tris-(O-*tert*-butyldimethylsilyl)guanosine (**131**) produced spirodiimidohydantoin (**135**).[127] A facile rearrangement occurred because the guanosine peroxide bore a 8-H substituent. A possible mechanism for the conversion of guanosine **131** to **135** is given in Scheme 31. The secondary photooxidation of 8-oxoG **132** yielded 5-hydroperoxy-8-oxo-7,8-dihydroguanosine (**133**) at low temperature. Reduction of **133** yielded the corresponding alcohol (**134**), which rearranged to a stable final product spirodiimidohydantoin (**135**).

Scheme 31

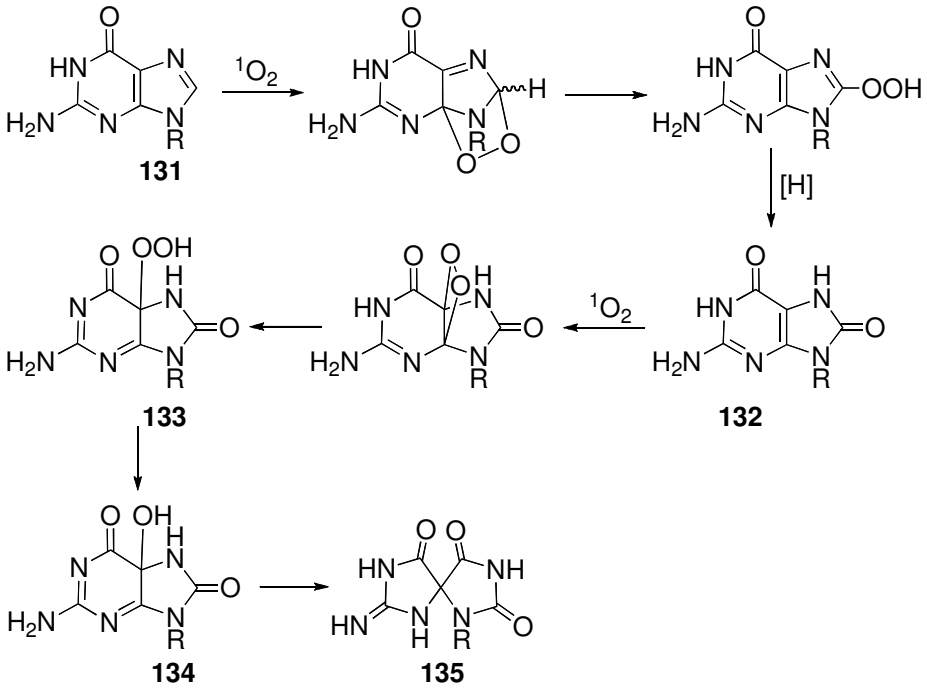

The first report of the structure of the spirodiimidohydantoin nucleoside coming from 8-oxoG was in 2000,[128] in which the oxidation of 8-oxoG by either Ir(IV) or singlet oxygen produced the same spiro compound according to polymerase,[129a] ^{13}C-, ^{15}N-, and ^{18}O-labeling,[129b] and density functional theory studies.[129c] The reaction of guanosine with singlet oxygen,[128-130] and the reaction of furans (such as, **123**) with singlet oxygen,[82,124] showed a similar tendency to form spiro compounds, although they appear to do so by different mechanisms.

5.5.5 Summary

The reactions in this section proceed through stepwise tandem additions of singlet oxygen. The overoxidation of unsaturated hydrocarbons **15** (in Freon-11 or acetone-d_6), **98**, **101**, **103**, **107**, **113**, **117**, **119**, **123**, **128**, and **131** led to the uptake of 2 equivalents of

oxygen. Compounds **15**, **98**, **101**, **103**, **107** led to the formation of bisperoxides. Growing experimental data has been accumulated for singlet oxygen reactions, which give rise to spiro compounds,[82,83,127-130] or yield bis- or polyperoxides, or polyepoxides.[42,58,114-120,131]

5.6 Conclusion

The chapter describes largely singlet oxygen reactions with synthetic potential. Dioxetanes, endoperoxides, hydroperoxides, and bisperoxides were target molecules in dye-sensitized photooxidations. Oxygen, sensitizer, and light were all needed to produce the peroxide products. Some polyunsaturated hydrocarbons were subject to singlet oxygen overoxidation reactions, others were efficient physical quenchers of singlet oxygen. Amine and metal-containing compounds also efficiently convert $^1O_2$ to $^3O_2$ (physical quenching) and chemically react slowly with singlet oxygen, which can represent a shortcoming for their use as substrates in this chemistry. Although a large body of photooxygenation data are available for peroxides, but only a fraction of it focuses on electron-transfer photooxidation chemistry,[29,32,132-134] and its broader synthetic utility has not yet been established.

5.7. References

[1] Suggested reading: (a) Medard, L. A. Accidental Explosions: Types of Explosive Substances; Ellis Horwood Limited: Chichester, 1989; Vol. 2. (b) Patnaik, P. A. Comprehensive Guide to the Hazardous Properties of Chemical Substances, 2nd ed.; John Wiley & Sons: New York, 1999.

[2] Singlet Oxygen; Wasserman, H. H., Murray, R. W., Eds.; Academic Press, Inc.: New York, 1979, especially pp 174-238, pp 244-283, pp 287-419, pp430-506.

[3] Wasserman, H. H., Ives, J. L. *Tetrahedron* **1981**, *37*, 1825.

[4] Hoffmann, N. *Chem. Rev.* **2008**, *108*, 1052.

[5] Wahlen, J.; De Vos, D. E.; Jacobs, P. A.; Alsters, P. L. *Adv. Synth. Catal.* **2004**, *346*, 152.

[6] (a) Blossey, E. C. N., D. C.; Thayer, A. L.; Schaap, A. P. *J. Am. Chem. Soc.* **1973**, *95*, 5820. (b) Fuchter, M. J.; Hoffman, B. M.; Barrett, A. G. M. *J. Org. Chem* **2006**, *71*, 724. (c) Shailaja, J.; Sivaguru, J.; Robbins, R. J.; Ramamurthy, V.; Sunoj, R. B.; Chandrasekhar, J. *Tetrahedron* **2000**, *56*, 6927.

[7] Schweitzer, C.; Schmidt, R. *Chem. Rev.* **2003**, *103*, 1685.

[8] Wilkinson, F.; Helman, W. P.; Ross, A. B. *J. Phys. Chem. Ref. Data* **1995**, *24*, 663.

[9] (a) Worrall, D. R., Abdel-Shafi, A. A., Wilkinson, F. *J. Phys. Chem. A* **2001**, *105*, 1270. (b) Bourne, R. A., Han, X., Chapman, A. O., Arrowsmith, N. J., Kawanami, H., Poliakoff, M., George, M. W. *Chem. Comm.* **2008**, 4457.

[10] Matsumoto, M. Synthesis with singlet oxygen, In *Singlet O_2*; Frimer, A. A., Ed.; CRC Press Volume 2, Boca Raton, FL, 1985, pp 205-274.

[11] (a) The full potential of synthetic organic reactions in water has not yet been realized: Grieco, P. A. (ed.) (1998) *Organic Synthesis in Water,* Blackie Academic & Professional Press: London; (b) Lindström, U. M. *Chem. Rev.* **2002**, *102*, 2751.

[12] (a) Gorman, A. A.; Lovering, G.; Rodgers, M. A. J. *J. Am. Chem. Soc.* **1979**, *101*, 3050. (b) Greer, A. *Science* **2003**, *302*, 235.

[13] Schuster, G. B.; Turro, N. J.; Steinmetzer, H. C.; Schaap, A. P.; Faler, G.; Adam, W. *J. Am. Chem. Soc.* **1975**, *97*, 7110.

[14] (a) Bastos, E. L.; Ciscato, L. F. M. L.; Weiss, D.; Beckert, R.; Badder, W. J. *Synthesis* **2006**, 1781. (b) Adam, W.; Reinhardt, D. *J. Chem. Soc., Perkin Trans. 2* **1997**, 1453.

[15] Sawa, M.; Imaeda, Y.; Hiratake, J.; Fujii, R.; Umeshita, R.; Watanabe, M.; Kondo, H.; Oda, J. *Bioorg. Med. Chem. Lett* **1998**, *8*, 647.

[16] Latch, D. E.; McNeill, K. *Science* **2006**, *311*, 1743.

[17] Grandbois, M.; Latch, D. E.; McNeill, K. *Environ. Sci. Technol.* **2008**, *42*, 9184.

[18] Bartlett, P. D.; Schaap, A. P. *J. Am. Chem. Soc.* **1970**, *92*, 3223.

[19] Mazur, S.; Foote, C. S. *J. Am. Chem. Soc.* **1970**, *92*, 3225.

[20] Zaklika, K. A.; Thayer, A. L.; Schaap, A. P. *J. Am. Chem. Soc.* **1978**, *100*, 4916.

[21] Zaklika, K. A.; Burns, P. A.; Schaap, A. P. *J. Am. Chem. Soc.* **1978**, *100*, 318.

[22] Matsumoto, M.; Watanabe, N.; Kasuga, N. C.; Hamada, F.; Tadokoro, K. *Tetrahedron Lett.* **1997**, *38*, 2863.

[23] Einaga, H.; Nojima, M.; Abe, M. *J. Chem. Soc., Perkin Trans. 1* **1999**, 2507.

[24] Schapp, A. P.; Burns, P. A.; Zaklika, D. A. *J. Am. Chem. Soc.* **1977**, *99*, 1270.

[25] Matsumoto, M.; Nasu, S.; Takeda, M.; Murakami, H.; Watanabe, N. *Chem. Comm.* **2000**, 821.

[26] Boyd, J. D.; Foote, C. S. *J. Am. Chem. Soc.* **1979**, *101*, 6758.

[27] Berdahl, D. R.; Wasserman, H. H. *An account of current research. Israel Journal of Chemistry* **1983**, *23*, 409.

[28] Sauter, M.; Adam, W. *Acc. Chem. Res.* **1995**, *28*, 289.

[29] Ohkubo, K.; Nanjo, T.; Fukuzumi, S. *Org. Lett.* **2005**, *7*, 4265.

[30] Adam, W., Trofimov, A. V. (2006) Contemporary trends in dioxetane chemistry. Rappoport, Z., Ed. Chemistry of Peroxides, 2(Pt. 2), 1171-1209.

[31] Adam, W.; Heil, M.; Mosandl, T.; Saha-Moeller, C. R. *Organic Peroxides* **1992**, 221.

[32] Kotani, H.; Ohkubo, K.; Fukuzumi, S. *J. Am. Chem. Soc.* **2004**, *126*, 15999.

[33] Baumstark, A. L. Thermolysis of alkyl-1,2-dioxetanes. In *Advances in Oxygenated Processes*; Baumstark, A. L.; Ed.; JAI Press: Greenwich, CT 1988, pp 31-84.

[34] Bartlett, P. D.; Baumstark, A. L.; Landis, M. E. *J. Am. Chem. Soc.* **1977**, *99*, 1890.

[35] Baumstark, A. L.; Vasquez, P. C. *J. Org. Chem.* **1984**, *49*, 793.

[36] Bartlett, P. D.; Baumstark, A. L.; Landis, M. E. *J. Am. Chem. Soc.* **1973**, *95*, 6486.

[37] Vasquez, P. C., Chen, Y.-X., Baumstark, A. L. The reaction of trivalent phosphorus compounds with 1,2-dioxetanes and 1,2-dioxolanes. In *Advances in Oxygenated Processes*; Baumstark, A. L.; Ed.; JAI Press: Greenwich, CT 1995, pp 203-224.

[38] Clennan, E. L., Foote, C. S. in Organic Peroxides Ando, W., Ed.; Wiley, Chichester, UK, (1992), pp 255-318.

[39] Balci, M. *Chem. Rev.* **1981**, *81*, 91.

[40] Bartoschek, A.; El-Idreesy, T. T.; Griesbeck, A. G.; Höink, L.-O.; Lex, J.; Miara, C.; Neudörfl, J. M. *Synthesis* **2005**, 2433.

[41] Clennan, E. L. *Tetrahedron* **1991**, *47*, 1343.

[42] Van den Heuvel, C. J. M.; Hofland, A.; Steinberg, H.; De Boer, T. J. *Recueil des Travaux Chimiques des Pays-Bas* **1980**, *99*, 275.

[43] Heuvel, C. J. M.; Steinberg, H.; De Boer, T. J. *Recueil des Travaux Chimiques des Pays-Bas* **1977**, *96*, 157.

[44] Briviba, K.; Debasagayam, T. P. A.; Sies, H.; Steenken, S. *Chem. Res. Toxicol.* **1993**, *6*, 548.

[45] A similar reaction was conducted with 1,5-dihydroxynaphthalene: Shimakoshi, H.; Baba, T.; Iseki, Y.; Endo, A.; Adachi, C.; Watanabe, M.; Hisaeda, Y. *Tetrahedron Lett.* **2008**, *49*, 6198.

[46] Aubry, J.-M.; Pierlot, C.; Rigaudy, J.; Schmidt, R. *Acc. Chem. Res.* **2003**, *36*, 668.

[47] Wasserman, H. H.; Larsen, D. L. *J. Chem. Soc., Chem. Commun.* **1972**, *253*, 253.

[48] Wasserman, H. H.; Wiberg, K. B.; Larsen, D. L.; Parr, J. *J. Org. Chem* **2005**, *70*, 105.

[49] Hart, H.; Oku, A. *J. Chem. Soc., Chem. Commun.* **1972**, *253*, 254.

[50] Martinez, G. R.; Ravanat, J.-L.; Medeiros, M. H. G.; Cadet, J.; Di Mascio, P. *J. Am. Chem. Soc.* **2000**, *122*, 10212.

[51] Pierlot, C.; Aubry, J.-M. *J. Chem. Soc., Chem. Commun.* **1997**, 2289.

[52] Pierlot, C.; Poprawski, J.; Marko, J.; Aubry, J.-M. *Tetrahedron Lett.* **2000**, *41*, 5063.

[53] Aubry, J.-M.; Mandard-Cazin, B.; Rougee, M.; Bensasson, R. V. *J. Am. Chem. Soc.* **1995**, *117*, 9159.

[55] Barrett, A. G. M.; Hopkins, B. T.; Kibberling, J. *Chem. Rev.* **2002**, *102*, 3301.

[56] Schmidt, R.; Drews, W.; Bauer, H.-D. *J. Photochem.* **1982**, *18*, 365.

[57] Bauer, H.-D.; Schmidt, R. *J. Phys. Chem. A* **2000**, *104*, 164.

[58] Linker, T.; Fudickar, W. *Chem. Eur. J.* **2006**, *12*, 9276.

[59] Nardello, V.; Aubry, J.-M. *Methods Enzymol.* **2000**, *319*, 50.

[60] Adam, W.; Prein, M. *Acc. Chem. Res.* **1996**, *29*, 275.

[61] Frizsche, J. (1867) Compt. Rend. 64, 1035-1037.

[62] Liang, Z.; Zhao, W.; Wang, S.; Tang, Q.; Lam, S.-C.; Miao, Q. *Org. Lett* **2008**, *10*, 2007.

[63] Ono, K.; Totani, H.; Hiei, T.; Yoshino, A.; Saito, K.; Eguchi, K.; Tomura, M.; Nishida, J.-I.; Yamashita, Y. *Tetrahedron* **2007**, *63*, 9699.

[64] Yamada, H.; Yamashita, Y.; Kikuchi, M.; Watanabe, H.; Okujima, T.; Uno, H.; Ogawa, T.; Ohara, K.; Ono, N. *Chem. Eur. J.* **2005**, *11*, 6212.

[65] Sparfel, D.; Gobert, F.; Rigaudy, J. *Tetrahedron* **1980**, *36*, 2225.

[66] Hamon, M. A.; Stensaas, K. L.; Sugar, M. A.; Tumminello, K. C.; Allred, A. K. *Chem. Phys. Lett.* **2007**, *447*, 1.

[67] Lebedkin, S.; Kareev, I.; Hennrich, F.; Kappes, M. M. *J. Phys. Chem. C* **2008**, *112*, 16236.

[68] Zhu, Z.; Tang, Z.; Phillips, J. A.; Yang, R.; Wang, H.; Tan, W. *J. Am. Chem. Soc.* **2008**, *130*, 10856.

[69] O'Shea, K.; Foote, C. S. *J. Org. Chem.* **1989**, *54*, 3475.

[70] Rigaudy, J.; Capdevielle, J.; Combrisson, S.; Maumy, M. *Tetrahedron Lett.* **1974**, *2757-2760*.

[71] Manring, L. E.; Foote, C. S. *J. Am. Chem. Soc.* **1983**, *105*, 4710.

[72] Clennan, E. L.; Mohrsheikh-Mohammadi, M. E. *J. Am. Chem. Soc.* **1984**, *106*, 7112.

[73] O'Neill, P. M.; Rawe, S. L.; Storr, R. C.; Ward, S. A.; Posner, G. H. *Tetrahedron Lett.* **2005**, *46*, 3029.

[74] Coughlin, D. J.; Salomon, R. G. *J. Am. Chem. Soc.* **1977**, *99*, 655.

[75] Kao, T.-C.; Chuang, G. J.; Liao, C.-C. *Angew. Chem. Int. Ed.* **2008**, *47*, 7325.

[76] Gollnick, K.; Griesbeck, A. G. *Angew. Chem. Int. Ed.* **1983**, *22*, 726.

[77] Kang, P.; Foote, C. S. *Tetrahedron Lett.* **2000**, *41*, 9623.

[78] Sheu, C.; Foote, C. S. *J. Am. Chem. Soc.* **1993**, *115*, 10446.

[79] Greer, A. *Acc. Chem. Res.* **2006**, *39*, 797.

[80] Foote, C. S.; Wexler, S. *J. Am. Chem. Soc.* **1964**, *86*, 3880.

[81] Patil, S. N.; Stephens, B. E.; Liu, F. *Tetrahedron* **2008**, *64*, 10831.

[82] Montagnon, T.; Tofi, M.; Vassilikogiannakis, G. *Acc. Chem. Res.* **2008**, *41*, 1001.

[83] Georgiou, T.; Montagnon, T.; Tofi, M.; Vassilikogiannakis, G. *Org. Lett.* **2006**, *8*, 1945.

[84] Boger, D. L.; Baldino, C. M. *J. Org. Chem* **1991**, *56*, 6942. Also see: Mayo, P. de.; Reid, S. T. *Chemistry & Industry* **1962**, *35*, 1576.

[85] (a) Dastan, A.; Balci, M. *Tetrahedron* **2006**, *67*, 4003. (b) Mete, E.; Altundas, R.; Secen, H.; Balci, M. *Turkish Journal of Chemistry* **2003**, *27*.

[86] Scott, L. T.; Erden, I.; Brunsvold, W. R.; Schultz, T. H.; Houk, K. N.; Paddon-Row, M. N. *J. Am. Chem. Soc.* **1982**, *104*, 3659.

[87] Gandy, M. N.; Piggott, M. J. *J. Nat. Prod.* **2008**, *71*, 866.

[88] Clennan, E. L.; Heah, P. C. *J. Org. Chem.* **1984**, *49*, 2284.

[89] Stratakis, M.; Orfanopoulos, M. *Tetrahedron* **2000**, *56*, 1595.

[90] (a) Alberti, M. N.; Orfanopoulos, M. *Tetrahedron* **2006**, *62*, 10660. (b) Stratakis, M.; Orfanopoulos, M. *Tetrahedron* **2000**, *56*, 1595.

[91] Lissi, E. A.; Lemp, E.; Zanocco, A. L. Singlet-Oxygen Reactions: Solvent and Compartmentalization Effects. In Understanding and manipulating excited state processes, Ramamurthy, V.; Schanze, K. S., Eds. Marcel Dekker Inc.: 2001; Vol. 8, pp. 287-316.

[92] Clennan, E. L. *Molecular and Supramolecular Photochemistry* **2003**, *9*, 275.

[93] Hino, T.; Anzai, T.; Kuramoto, N. *Tetrahedron Lett.* **2006**, *47*, 1429.

[94] Griesbeck, A. G.; El-Idreesy, T. T.; Bartoschek, A. *Pure Appl. Chem.* **2005**, *77*, 1059.

[95] Bartoschek, A.; El-Idreesy, T. T.; Griesbeck, A. G.; Höinck, L.-O.; Lex, J.; Miara, C.; Neudörfl, J. M. *Synthesis* **2005**, *14*, 2433.

[96] Fröhlich, L.; Torsten, L. *Synlett* **2004**, 2725.

[97] Stratakis, M.; Orfanopoulos, M.; Foote, C. S. *J.Org. Chem.* **1998**, *63*, 1315.

[98] Stratakis, M.; Orfanopoulos, M. *Synth. Comm.* **1993**, *23*, 425.

[99] Griesbeck, A. G.; El-Idreesy, T. T.; Fiege, M.; Brun, R. *Org. Lett.* **2002**, *4*, 4193.

[100] Singh, C.; Malik, H. *Org. Lett.* **2005**, *7*, 5673.

[101] Singh, C.; Pandey, S.; Saxena, G.; Srivastava, N.; Sharma, M. *J.Org. Chem.* **2006**, *71*, 9057.

[102] Stensaas, K. L.; Bajaj, A.; Al-Turk, A. *Tetrahedron Lett.* **2005**, *46*, 715.

[103] Stensaas, K. L.; Bajaj, A. *Synthesis* **2005**, 2623.

[104] Natarajan, A.; Kaanumalle, L. S.; Gibb, S. J. C. L. D.; Gibb, B. C.; Turro, N. J.; Ramamurthy, V. *J. Am. Chem. Soc.* **2007**, *129*, 4132.

[105] Greer, A. *Nature* **2007**, *447*, 273.

[106] Aebisher, D.; Azar, N. S.; Zamadar, M.; Gandra, N.; Gafney, H. D.; Gao, R.; Greer, A. *J. Phys. Chem. B* **2008**, *112*, 1913.

[107] DiMagno, S. G.; Dussault, P. H.; Schultz, J. A. *J. Am. Chem. Soc.* **1996**, *118*, 5312.

[108] Midden, W. R.; Wang, S. Y. *J. Am. Chem. Soc.* **1983**, *105*, 4129.

[109] Pace, A. P. P.; Buscemi, S.; Vivona, N.; Clennan, E. L. *J. Org. Chem.* **2007**, *72*, 2644. Also see: Pace, A. P. P.; Clennan, E. L. *J. Am. Chem. Soc.* **2002**, *124*, 11236. Cojocaru, B., Laferrière, M., Carbonell, E., Parvulescu, V., García, H., Scaiano, J. C. *Langmuir* **2008**, *24*, 4478.

[110] Clennan, E. L. *Adv. Phys. Org. Chem.* **2008**, *42*, 225.

[111] Stratakis, M.; Raptis, C.; Sofikiti, N.; Tsangarakis, C.; Kosmas, G.; Zaravinos, I.-P.; Kalaitzakis, D.; Stavroulakis, D.; Baskakis, C.; Stathoulopoulou, A. *Tetrahedron* **2006**, *62*, 10623.

[112] Li, X.; Ramamurthy, V. *J. Am. Chem. Soc.* **1996**, *118*, 10666.

[113] Singleton, D. A.; Szymanski, M. J.; Meyer, M. P.; Leach, A. G.; Kuwata, K. T.; Chen, J. S.; Greer, A.; Foote, C. S.; Houk, K. N. *J. Am. Chem. Soc.* **2003**, *125*, 1319.

[114] Adam, W.; Cheng, C. C.; Cueto, O.; Erden, I.; Zinner, K. *J. Am. Chem. Soc.* **1979**, *101*, 4735.

[115] Rio, G.; Bricout, D.; Lacombe, L. *Tetrahedron Lett.* **1972**, 3583.

[116] Rio, G.; Bricout, D.; Lacombe, L. *Tetrahedron* **1973**, *29*, 3553.

[117] Zhang, X.; Feng, L.; Foote, C. S. *J. Org. Chem* **1995**, *60*, 1333.

[118] Salamci, E.; Secen, H.; Sütbeyaz, Y.; Balci, M. *J. Org. Chem* **1997**, *62*, 2453.

[119] Adam, W.; Balci, M.; Kilic, H. *J. Org. Chem* **2000**, *65*, 5926.

[120] Gültekin, M. S.; Salamci, E.; Balci, M. *Carbohydr. Res.* **2003**, *338*, 1615.

[121] Kishali, N. H.; Sahin, E.; Kara, Y. *Org. Lett.* **2006**, *8*, 1791.

[122] Blay, G.; Garcia, B.; Molina, E.; Pedro, J. R. *org. Lett.* **2005**, *7*, 3291.

[123] Adam, W.; Balci, M.; Kilic, H. *J. Org. Chem.* **1998**, *63*, 8544.

[124] Sofikiti, N.; Tofi, M.; Montagnon, T.; Vassilikogiannakis, G.; Stratakis, M. *Org. Lett.* **2005**, *7*, 2357.

[125] Adam, W.; Rodriguez, A. *Tetrahedron Lett.* **1981**, *22*, 3505.

[126] Margaros, I.; Montagon, T.; Vassilikogiannakis, G. *Org. Lett.* **2007**, *7*, 2357.

[127] McCallum, J. E. B.; Kuniyoshi, C. Y.; Foote, C. S. *J. Am. Chem. Soc.* **2004**, *126*, 16777.

[128] Luo, W.; Muller, J. G.; Rachlin, E. M.; Burrows, C. J. *Org. Lett.* **2000**, *2*, 613.

[129] (a) Duarte, V.; Muller, J. G.; Burrows, C. J. *Nucleic Acids Res.* **1999**, *27*, 496. (b) Ye, Y., Muller, J. G., Luo, W., Mayne, C. L., Shallop, A. J., Jones, R. A., Burrows, C. J. *J. Am. Chem. Soc.* **2003**, *125*, 13926. (c) Munk, B. H., Burrows, C. J., Schlegel, H. B. *J. Am. Chem. Soc.* **2008**, *130*, 5245.

[130] (a) Cadet, J.; Douki, T.; Ravanat, J. L. *Acc. Chem. Res.* **2008**, *41*, 1075. (b) Gimisis, T.; Cismas, C. *Eur. J. Org. Chem.* **2006**, 1351.

[131] Washington, I.; Jockosch, S.; Itagaki, Y.; Turro, N. J.; Nakanishi, K. *Angew. Chem. Int. Ed.* **2005**, *44*, 7097.
[132] Bonesi, S. M.; Fagnoni, M.; Albini, A. *Eur. J. Org. Chem.* **2008**, 2612.

[133] Baciocchi, E.; Del Giacco, T.; Elisei, F.; Gerini, M. F.; Guerra, M.; Lapi, A.; Liberali, P. *J. Am. Chem. Soc.* **2003**, *125*, 16444.

[134] Zhou, W. C., Edward L. *J. Am. Chem. Soc.* **1999**, *121*, 2915.